NASA CR-137928

ADVANCED AIRFOIL DESIGN EMPIRICALLY BASED TRANSONIC AIRCRAFT-DRAG BUILDUP TECHNIQUE

FINAL REPORT

by W. D. Morrison, Jr.

January 1976

Prepared Under Contract No. NAS2-8612

for

Ames Research Center

National Aeronautics and Space Administration

by

Lockheed-California Company

Burbank, California

ADVANCED AIRFOIL DESIGN EMPIRICALLY BASED TRANSONIC AIRCRAFT-DRAG BUILDUP TECHNIQUE

W. D. MORRISON

LOCKHEED-CALIFORNIA COMPANY
BURBANK, CALIFORNIA

JANUARY 1976

NASA CR-137928

ADVANCED AIRFOIL DESIGN EMPIRICALLY BASED TRANSONIC AIRCRAFT-DRAG BUILDUP TECHNIQUE

FINAL REPORT

by W. D. Morrison, Jr.

January 1976

Prepared Under Contract No. NAS2-8612

for

Ames Research Center

National Aeronautics and Space Administration

by

Lockheed-California Company

Burbank, California

1. REPORT NO.	2. GOVERNMENT ACCESSION NO.	3. RECIPIENT'S CATALOG NO.
NASA CR-137928		

4. TITLE AND SUBTITLE	5. REPORT DATE
Advanced Airfoil Design - Empirically Based - Transonic Aircraft Drag Buildup Technique	January 1976
	6. PERFORMING ORG CODE
7. AUTHOR(S)	8. PERFORMING ORG REPORT NO.
W. D. Morrison, Jr.	LR 27524
9. PERFORMING ORGANIZATION NAME AND ADDRESS	10. WORK UNIT NO.
LOCKHEED-CALIFORNIA COMPANY P.O. BOX 551 BURBANK, CALIFORNIA 91520	11. CONTRACT OR GRANT NO. NAS2-8612
12. SPONSORING AGENCY NAME AND ADDRESS	13. TYPE OF REPORT AND PERIOD COVERED
National Aeronautics and Space Administration Ames Research Center Moffit Field, California	Contractor Report-Final
	14. SPONSORING AGENCY CODE

15. SUPPLEMENTARY NOTES

16. ABSTRACT

Advances in airfoil section design applicable to aircraft optimized for transonic cruise offer improvements in the range factor $M\frac{L}{D}$, increases in wing thickness ratios, increases in wing aspect ratio, or reductions in wing sweep if applied to current transonic aircraft.

To systematically investigate the potential of advanced airfoils in Advance Preliminary Design studies, empirical relationships have been derived, based on available wind tunnel test data, through which total drag can be determined recognizing all major aircraft geometric variables. This technique recognizes a single design lift coefficient and Mach number for each aircraft. Using this technique drag polars can be derived for all Mach numbers up to $M_{Design} + 0.05$ and lift coefficients -0.40 to +0.20 from $C_{L_{Design}}$.

17. KEY WORDS (SUGGESTED BY AUTHOR(S))	18. DISTRIBUTION STATEMENT
Advanced Airfoils Drag Correlation Transonic Aerodynamics Supercritical Airfoils	

19. SECURITY CLASSIF. (OF THIS REPORT)	20. SECURITY CLASSIF. (OF THIS PAGE)	21. NO. OF PAGES	22. PRICE*
UNCLASSIFIED	UNCLASSIFIED		

FOREWORD

The study summarized in this (unclassified final) report (NASA CR-137928) and the Confidential Appendix (NASA CR-137929), under separate cover, was performed by the Lockheed-California Company for the National Aeronautics and Space Administration, Ames Research Center, under Contract No. NAS2-8612. Mr. L. J. Williams was the NASA technical monitor. Mr. W. D. Morrison was the principal investigator.

TABLE OF CONTENTS

LIST OF FIGURES AND TABLES

LIST OF FIGURES AND TABLES (Continued)

LIST OF FIGURES AND TABLES (Continued)

LIST OF SYMBOLS

AR	Wing aspect ratio	b^2/S_{ref}
b	Wing span-tip to wing-body ℄	ft
c	Local Wing Chord	ft
$\bar{c}$	Wing mean aerodynamic chord	ft
℄	Centerline	
C_d	2-dimensional drag coefficient	$\frac{d}{qc}$
C_D	3-dimensional drag coefficient	$\frac{D}{q\ S_{ref}}$
$C_{d_{pmin}}$	Minimum 2-dimensional pressure drag coefficient @ M 0.60	from TEST DATA
$C_{D_{pmin}}$	Minimum 3-dimensional pressure drag coefficient @ M 0.60	from TEST DATA
$C_{D_{pmin}}$	Zero lift drag coefficient	C_f X F.F. $\frac{S_{wet}}{S_{ref}}$
C_{D_i}	Induced drag coefficient	$C_L^2/\pi AR$
C_{D_c}	Compressibility drag coefficient	(f) ΔM , t/c, h/c
C_{D_p}	Pressure drag coefficient	(f) ΔM, ΔC_L, t/c, h/c
C_f	Skin friction drag coefficient	(f) RN'
C_{f_i}	Incompressible skin friction drag coefficient	(f) RN
C_ℓ	2-dimensional lift coefficient	$\frac{\ell}{qc}$
C_n	2-dimensional normal force coefficient	$\frac{n}{qc}$
C_L	3-dimensional lift coefficient	$\frac{L}{q\ S_{ref}}$
C_{L_B}	Lift coefficient for buffet onset	
$C_{L_{Design}}$	Design lift coefficient	C_L @ $(0.99\ M \frac{L}{D})_{max}$
$C_f/C_{f_{incomp.}}$	Compressibility correction to skin friction coefficient	

LIST OF SYMBOLS (Continued)

ΔC_L	$\Delta C_L = C_L - C_{L_{Design}}$	
C_{m_o}	Zero lift pitching moment coefficient	$\frac{M}{q\, S_{ref}\, \bar{c}}$
C_p	Pressure coefficient	$\frac{p_\ell - p_s}{q}$
$C_{p_{critical}}$	Pressure coefficient @ $M_\ell = 1.00$	f(M)
F.F.	Form factor - wing section	f(t/c)
F.F.	Form factor - bodies	$f(\ell/d)$
H	Total pressure (static and dynamic)	lb/ft^2
h/c	Wing camber @ $.70Y/\frac{b}{2}$	$\left(\frac{\frac{Z_{upper}}{c} + \frac{Z_{lower}}{c}}{2}\right)100$
L/D	Lift to drag ratio	
ℓ/d	Body fineness ratio	
ℓ_t	Horizontal tail length	ft
M or M_∞	Freestream Mach number	
M_{Design}	Design Mach number	$M\ @(0.99\ M\frac{L}{D})_{max}$ @ $C_{LDES.}$
$M_{D\ 2\text{-}D}$	2-dimensional drag divergence Mach number	$\frac{d\, C_d}{d\, M} = 0.10$
$M_{D\ 3\text{-}D}$	3-dimensional drag divergence Mach number	$\frac{d\, C_D}{d\, M} = 0.10$
ΔM_{AR}	Correction to divergence Mach number due to aspect ratio	
ΔM_Λ	Correction to divergence Mach number due to sweep	
$M_{DES} = M_{D\ 3\text{-}D} = \left(M_{D\ 2\text{-}D} + \Delta M_{AR} + \Delta M_\Lambda\right)$	@ $C_{L_{Design}}$	
p_ℓ	Local static pressure	lb/ft^2
p_s	Freestream static pressure	lb/ft^2
P/H	ratio of static to total pressure	

LIST OF SYMBOLS (Continued)

q	Dynamic pressure	lb/ft^2
RN RN_ℓ	Reynolds number	$\rho\frac{V\ell}{\mu}$
S_{ref}	Reference wing area - continue basic wing panel leading and trailing edge to ℄	ft^2
S_{wet}	Wetted area of airplane component	ft^2
t/c	Wing section thickness ratio	
t/c_{eff}	Effective thickness ratio - wing frontal area divided by wing plan area to wing-body intersection - include gloves	
W	Aircraft weight	lb
x,y,z	Cartesian coordinate system	
max.	Maximum value	
(f)	Function of	
$\Lambda_{\frac{c}{4}}$	Sweep of basic wing panel quarter chord	deg
ρ		$slug/ft^3$
μ		slug/ft-sec

ADVANCED AIRFOIL DESIGN
EMPIRICALLY BASED
TRANSONIC AIRCRAFT-DRAG BUILDUP TECHNIQUE

By W. D. Morrison, Jr.
Lockheed-California Company

SUMMARY

Advances in airfoil section design applicable to aircraft optimized for transonic cruise offer improvements in the range factor $M\frac{L}{D}$, increases in wing thickness ratios, increases in wing aspect ratio, or reductions in wing sweep if applied to current transonic aircraft.

To systematically investigate the potential of advanced airfoils in Advance Preliminary Design studies, empirical relationships have been derived, based on available wind tunnel test data, through which total drag can be determined recognizing all major aircraft geometric variables. This technique recognizes a single design lift coefficient and Mach number for each aircraft. Using this technique, drag polars can be derived for all Mach numbers up to M_{Design} +0.05 and lift coefficients -0.40 to +0.20 from $C_{L_{Design}}$.

1. INTRODUCTION

In the preliminary design of advanced aircraft there is always the objective of incorporating into the design the most advanced technologies to evaluate their potential for future products.

The concept of controlled supersonic flow development used in present day advanced airfoil design practices has evolved section characteristics exhibiting improvements over more conventional airfoils for application to aircraft designed for transonic cruise. The expression controlled supersonic flow development implies that as the region of local supersonic flow develops and grows in extent over the airfoil chord, the shock wave terminating such a region remains weak. This phenomenon is in contrast to the very strong upper surface shock associated with more conventional design practices.

A number of prominent investigators have applied descriptive terms to their advanced airfoil design philosophy, i.e., Dr. R. Whitcomb's supercritical airfoils, Pearcy's peaky airfoils, and Korn-Garabedian shockless airfoils. In addition, industry and the universities have developed their own advanced airfoil design practices and all indicate improvements over the conventional airfoils. All of these resulting airfoils may be considered supercritical; however, it has become customary to apply the term supercritical to those airfoils that in addition to having controlled supersonic flow development, also carry a significant amount of aft loading due to an appreciable lower surface reflex near the trailing edge. Thus, of the above mentioned advanced airfoil designs, only those developed by Dr. Whitcomb of NASA fit into this more restrictive definition of the term supercritical.

At the present, limited nonsystematic 2- and 3-dimensional wind tunnel test data are available from these aforementioned sources. The explicit methods for the design and quantification of their characteristics reside with the principal investigators. Only the test results are available.

This study has been undertaken, not in an attempt to devise an advanced airfoil design procedure, but rather to collect available 2- and 3-dimensional test data under the generalized concept of "airfoils designed to a controlled supersonic flow development" and devise correlation techniques which will permit preliminary design evaluation of the potential of advanced airfoils for transonic flight applications.

2. STUDY PREMISES AND OBJECTIVES

State of the art and advanced airfoil 2-dimensional section shapes and approximate design condition pressure coefficients are shown in Figure 1. The state-of-the-art airfoil shown here represents one of the sections tested during the development phase of the L-1011. The advanced airfoil shown is representative of an outboard wing section employed on an advanced L-1011 wind tunnel model. Both sections are characterized by controlled upper surface supersonic flow development. However, the advanced airfoil rounder leading edge, flatter upper surface, and more reflexed trailing edge reduces the leading edge pressure coefficient peakiness, extends the near sonic flow further aft on the airfoil,

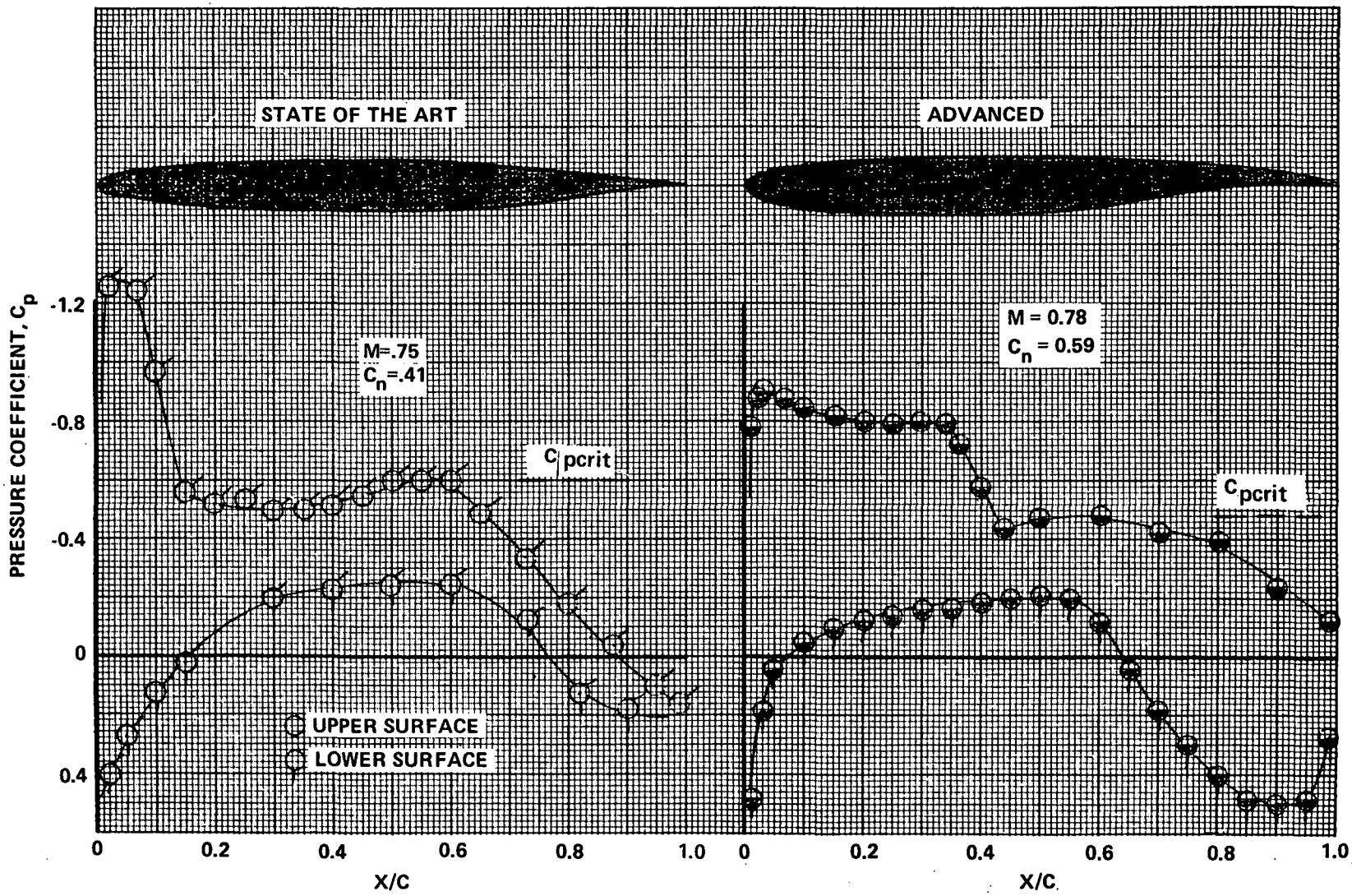

Figure 1. State of the Art and Advanced Airfoil Section Characteristics

and produces a more highly aft loaded section; all contributing to a higher freestream drag divergence Mach number at a somewhat higher lift coefficient. Application of a similar pressure distribution to a 3-dimentional wing involves a design process which is complicated, undoubtedly varies between principal investigators, and to date employs empirical or other approximations (Reference 1). In spite of these complications and probable variations, consideration was given prior to initiating this correlation in an attempt to insure a degree of compatibility of definition and identification of parameters which might aid in the development or validation of theoretical programs.

To this end, the assumption is made that a commonality exists between most theoretical design programs that a specified design-to pressure distribution, P/H, over the airfoil is stipulated at the critical or design lift coefficient and Mach number. This implies that for all advanced airfoil design wind tunnel models there exists a somewhat common level of local Mach number over the airfoil at design conditions or for correlation purposes the same level of pressure drag. The freestream Mach number at which these design conditions are met can be varied by the geometric parameters of sweep, aspect ratio, and thickness ratio.

This suggests that the 3-dimensional wind tunnel test results can be correlated to 2-dimensional equivalence through relationships of design lift coefficient, design Mach number, model geometry, and a relationship of the freestream Mach number to the design Mach number.

3. APPROACH TO DATA CORRELATION

Following the assumptions previously stated, and guided by the NACA work in developing data correlation techniques by means of the Transonic Similarity Rules (Reference 2), a data correlating procedure was evolved and is descriptively noted on Figures 2, 3, and 4.

Two paths of data correlation are shown. Path I involves the determination of design Mach number, design lift coefficient, and drag divergence

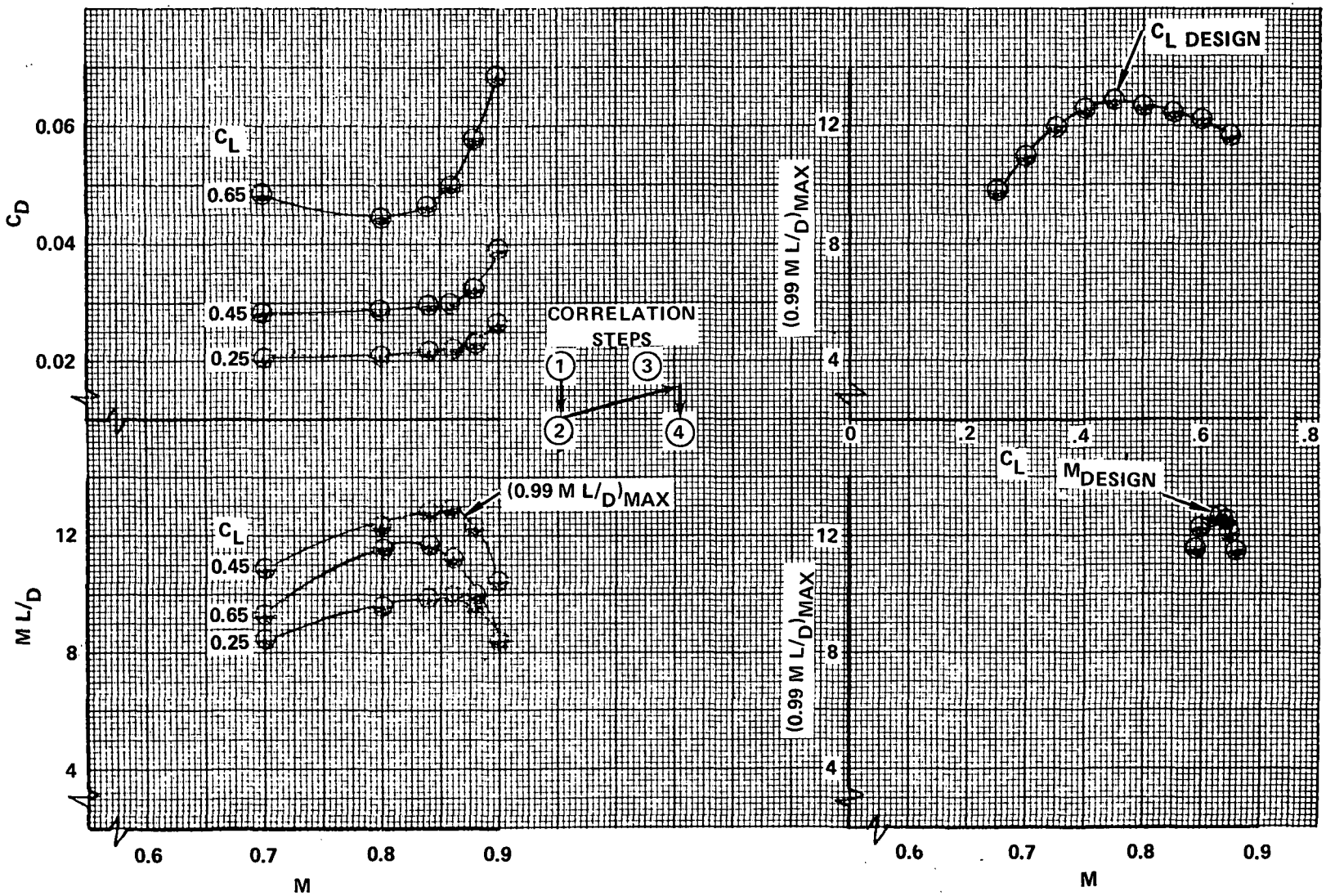

Figure 2. Path I of Data Correlation Technique - $C_{L\ Design}$ and M_{Design} Derivation

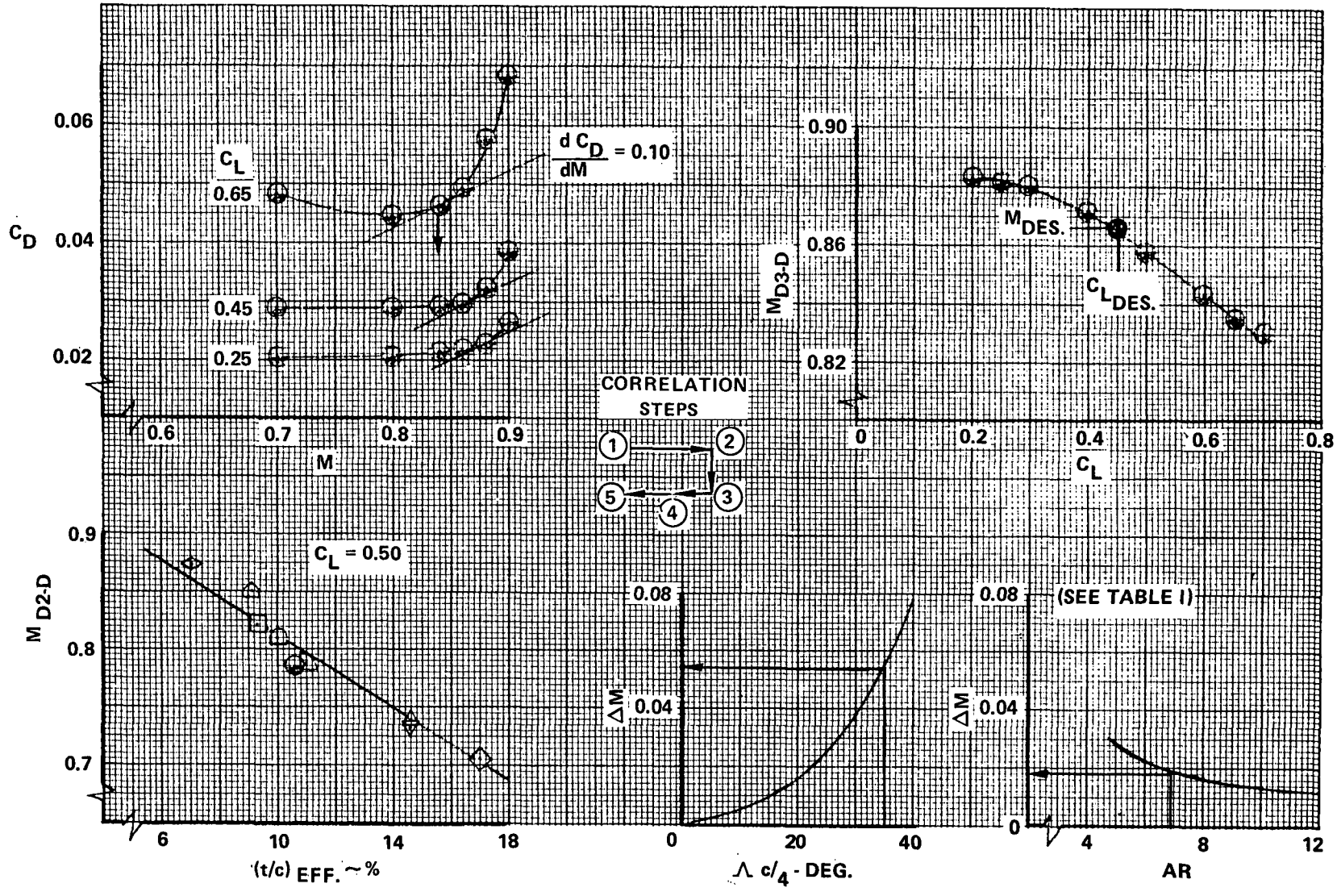

Figure 3. Path I of Data Correlation Technique - Drag Divergence Mach Number Derivation

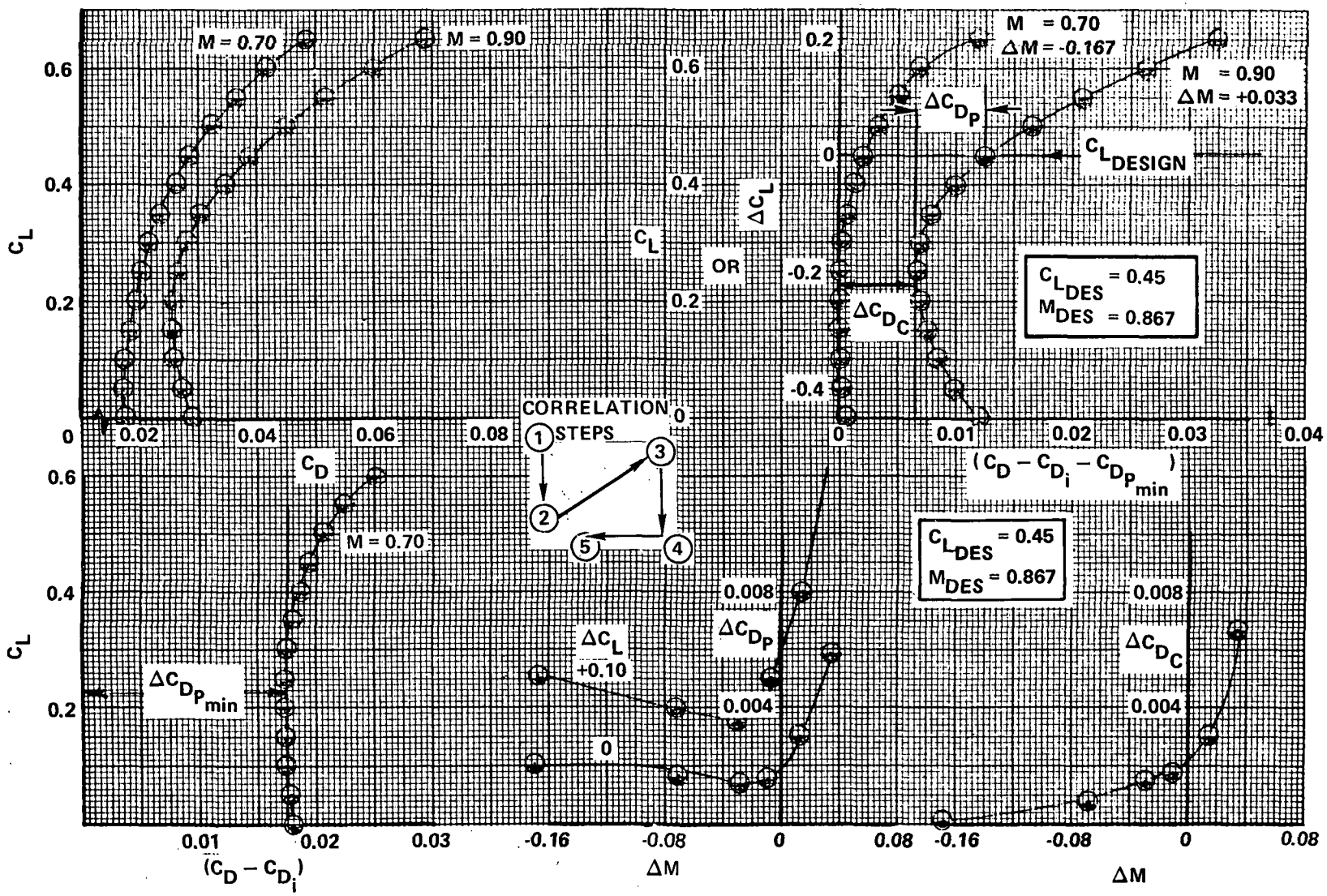

Figure 4. Path II Data Correlation Technique - Incremental Compressibility and Pressure Drag Derivation

Mach number. Path II involves determination of the compressibility and pressure drag.

- Path I: Initial steps require the crossplotting of each wing-body data set as drag versus Mach number at constant lift coefficients; then computing M L/D for each data point and replotting as M L/D versus Mach number at constant lift coefficients. For maximum range, the lift coefficient and Mach number at which the peak value occurs will, in general, be the airplane cruise or design condition. For practical reasons, i.e., flatness of the curve and to insure cruise at the highest speed, an arbitrary value of 0.99 $(M\ L/D)_{max}$ was selected as the design point for M_{Design} and $C_{L_{Design}}$.

  Using the same data crossplots of drag coefficient versus Mach number at constant lift coefficients, the three-dimensional drag divergence characteristics are then determined. To these data, ΔM corrections due to aspect ratio and sweep are applied to arrive at 2-D equivalent characteristics. Divergence has been defined as that Mach number at a constant lift coefficient at which the rate of change in drag coefficient with Mach number reaches a value of $\frac{dC_D}{dM} = 0.10$.

  At the design C_L, Mach divergence, and design are synonymous.

- Path II: The basic drag polar, plotted as drag coefficient versus lift coefficient at constant Mach number, is selected for the determination of the incremental compressibility and pressure drag contributions. Idealized induced drag is computed, as $\frac{C_L^2}{AR}$; e = 1.0, and this quantity is removed from each polar. At the lowest test Mach number, at least a $\Delta M = 0.30$ below design, the minimum profile drag is determined as the bucket of the curve and this drag quantity is removed from all polars. Referring back to Path I of the data correlation, M_{Design} and $C_{L_{Design}}$ are selected and the adjusted polars are replotted at a constant ΔM from M_{Design} versus ΔC_L from $C_{L_{Design}}$. The drag bucket of each of these polars is defined as the incremental compressibility drag and assumed to vary as a function of ΔM from M_{Design}, independent of lift coefficient. The remaining incremental drag above and below $\Delta C_L = 0$, i.e., $C_{L_{Design}}$, is defined as the pressure drag and is assumed to vary as a function of ΔM from M_{Design} at a constant ΔC_L from $C_{L_{Design}}$.

The above data reduction process was applied to each wing-body data set and the resulting data correlation is presented in the following sections. Where appropriate, 2-dimensional data were included.

4. DATA CORRELATION/EMPIRICAL RELATIONSHIPS

4.1 Data Base Summary

The wing-body wind tunnel models incorporating advanced airfoil design sections are noted as W_3 through W_{10} (see Figure 5); 2-dimensional data as W_{11} through W_{14}. The L-1011 flight test and wind tunnel results, W_1 and W_2, respectively, are included as a state of the art reference. W_3 is the L-1011 wind tunnel model test data incorporating an advanced airfoil section. Conventional wing design test data base, not noted on the figure but included in the correlation as another datum reference, was that obtained from References 3, 4, and 5. W_4 through W_{14} test data were reported in References 6 through 18, respectively. The remaining references, 19 through 31, are included as a bibliography of advanced airfoil design tests.

W_1, W_2, and W_3 are the wing designs of Mr. L. R. Miranda of the Lockheed-California Company. W_6 embodies supercritical sections designed by Mr. J. A. Blackwell of the Lockheed-Georgia Company. W_8 is the oblique wing of Dr. R. T. Jones of NASA-Ames with an airfoil section design by Dr. P. Garabedian. W_{10} is a wing-body design by the Boeing Company of Seattle. The remaining wing and wing body models incorporate the supercritical wing sections of Dr. R. Whitcomb of NASA-Langley.

The boxed-in numbers simply highlight the minimum and maximum geometric and design variables associated with this data base.

4.2 Mach and C_L Drag Divergence

A comparison of conventional, state-of-the-art, and advanced airfoil design wing section drag divergence characteristics at a lift coefficient of 0.50 is noted on Figure 6. The data points represent either 2-D test results or 3-D data corrected for the effects of aspect ratio and sweep using Table I. As an example, for an effective thickness ratio of 11 percent, advanced airfoil design gains over conventional airfoils are of the order of $\Delta M = +0.07$. Compared to state-of-the-art airfoils, these gains are of the order of $\Delta M = +0.03$ to $+0.04$. Limiting thickness ratios, minimum and maximum, for incorporating advanced airfoil design practices have not been reported on to date and caution should be exercised in extrapolating much beyond the available data.

TABLE I. INCREMENTAL MACH NUMBER CORRECTION TO DRAG DIVERGENCE DUE TO ASPECT RATIO AND SWEEP

AR	ΔM	$\Lambda_{c/4}$°	ΔM
1.5	0.097	0	0
2.0	0.074	10	0.004
2.5	0.058	15	0.008
3.0	0.047	20	0.016
3.5	0.040	25	0.028
4.0	0.035	30	0.042
5.0	0.028	35	0.057
6.0	0.023	40	0.075
8.0	0.018	45	0.095
10.0	0.014	50	0.115
12.0	0.012	55	0.137
20.0	0.008	60	0.160

SYM.	WING – BODY	#	REF.	AR	Λc/4°	t/c EFF %	CAMBER h/c %	$C_{L_{DESIGN}}$	M_{DESIGN}	
○	W_1	6		6.95	35.0	10.5	1.3	0.46	0.85	3D
◌	W_2	7		6.95	35.0	10.5	1.3	0.45	0.84	
◒	W_3	8		6.95	35.0	10.5	1.6	0.45	0.867	
△	W_4	9		[8.63]	22.0	14.6	[2.6]	[0.55]	0.77	
▽	W_5	9		8.63	22.0	14.6	2.2	0.475	0.775	
□	W_6	10		7.64	40.0	9.3	1.9	0.47	0.916	
◇	W_7	11		5.07	[2.28]	[17.0]	2.1	0.50	[0.735]	
◇	W_8	12		6.48	[45.0]	7.07	0.99	0.325	[0.97]	
⌂	W_9	13		6.80	42.24	9.1	2.0	0.45	0.963	
▱	W_{10}	14		[3.5]	39.4	[5.0]	[0.40]	[0.275]	0.918	
◇	W_{11}	15		--	--	10.0	1.64	--	--	2D
⌂	W_{12}	16		--	--	10.0	1.64	--	--	
▱	W_{13}	17		--	--	11.0	2.03	--	--	
◺	W_{14}	18		--	--	11.0	2.05	--	--	

[ ] MAX., MIN. VARIATIONS

Figure 5. State of the Art and Advanced Airfoil - Flight and Wind Tunnel Model Data Base Summary

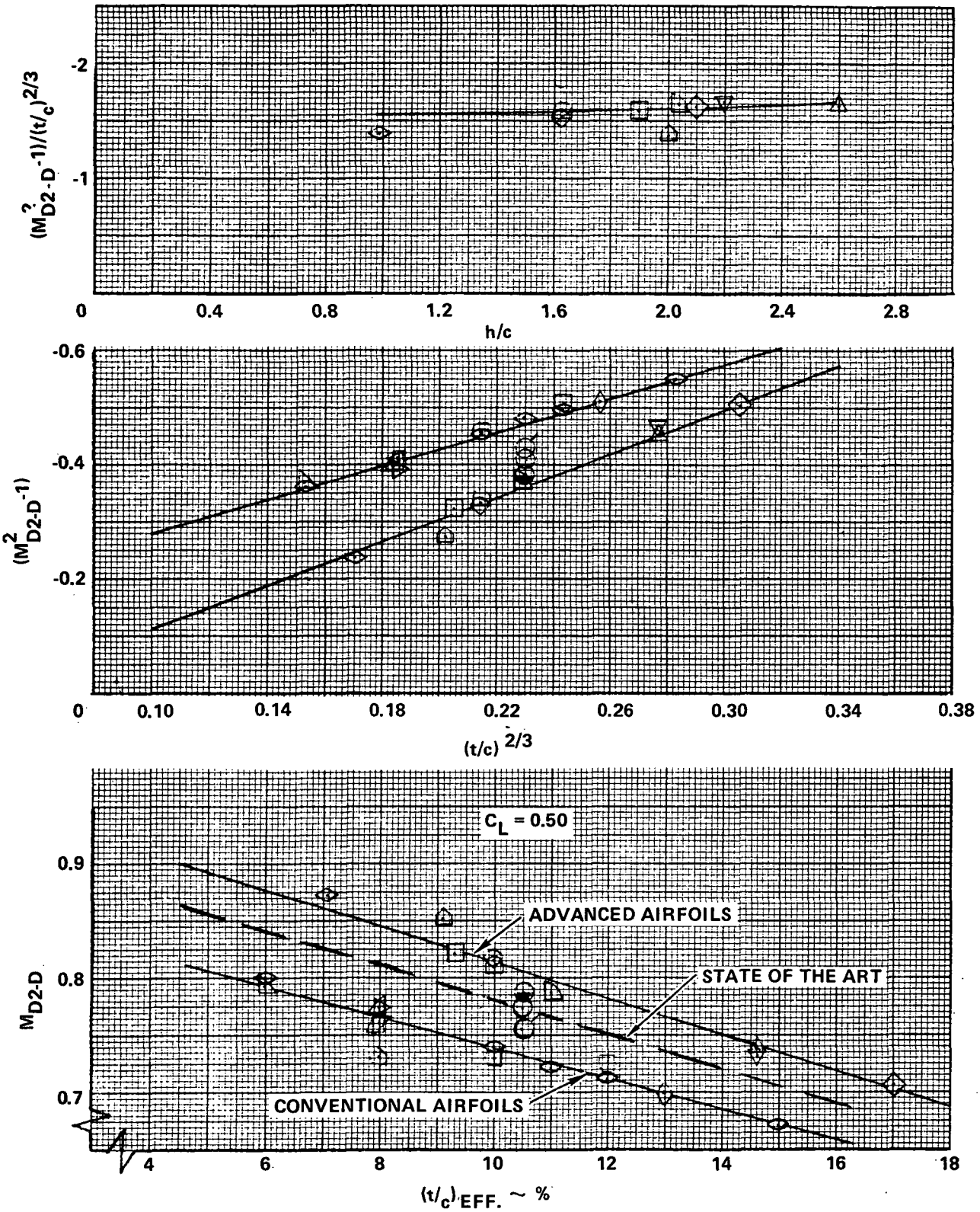

Figure 6. $M_{D\ 2\text{-}D}$ Correlation Approach - $C_L = 0.50$

Recognizing that drag divergence Mach number may also be sensitive to other first order airfoil geometric variables, additional correlating parameters were investigated and are noted on Figure 6. The parameter $(M_{D_{2-D}}^2 - 1)$ versus $(t/c)^{2/3}$ was suggested in Reference 2 and appears to improve the correlation. Effects of camber are also noted on this figure and reflect a slight variation in divergence Mach number with increased camber at this lift coefficient. At lower lift coefficients, the effects of high camber become more predominant. For purposes of this study, a linear variation of $(M_{D2-D}^2 - 1)$ vs $(t/c)^{2/3}$, representative of cambers up to $\approx$2.2%, is assumed and this correlation is presented for lift coefficients from 0.10 to 0.80 on Figures 7 through 14. Tables II and III are included to aid in determination of the M_{D2-D} and t/c relationships to the chosen parameters $(M_{D2-D}^2 - 1)$ and $(t/c)^{2/3}$.

4.3 Design Lift Coefficient

The determination of $C_{L_{Design}}$ is the key to this data correlation technique. Through this definition there is a single optimum polar selected for a given aircraft geometry.

The initial study premise, that each wing-body wind tunnel data set has its unique design lift coefficient, implied that certain configuration relationships would determine this lift coefficient. The classical definition of $C_{L_{optimum}}$ (the lift coefficient corresponding to (L/D_{max}) suggested those correlating parameters, since $C_{L_{opt.}} = f\left(\sqrt{e\pi AR}\ \sqrt{C_{D_o}}\right)$. On Figure 15 the $C_{L_{Design}}$ for the wing-body configurations of this study are noted as a function of wing aspect ratio. By normalizing those data to a single level of C_{D_o} = 0.0160 and recognizing section camber as a contributor to $C_{L_{Design}}$, the relationship shown on the left of Figure 15 was determined.

4.4 Compressibility and Pressure Drag

An assessment of the magnitude of the various incremental contributors to total drag is in order prior to review of the following section.

The percentage contribution of the compressibility plus pressure drag to the total drag of an existing wide-body transport at the design conditions of M = 0.85 and 0.46 lift coefficient is some 14 percent. This contribution

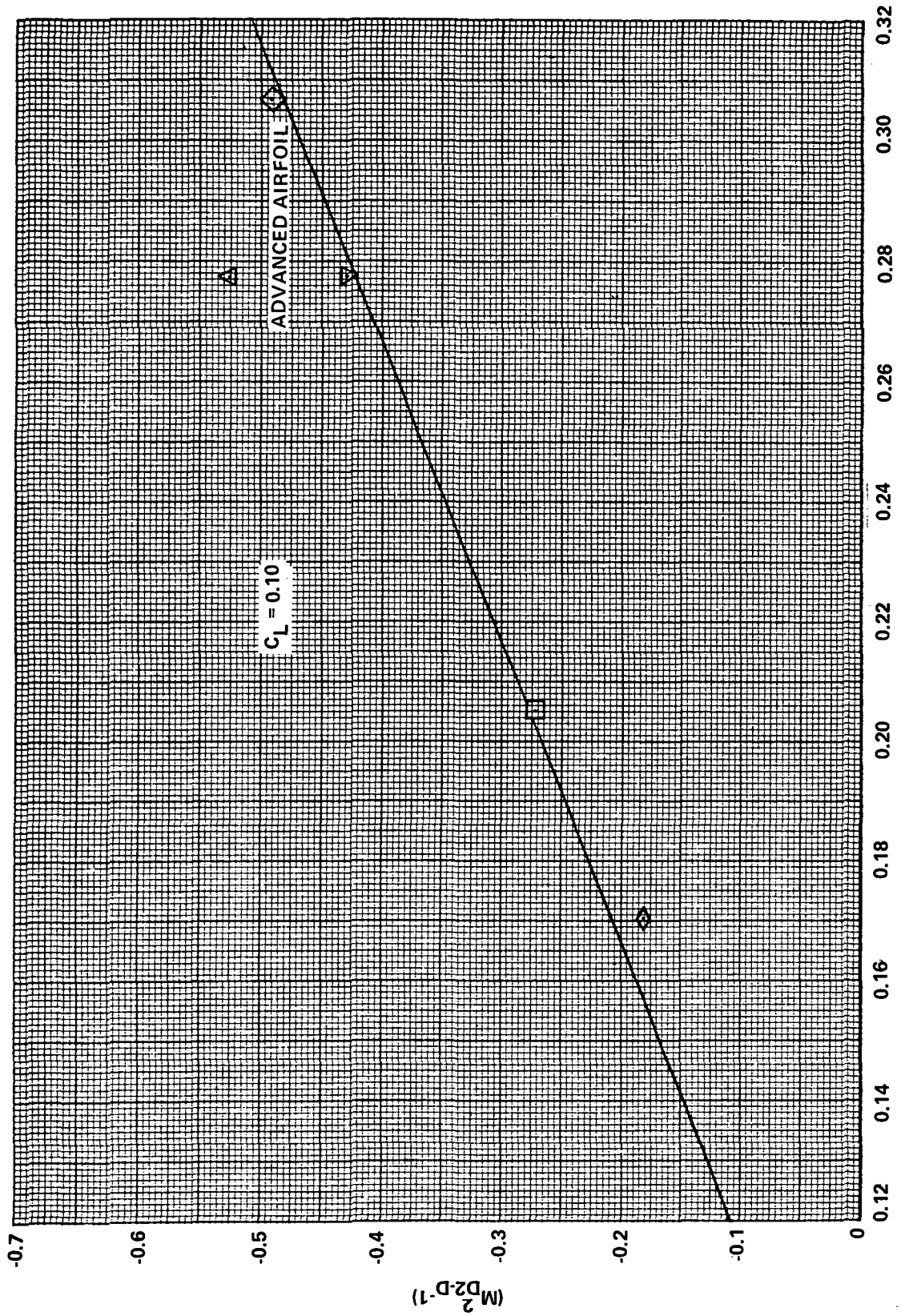

Figure 7. $M_{D\ 2\text{-}D}$ vs t/c Correlation - $C_L = 0.10$

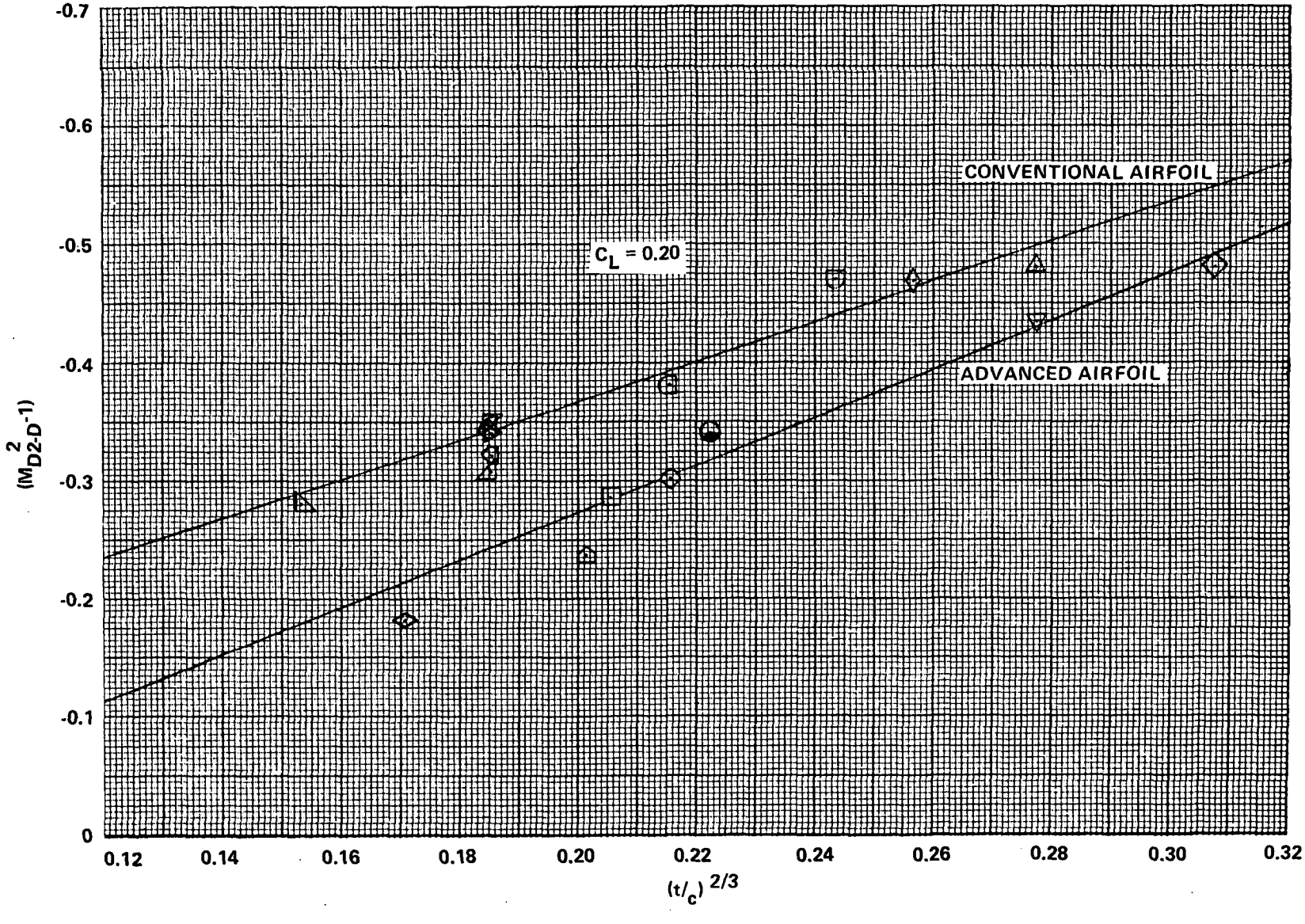

Figure 8. $M_{D\ 2\text{-}D}$ vs t/c Correlation - $C_L = 0.20$

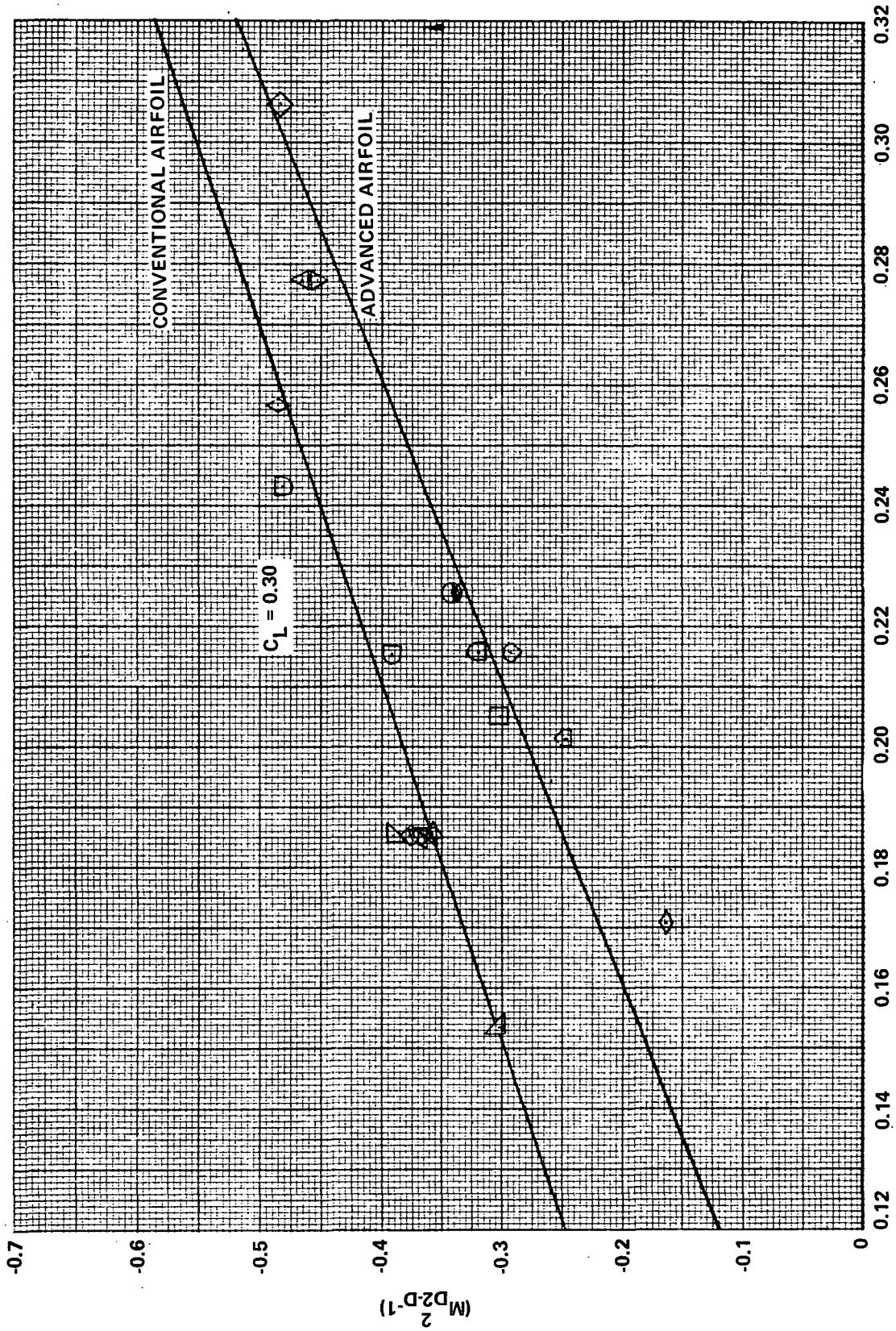

Figure 9. $M_{D\ 2\text{-}D}$ vs t/c Correlation - C_L = 0.30

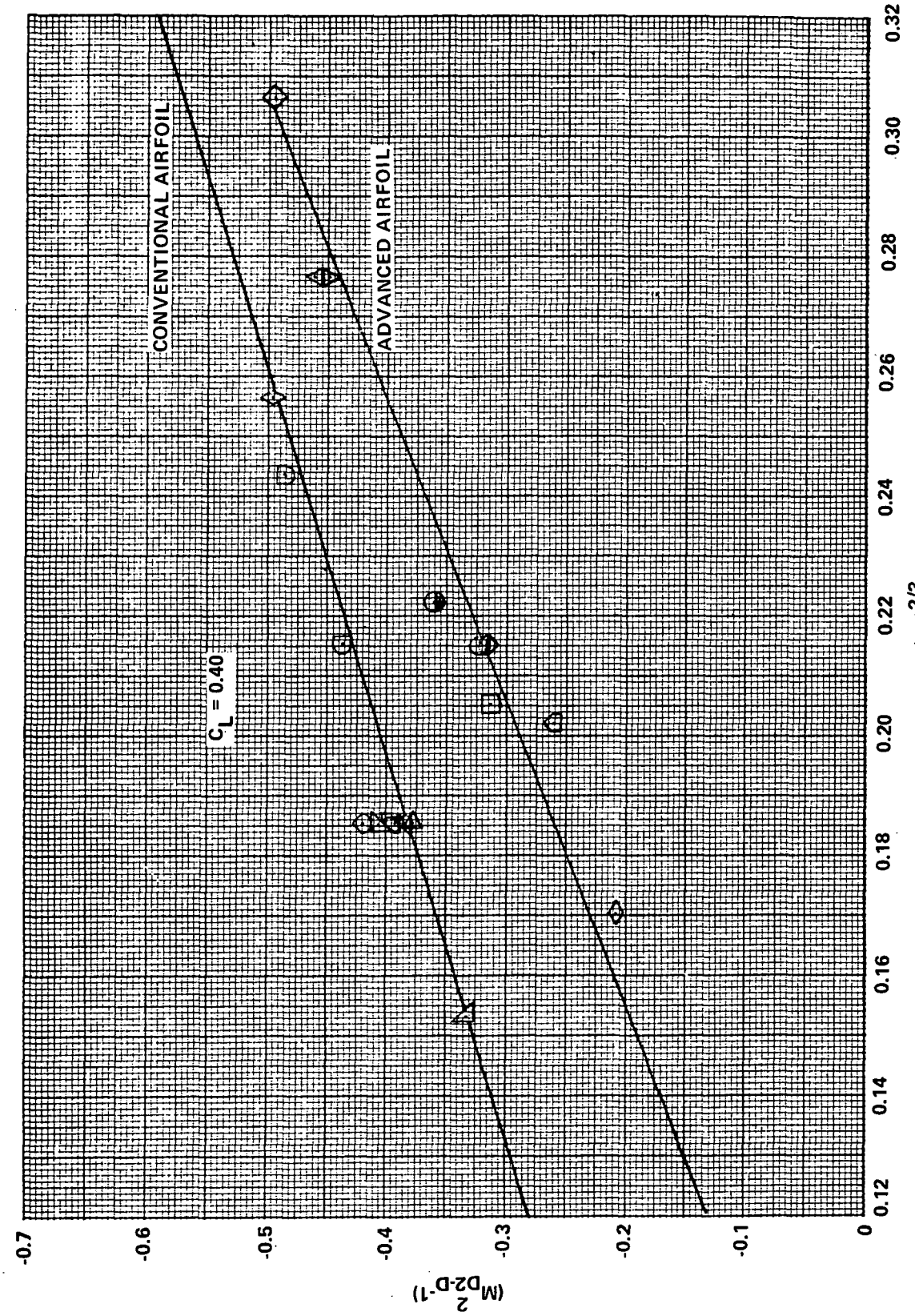

Figure 10. M_D 2-D vs t/c Correlation - $C_L = 0.40$

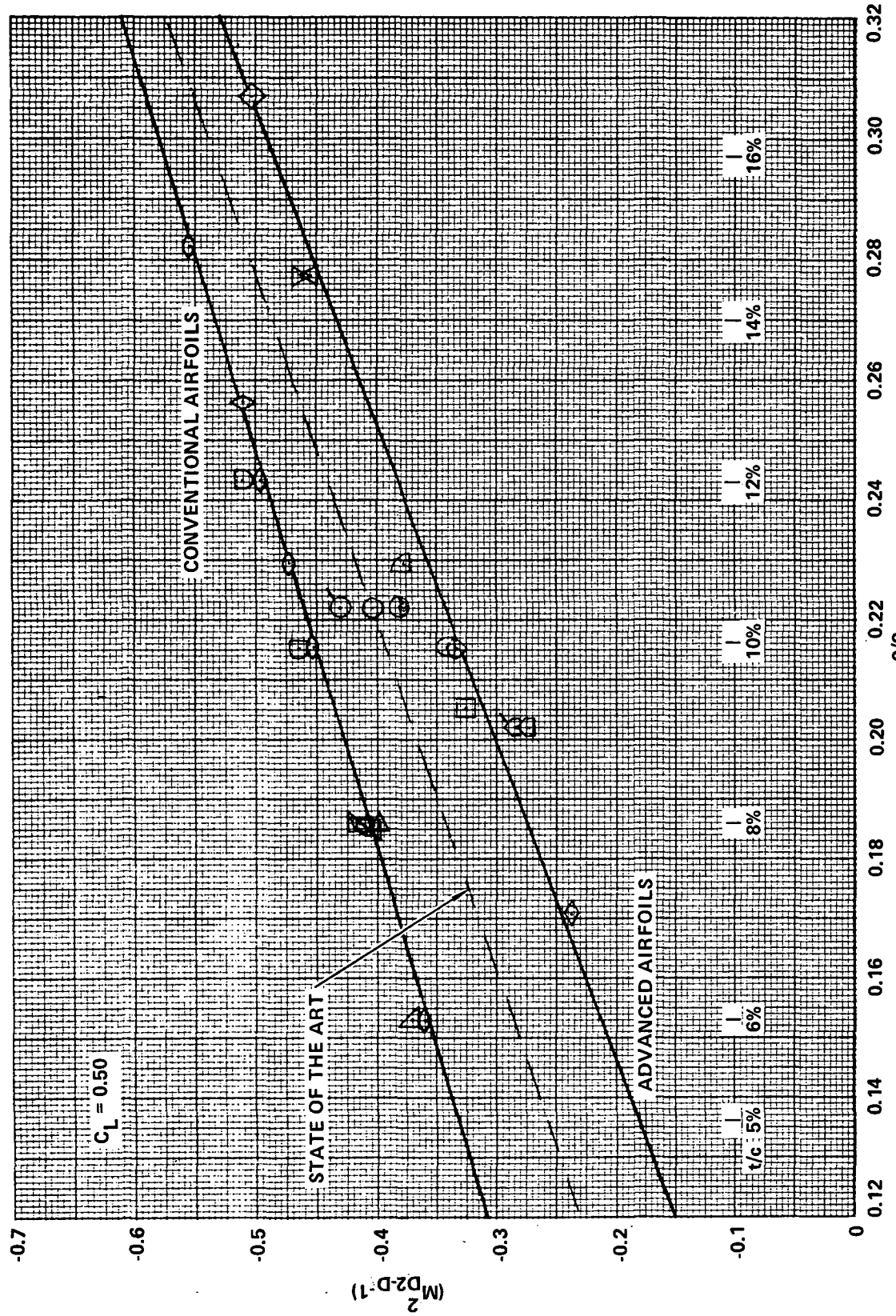

Figure 11. $M_{D\ 2\text{-}D}$ vs t/c Correlation - $C_L = 0.50$

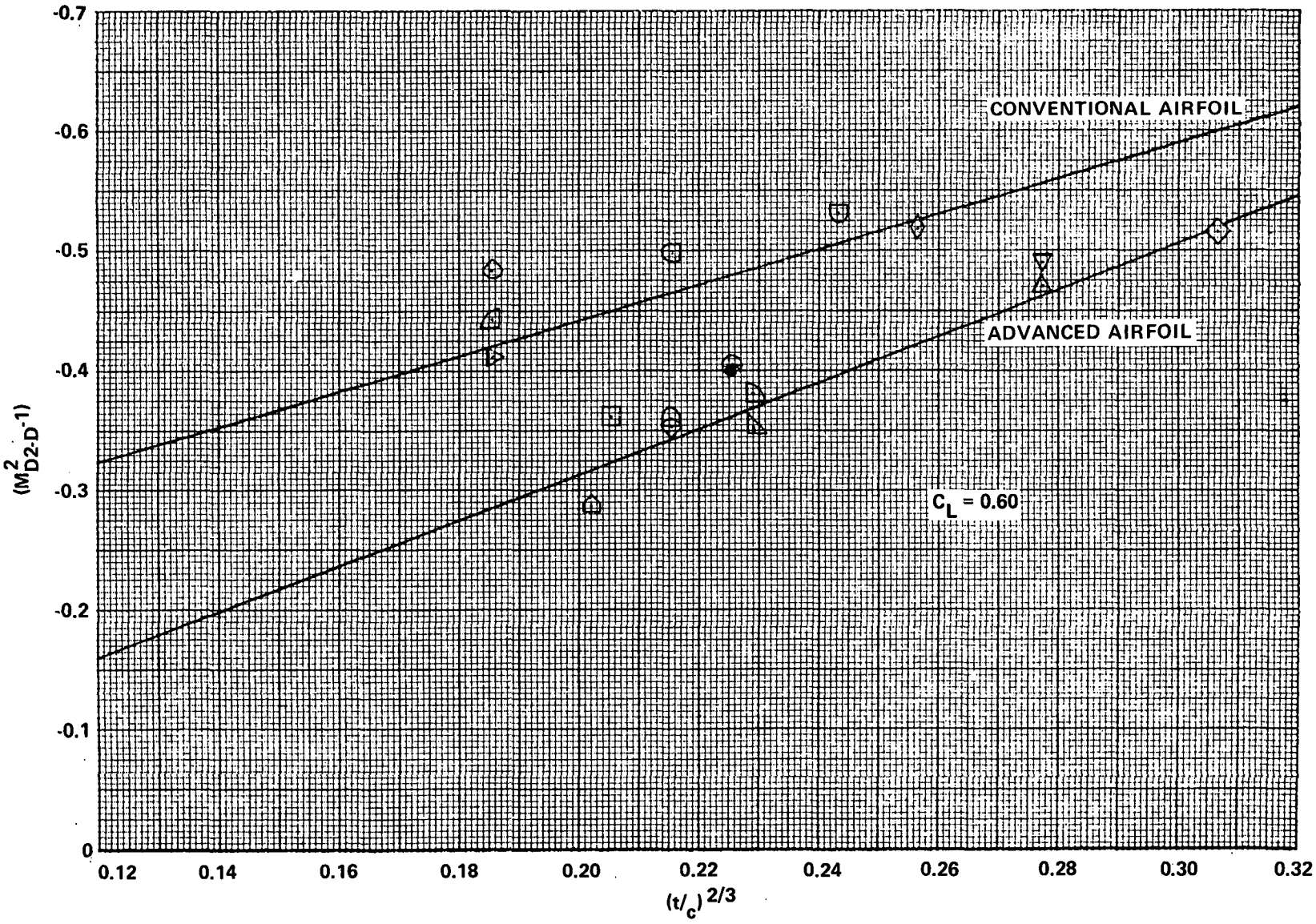

Figure 12. $M_{D\ 2\text{-}D}$ vs t/c Correlation - C_L = 0.60

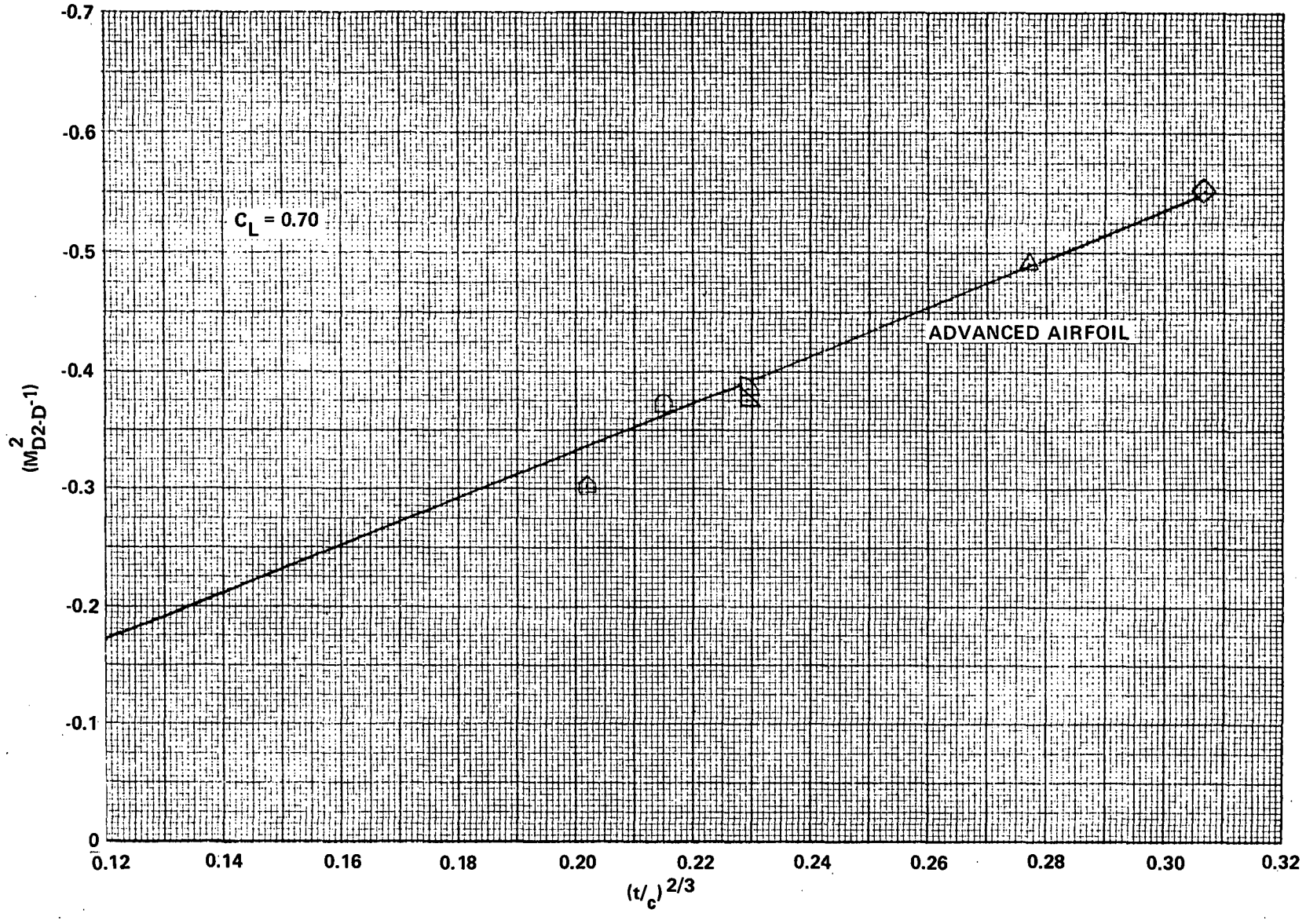

Figure 13. $M_{D\ 2\text{-}D}$ vs t/c Correlation - $C_L = 0.70$

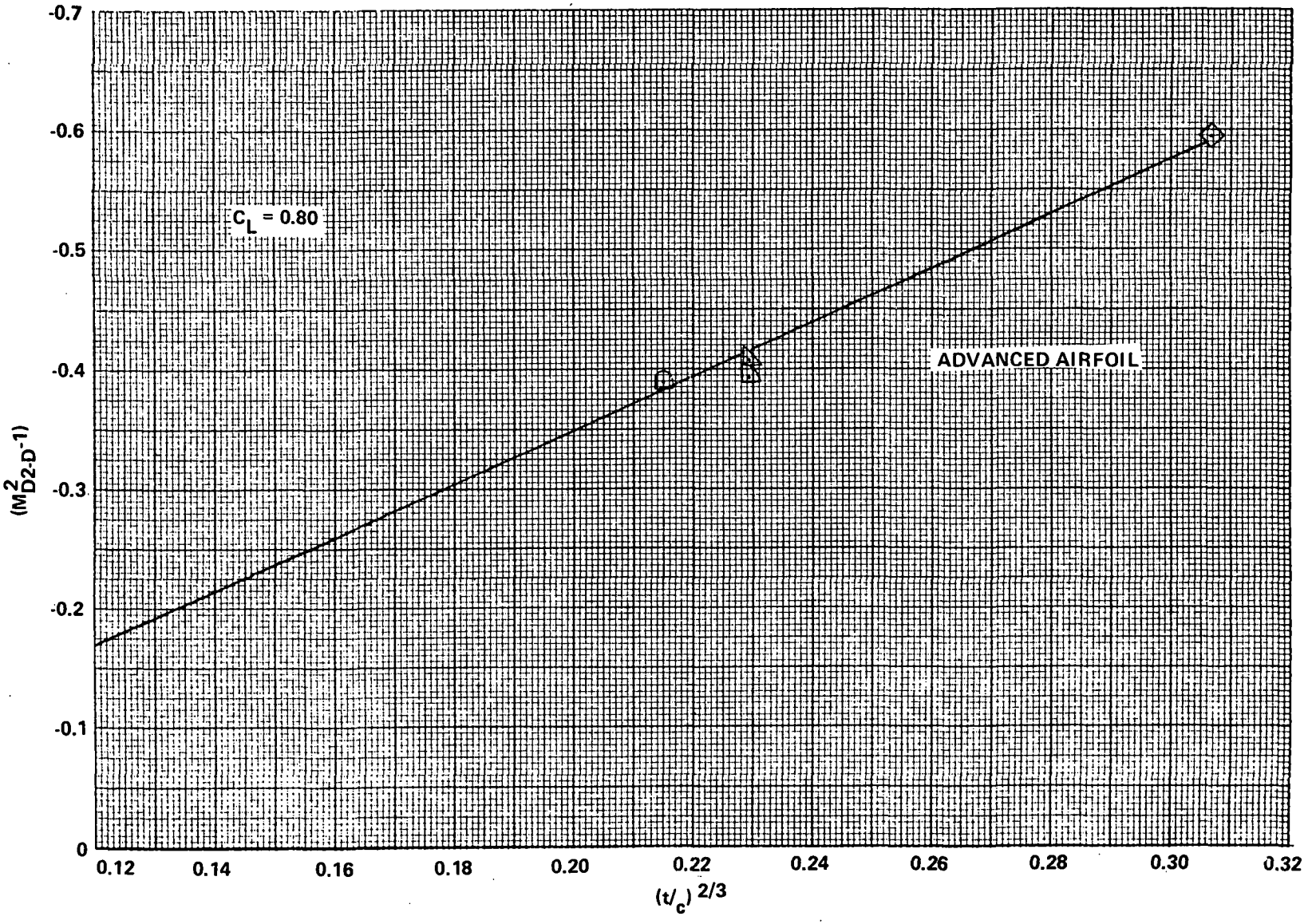

Figure 14. $M_{D\ 2\text{-}D}$ vs t/c Correlation - C_L = 0.80

TABLE II. $M_{D\ 2\text{-}D}$, $M^2_{D\ 2\text{-}D}$, and $(M^2_{D\ 2\text{-}D}{}^{-1})$ RELATIONSHIPS

$M_{D\ 2\text{-}D}$	$M^2_{D\ 2\text{-}D}$	$(M^2_{D\ 2\text{-}D}{}^{-1})$
0.60	0.3600	-0.6400
0.62	0.3844	-0.6156
0.64	0.4096	-0.5904
0.66	0.4356	-0.5644
0.68	0.4624	-0.5371
0.70	0.4900	-0.5100
0.72	0.5184	-0.4816
0.74	0.5476	-0.4524
0.76	0.5776	-0.4224
0.78	0.6084	-0.3916
0.80	0.6400	-0.3600
0.82	0.6724	-0.3276
0.84	0.7056	-0.2944
0.86	0.7396	-0.2604
0.88	0.7744	-0.2256
0.90	0.8100	-0.1900

TABLE III. t/c, $(t/c)^{5/3}$, $(t/c)^{2/3}$, and $(t/c)^{1/3}$ RELATIONSHIPS

t/c	$(t/c)^{5/3}$	$(t/c)^{2/3}$	$(t/c)^{1/3}$
0.04	0.00468	0.1170	0.3420
0.05	0.00679	0.1357	0.3684
0.06	0.00920	0.1533	0.3915
0.07	0.01189	0.1699	0.4121
0.08	0.01485	0.1857	0.4309
0.09	0.01807	0.2008	0.4481
0.10	0.02155	0.2154	0.4642
0.11	0.02526	0.2295	0.4791
0.12	0.02919	0.2433	0.4932
0.13	0.03337	0.2566	0.5066
0.14	0.03775	0.2696	0.5193
0.15	0.04235	0.2823	0.5313
0.16	0.04716	0.2947	0.5429
0.17	0.05218	0.3068	0.5540
0.18	0.05739	0.3187	0.5646
0.19	0.06280	0.3304	0.5749
0.20	0.06841	0.3419	0.5848

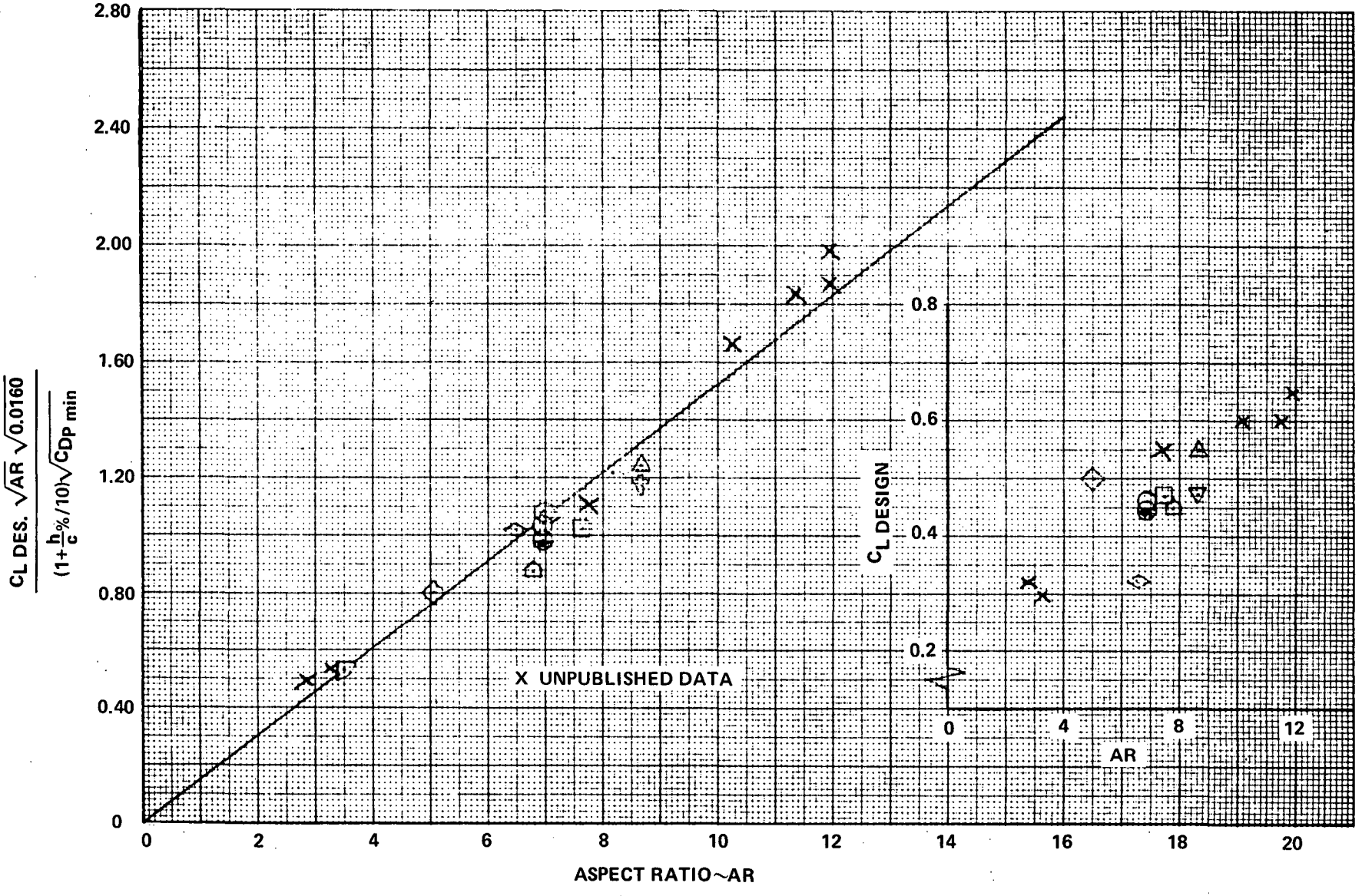

Figure 15. Correlation of Design Lift Coefficient

is essentially equally divided as 7 percent compressibility and 7 percent pressure. The remaining drag is comprised of 33 percent induced and 53 percent friction, dirtyness, leakage, and interference. As the Mach number is increased to 0.89, $\Delta M = +0.04$, the $(\Delta C_{D_c} + \Delta C_{D_p})$ contribution increases to some 30 percent. Reducing the Mach number to $M = 0.80$, $\Delta M = 0.05$, this contribution is in the order of 10 percent of total drag.

In evaluating the compressibility plus pressure drag of 2-dimensional or 3-dimensional wing-body test data, consideration must be given to the test Reynolds number, location of the boundary layer trip grit, and wind tunnel blockage. The sensitivity of $(\Delta C_{D_c} + \Delta C_{D_p})$ to Reynolds number is noted on Figure 16. The design conditions were approximately $C_n = 0.60$ at a Mach number of 0.79. As the test RN is increased, the level of $(\Delta C_{D_c} + C_{D_p})$ tends to reduce or bucket as the design Mach number is approached. These effects will be noted in the following 3-D correlations and are in the main evidenced in the ΔC_{D_p} term.

4.4.1 Compressibility Drag. - On Figure 17 ΔC_{D_c} is presented as a function of ΔM from M_{Design} for the wing-body data sets and the L-1011 state-of-the-art reference flight test and wind tunnel data. At the top of the figure, the unadjusted compressibility drag shows scatter on the order of 20 counts of drag, i.e., $\Delta C_D = 0.0020$. The correlating factors of $(t/c)^{5/3}$ and camber h/c % (lower curve, Figure 17) were those suggested in NACA TR 1253 - Correlation by Transonic Similarity Rules. Up to M_{Design} the correlation of data appears exceptionally good. Data scatter above M_{Design} may be attributable to varying test Reynolds number, test grit location, camber, and section variation with span, or to the degree of refinement of model following flow visualization studies of shock buildup across the span. A fairing of these data against a logorithmic scale is presented on Figure 18.

4.4.2 Pressure Drag. - Pressure drag is presented on Figure 19 through 28 for ΔC_L's ranging from minus 0.40 to plus 0.20. Figure 24 (upper curve) presents the uncorrelated data sets at $C_{L_{Design}}$. Design C_L for the data sets ranged from 0.275 to 0.55 and Mach design from 0.73 to 0.97. Approximately 20 counts of data scatter are noted up to design Mach number with increasing

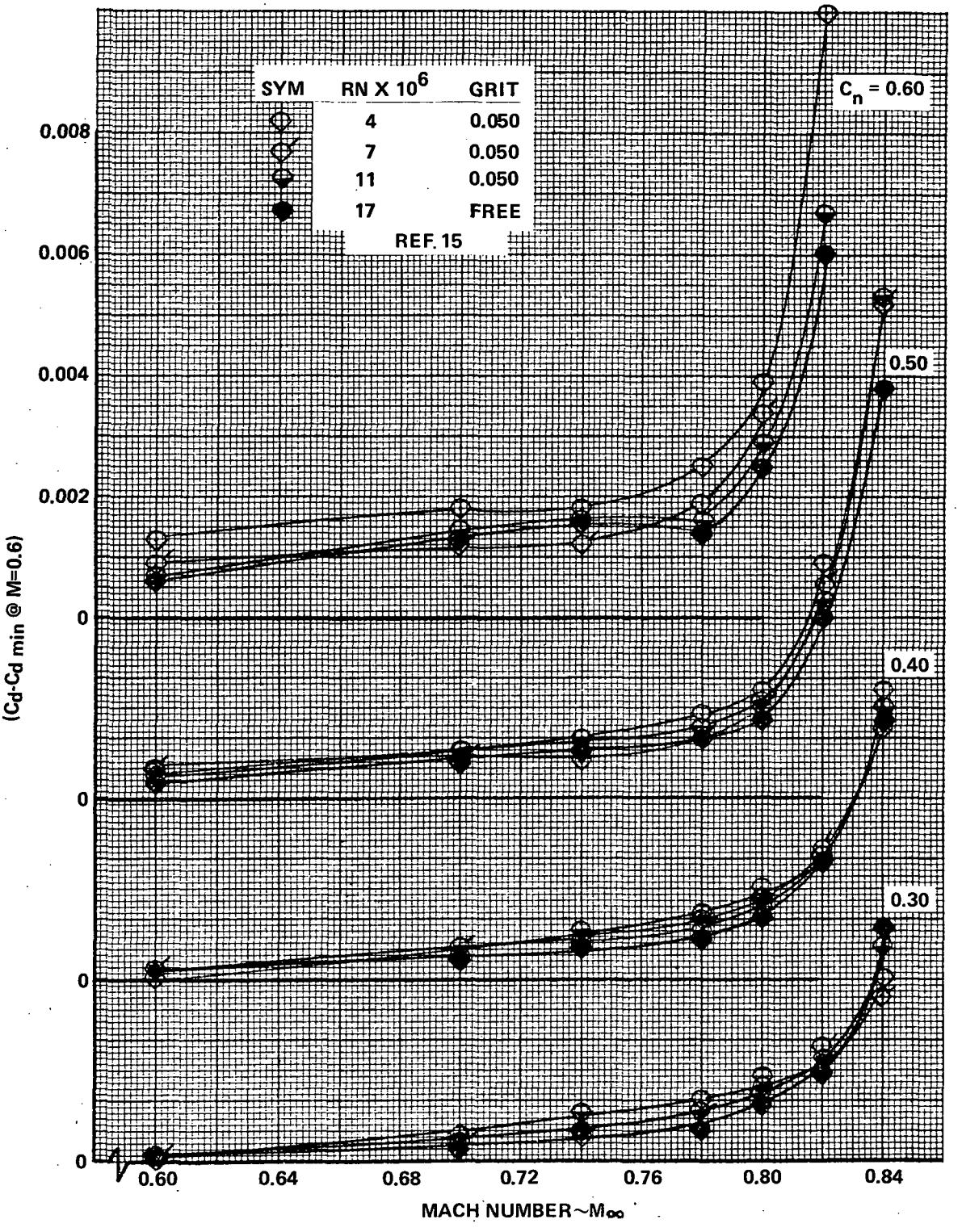

Figure 16. 2-D Compressibility and Pressure Drag Variation with Reynolds Number

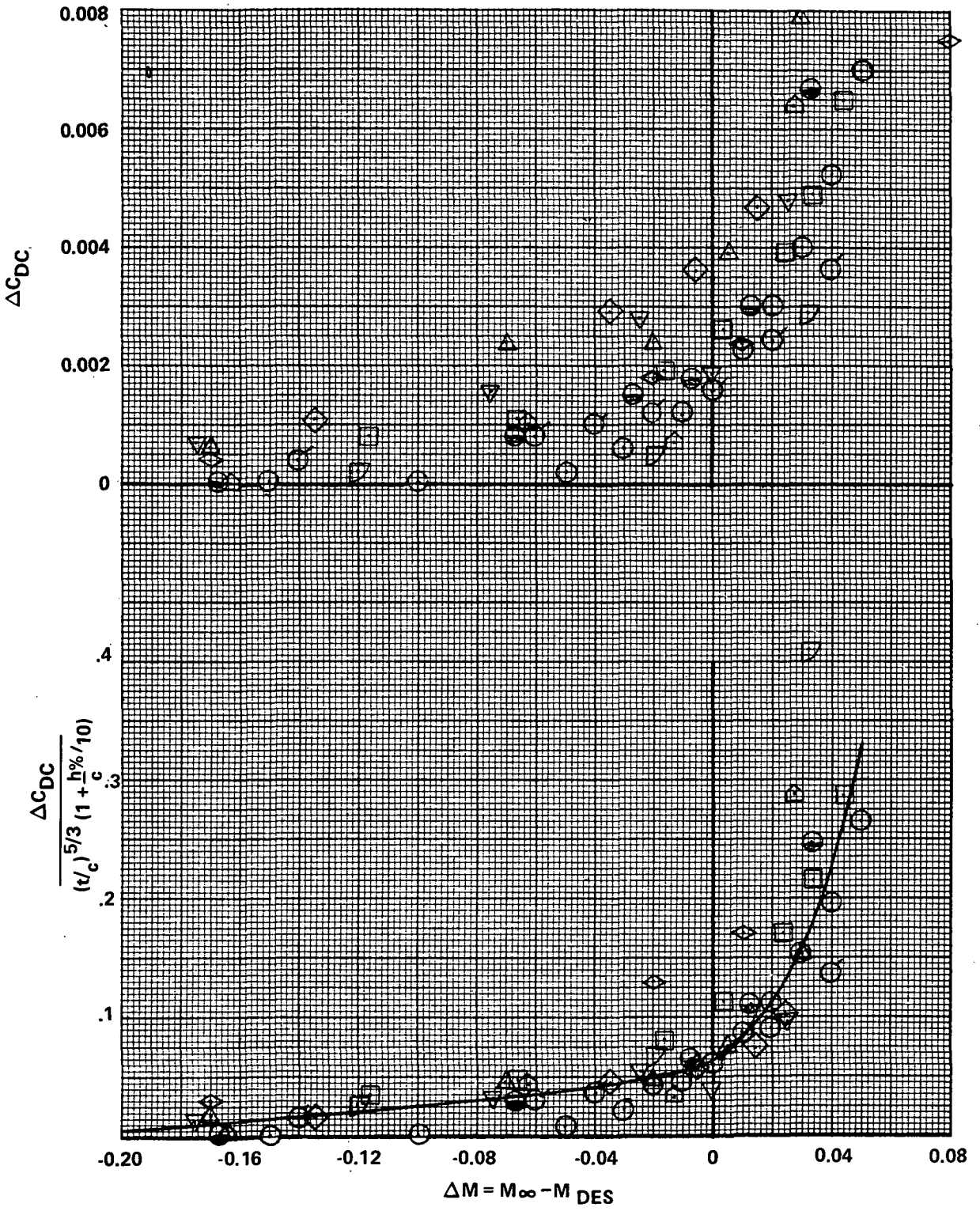

Figure 17. Incremental Compressibility Drag Variation with Incremental Mach Number from Mach Design

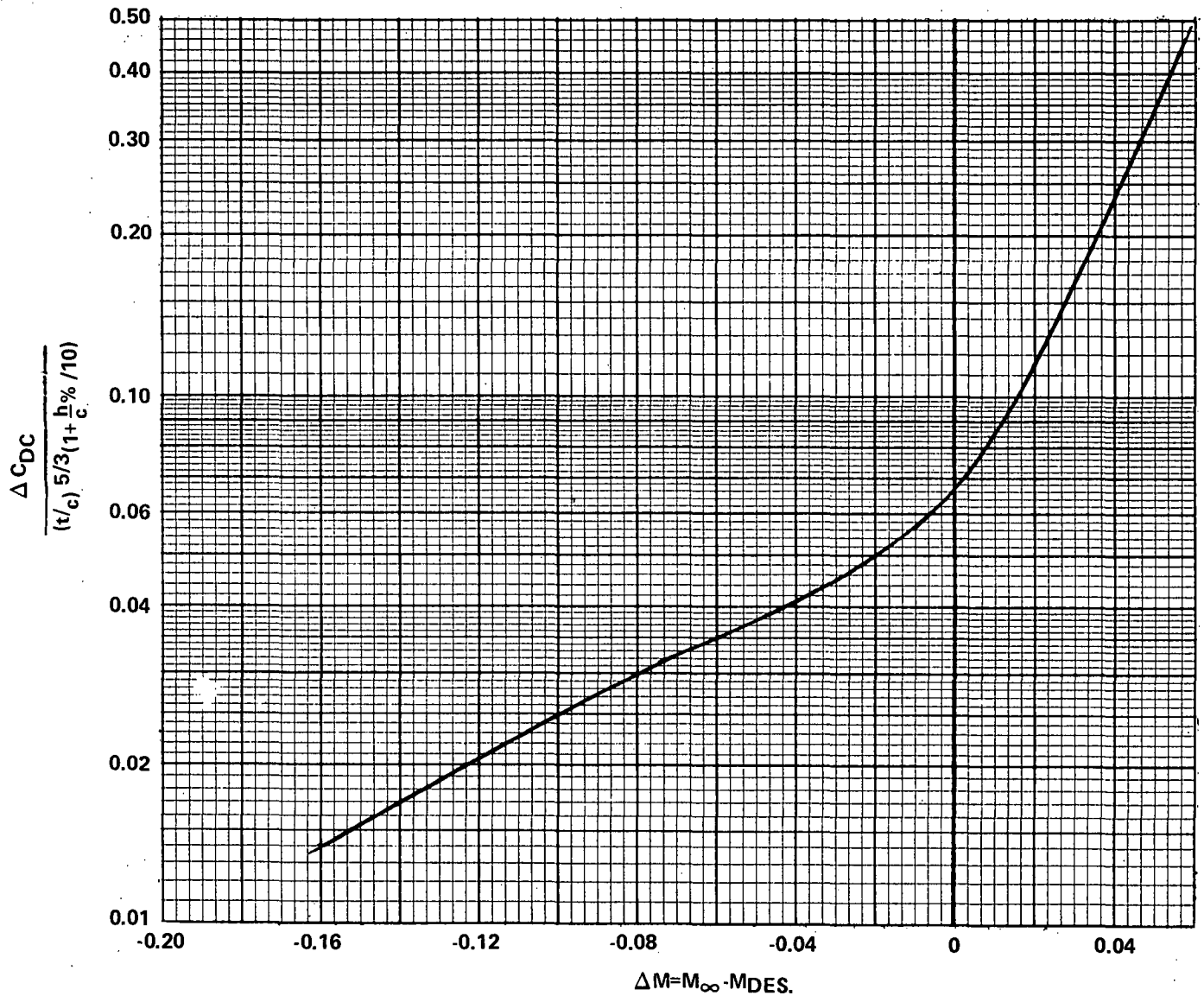

Figure 18. Fairing of Incremental Compressibility Drag - Summary

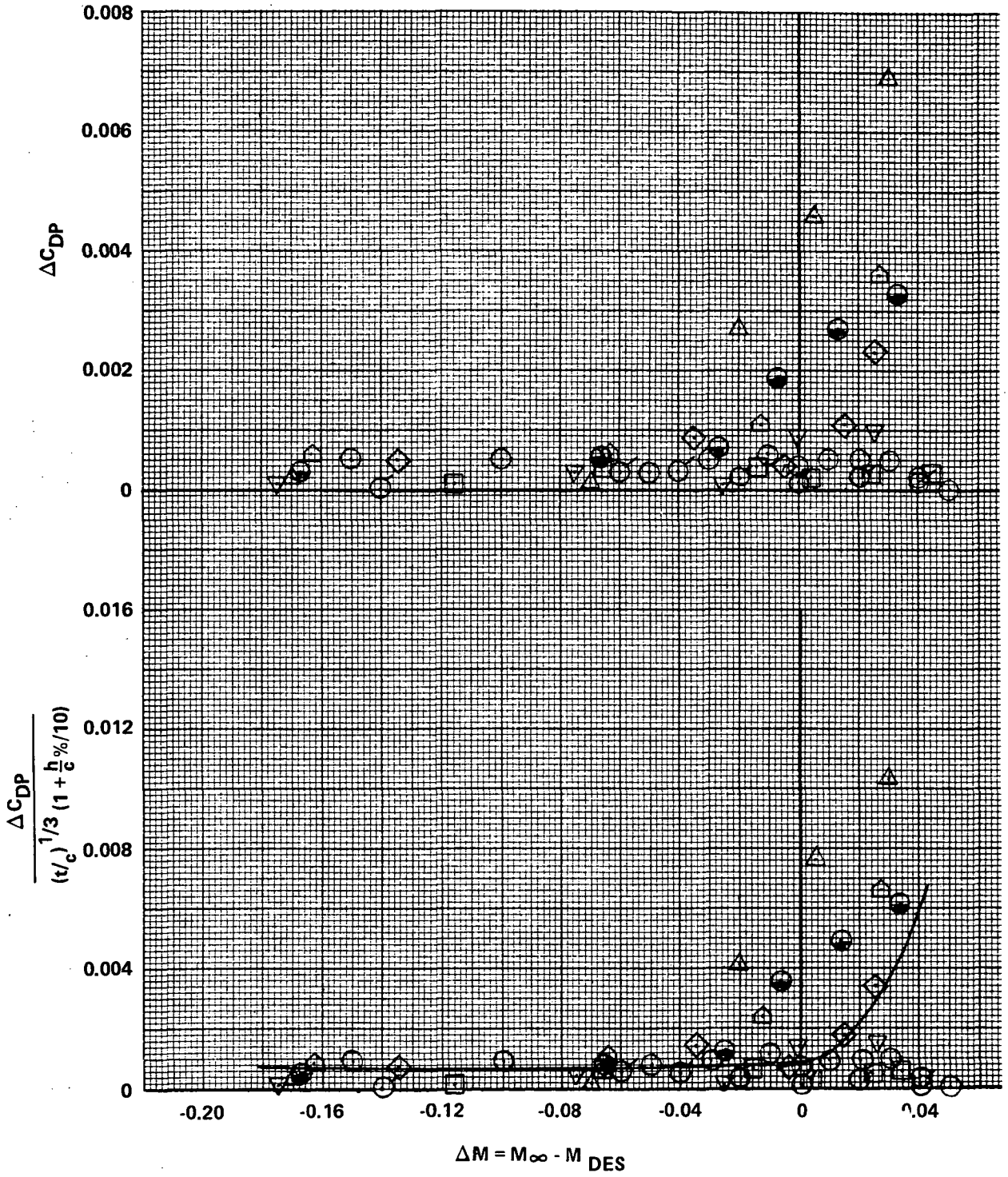

Figure 19. Incremental Pressure Drag Variation with Incremental Mach Number from Mach Design $\Delta C_L = -0.40$

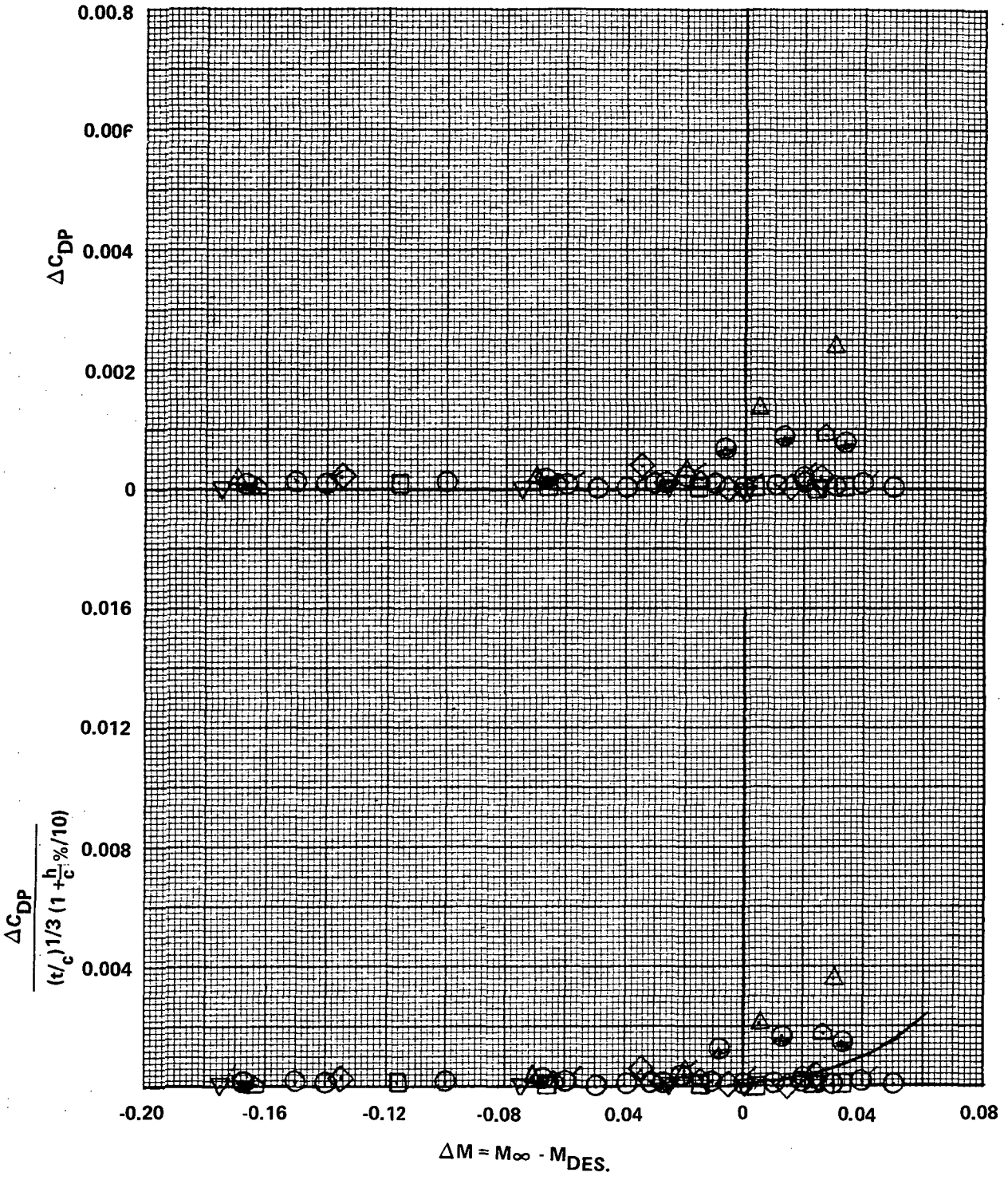

Figure 20. Incremental Pressure Drag Variation with Incremental Mach Number from Mach Design - ΔC_L = -0.30

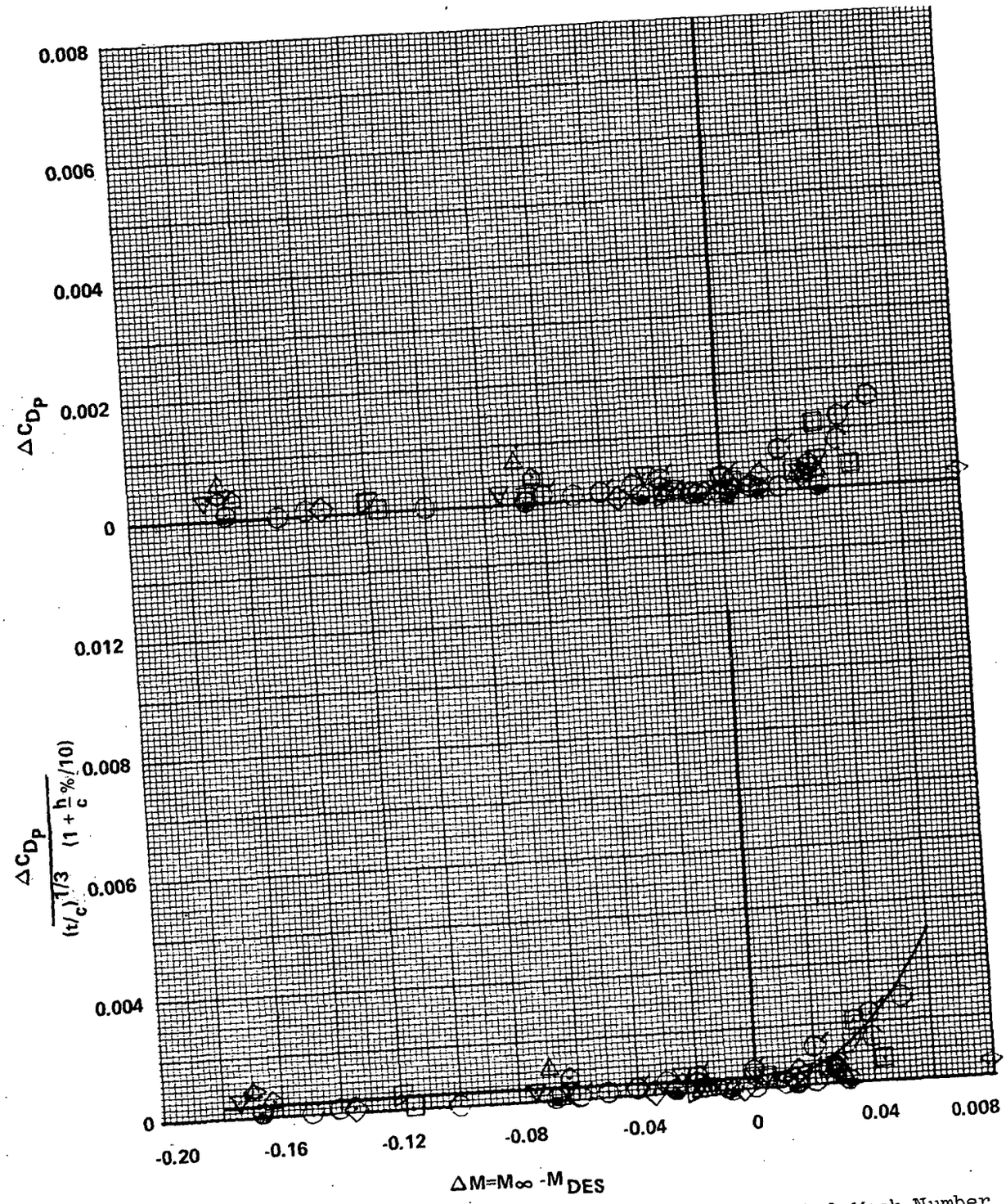

Figure 21. Incremental Pressure Drag Variation with Incremental Mach Number from Mach Design $-\Delta C_L = -0.20$

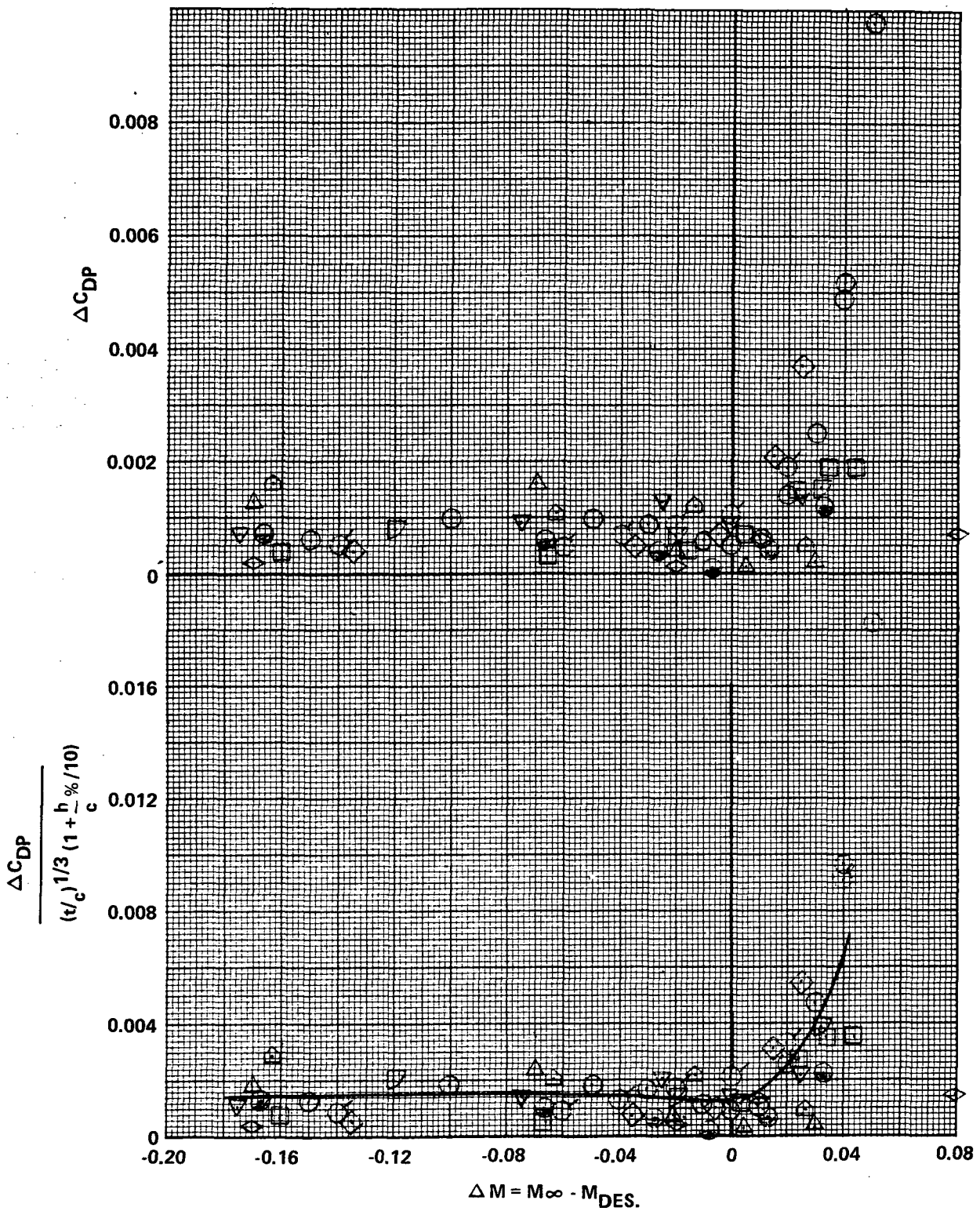

Figure 22. Incremental Pressure Drag Variation with Incremental Mach Number from Mach Design - ΔC_L = -0.10

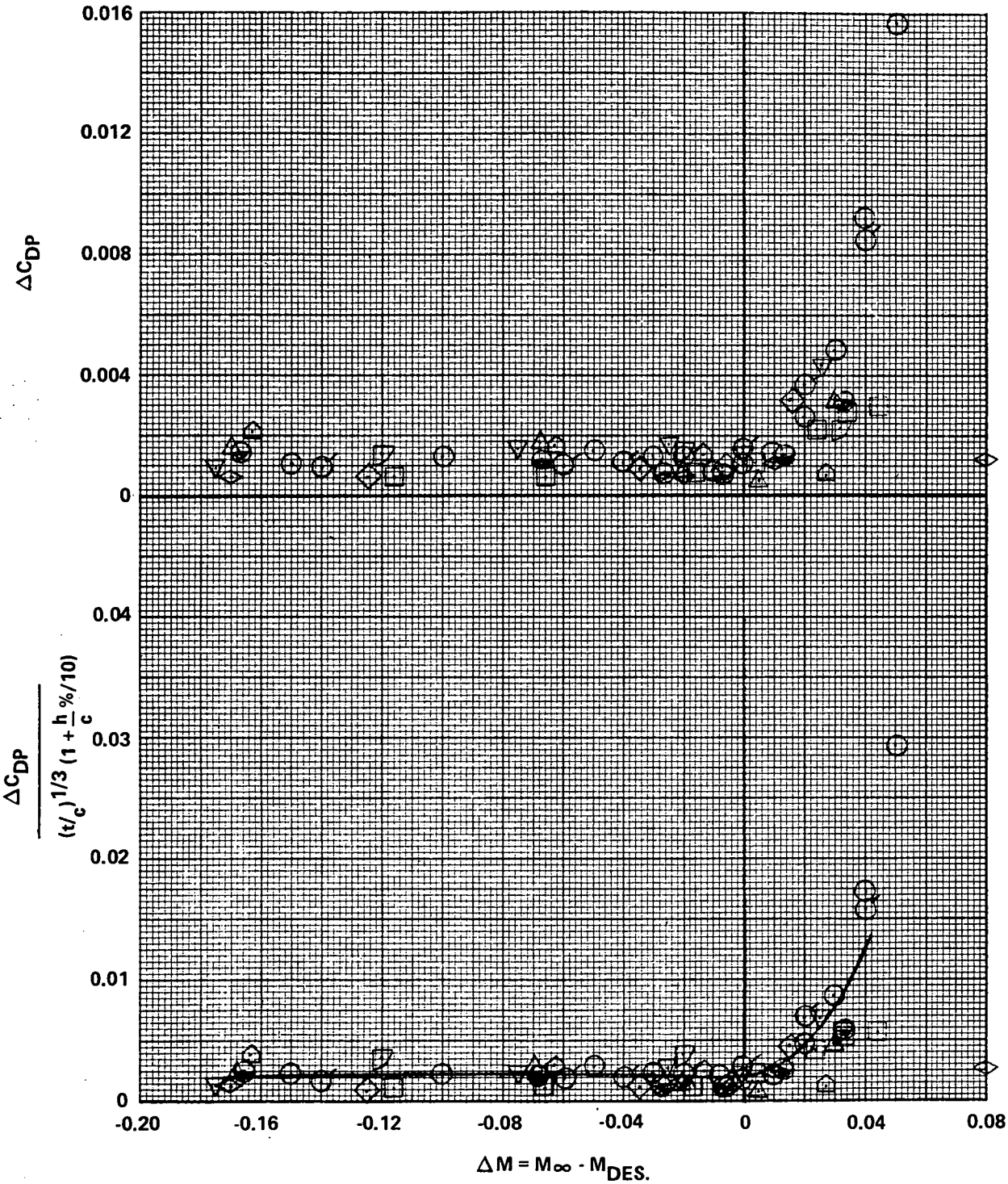

Figure 23. Incremental Pressure Drag Variation with Incremental Mach Number from Mach Design $-\Delta C_L = -0.05$

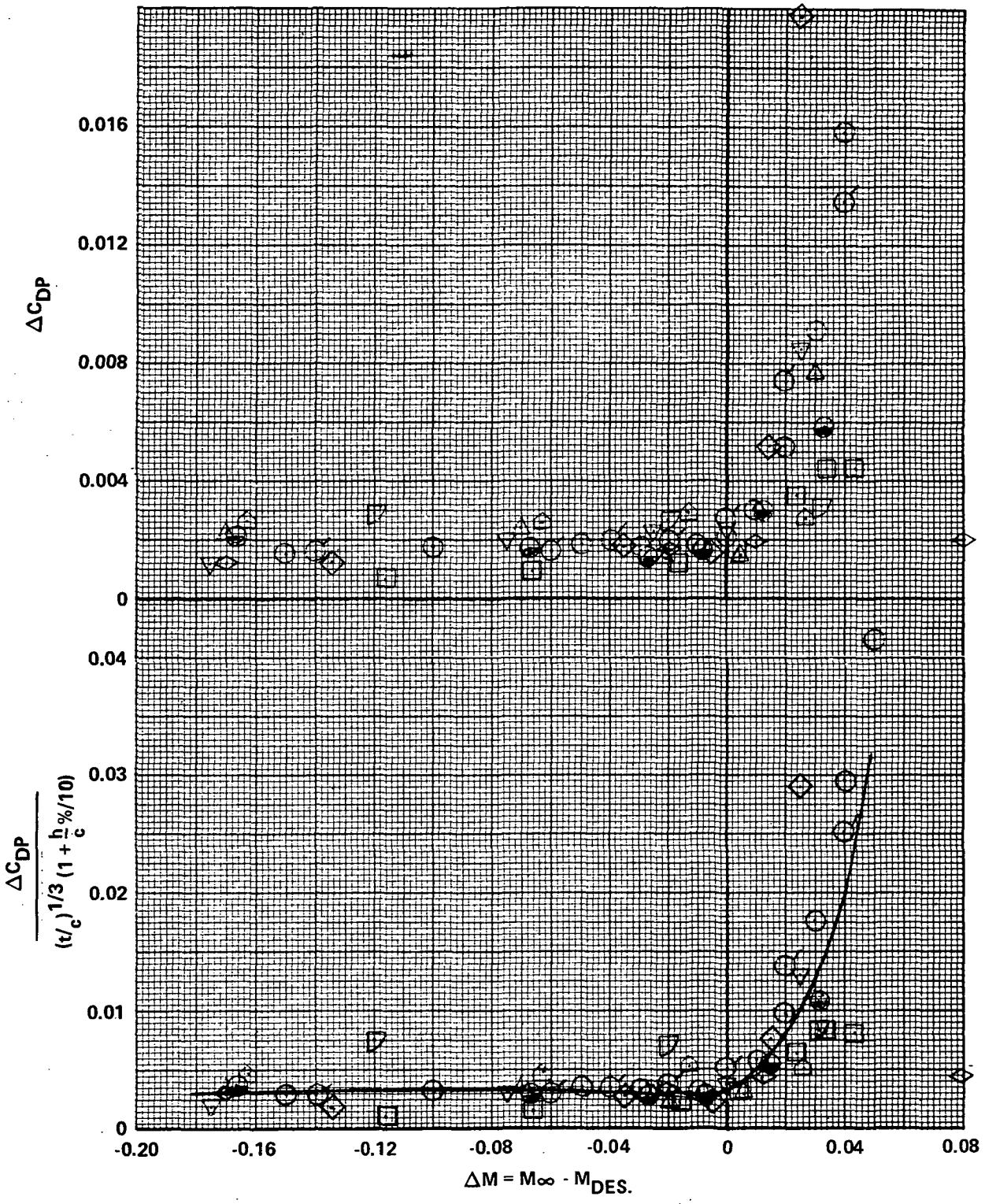

Figure 24. Incremental Pressure Drag Variation with Incremental Mach Number from Mach Design - $\Delta C_L = 0$

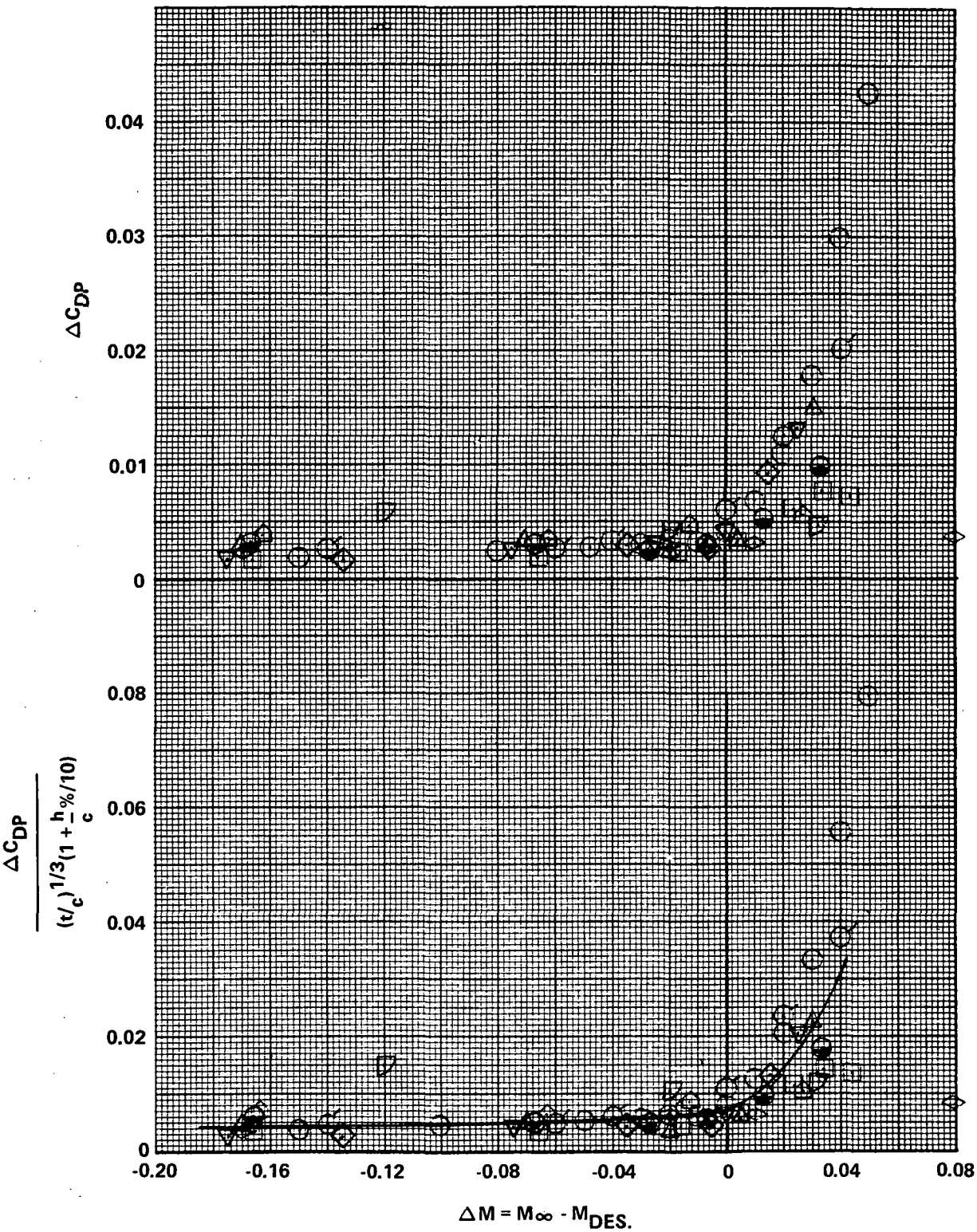

Figure 25. Incremental Pressure Drag Variation with Incremental Mach Number from Mach Design $-\Delta C_L = +0.05$

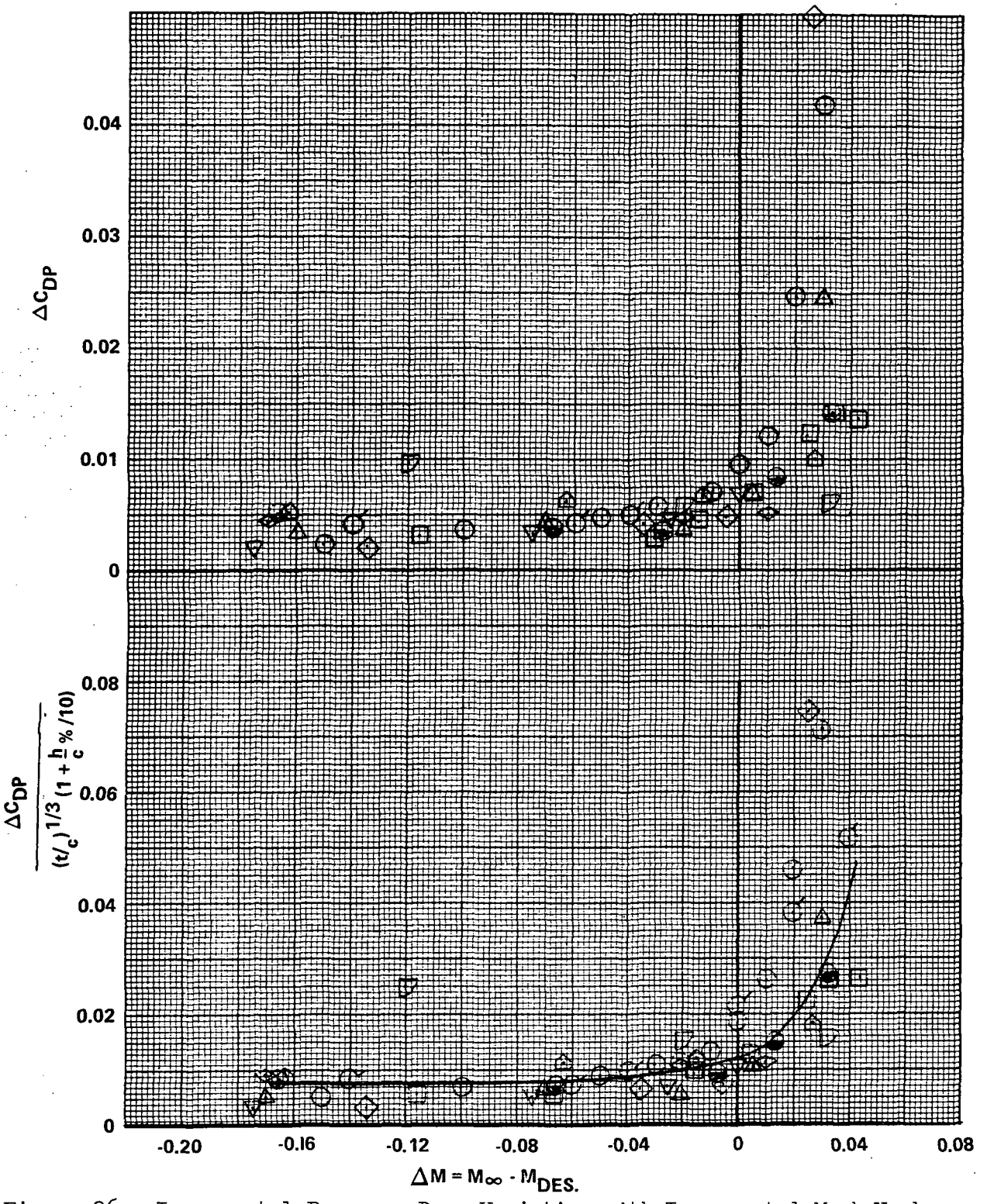

Figure 26. Incremental Pressure Drag Variation with Incremental Mach Number from Mach Design $-\Delta C_L = +0.10$

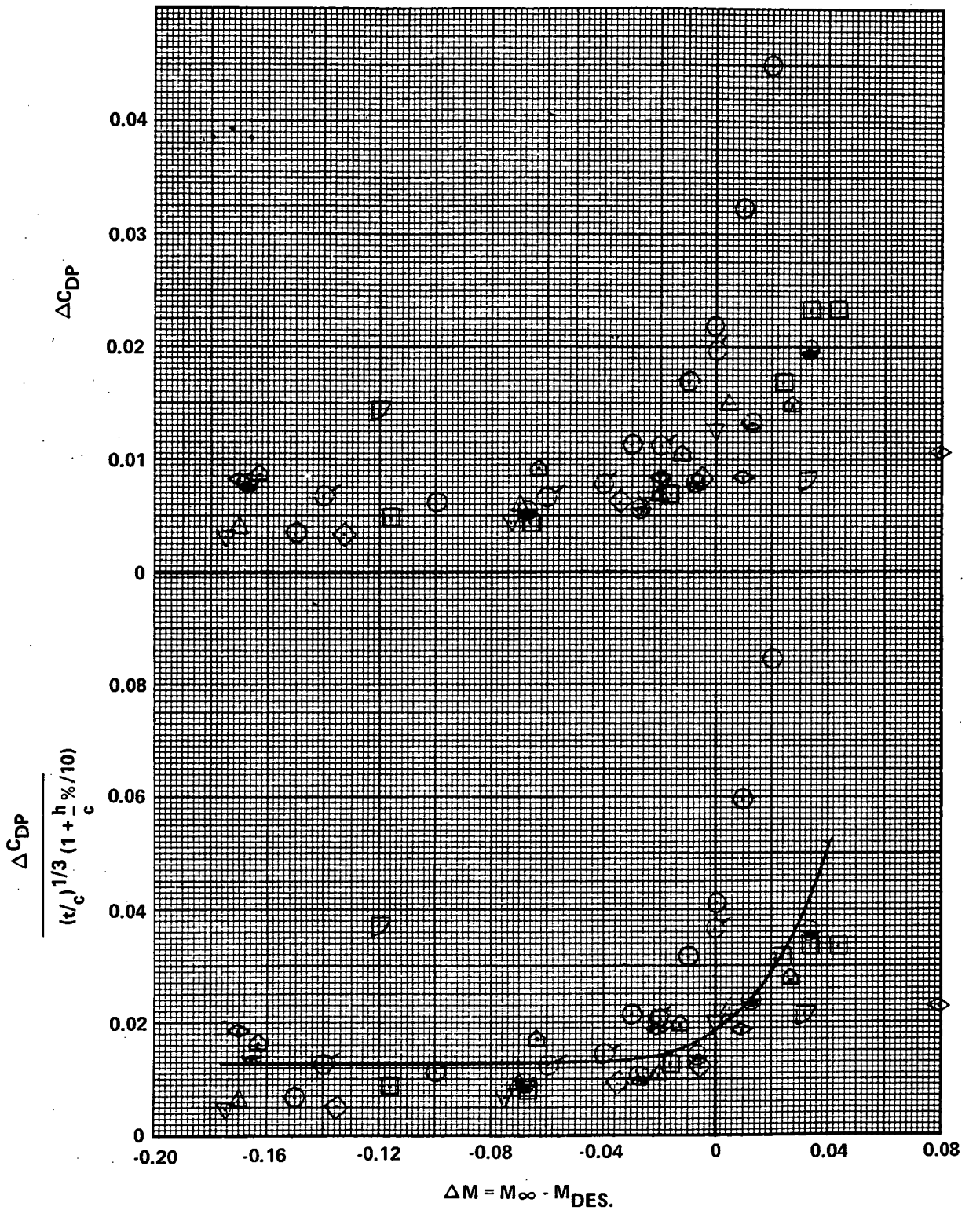

Figure 27. Incremental Pressure Drag Variation with Incremental Mach Number from Mach Design - $\Delta C_L = +0.15$

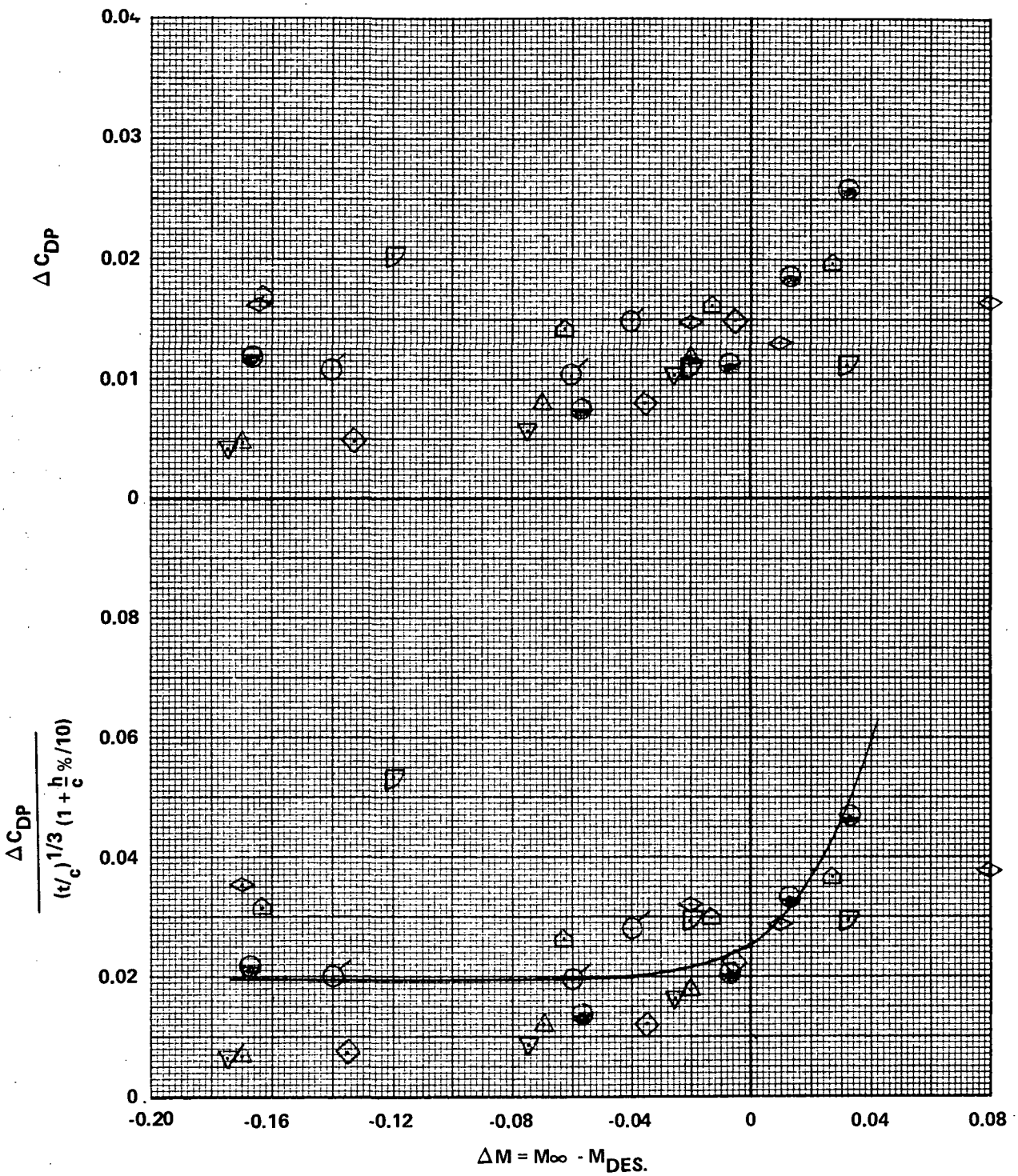

Figure 28. Incremental Pressure Drag Variation with Incremental Mach Number from Mach Design $-\Delta C_L = +0.20$

scatter above. Again, the correlating factors suggested in NACA TR 1253, i.e., $(t/c)^{1/3}$ and camber h/c %, were employed to adjust the data sets for varying geometries (lower curve, Figure 24). Again the correlation is improved up to design Mach number with increasing data scatter above.

Around M_{Design}, grouping of the data pinpoints the desirable reduction in pressure drag evidenced from the 2-D tests noted on Figure 16. Figures 19 through 21 and 25 through 28 present both uncorrected and adjusted ΔC_{D_p} for ΔC_L's ranging from -0.40 to +0.20. (Note scale changes.) At a $\Delta C_L = -0.40$, Figure 19, and ΔM's above M_{Design} the effects of camber do not appear to be sufficiently accounted for by the h/c correction. The deviation of the W_4 data may be attributable to lower surface shocks and separation which was also evidenced in the Mach divergence characteristics of Figure 7 through 14. It should be pointed out, however, the a $\Delta C_L = -0.40$ represents a very low lift coefficient, i.e., 0 to +0.15, for the majority of the data sets and is seldom a lift coefficient corresponding to any flight phase of a transport. Figure 29 summarizes the ΔC_{D_p} faired variation with ΔM for ΔC_L's of -0.40 to +0.20.

4.5 Zero Lift Pitching Moments

Large negative C_{m_o} has been associated with advanced airfoil design practices and raises a concern that this might impose significant trim penalties.

On Figure 30 the variation of C_{m_o} with ΔM indicates a fairly constant value up to M_{Design} with some reduction above. The upper curve of Figure 30 indicates at M_{Design} that C_{m_o} correlates as might be expected with camber.

For preliminary design purposes, the assumption may be made that under trimmed conditions and for configurations incorporating aft tails, the wing must carry an additional lift equal to but opposite in sign to the tail down load. This increment in lift is $\Delta C_L = -C_{m_o}/\frac{\ell t}{c}$. At the design C_1 and Mach number for a 10% thick airfoil cambered 1.6% with an $\frac{\ell t}{c} = 3.0$, the wing will carry approximately 3 counts of trim drag to provide extra ΔC_L. The increased down wash at the tail and resulting angle of the tail lift vector may subtract from this trim drag; however, this increment would be too difficult to predict in the normal preliminary design study.

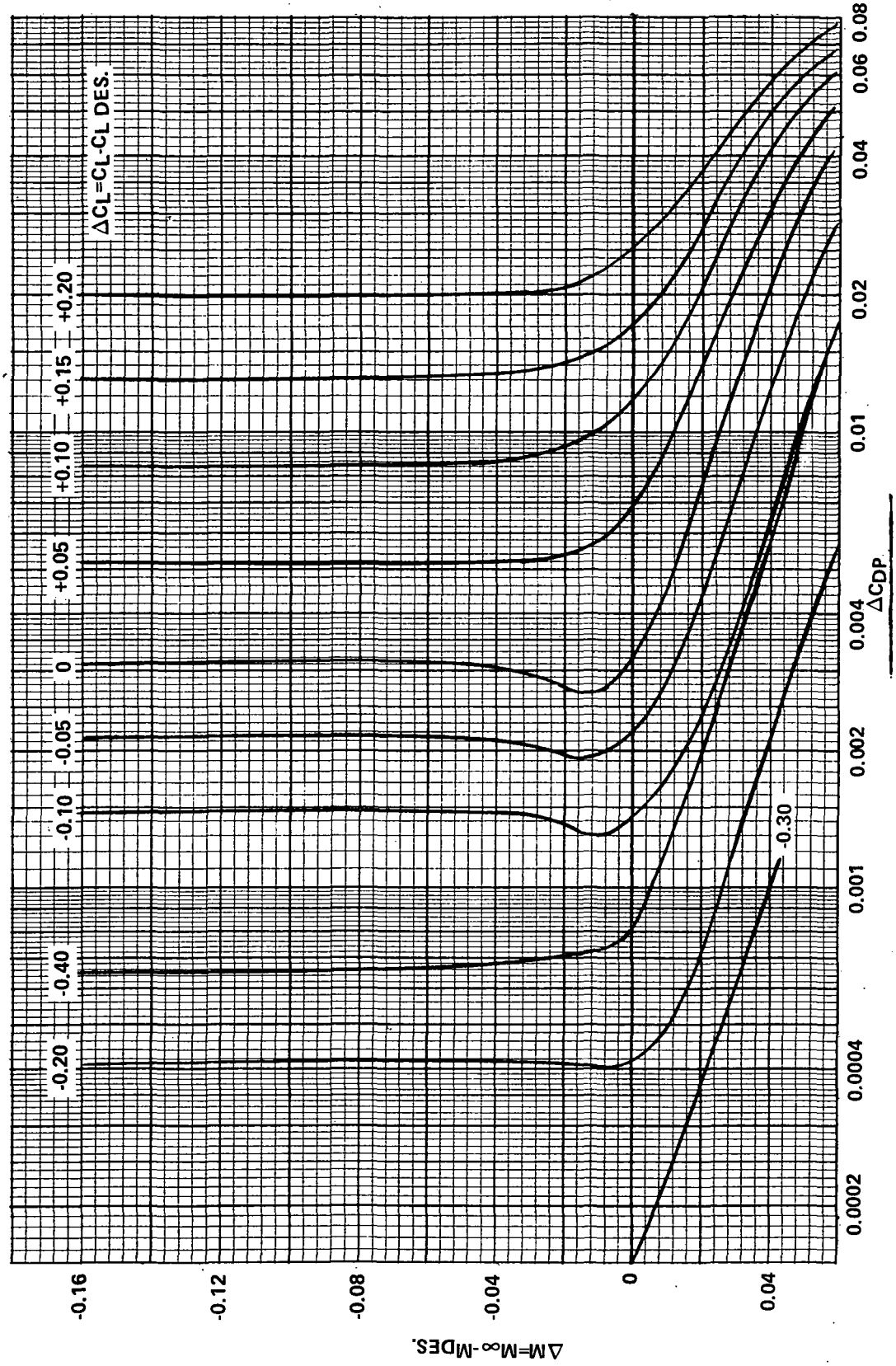

Figure 29. Fairing of Incremental Pressure Drag - Summary

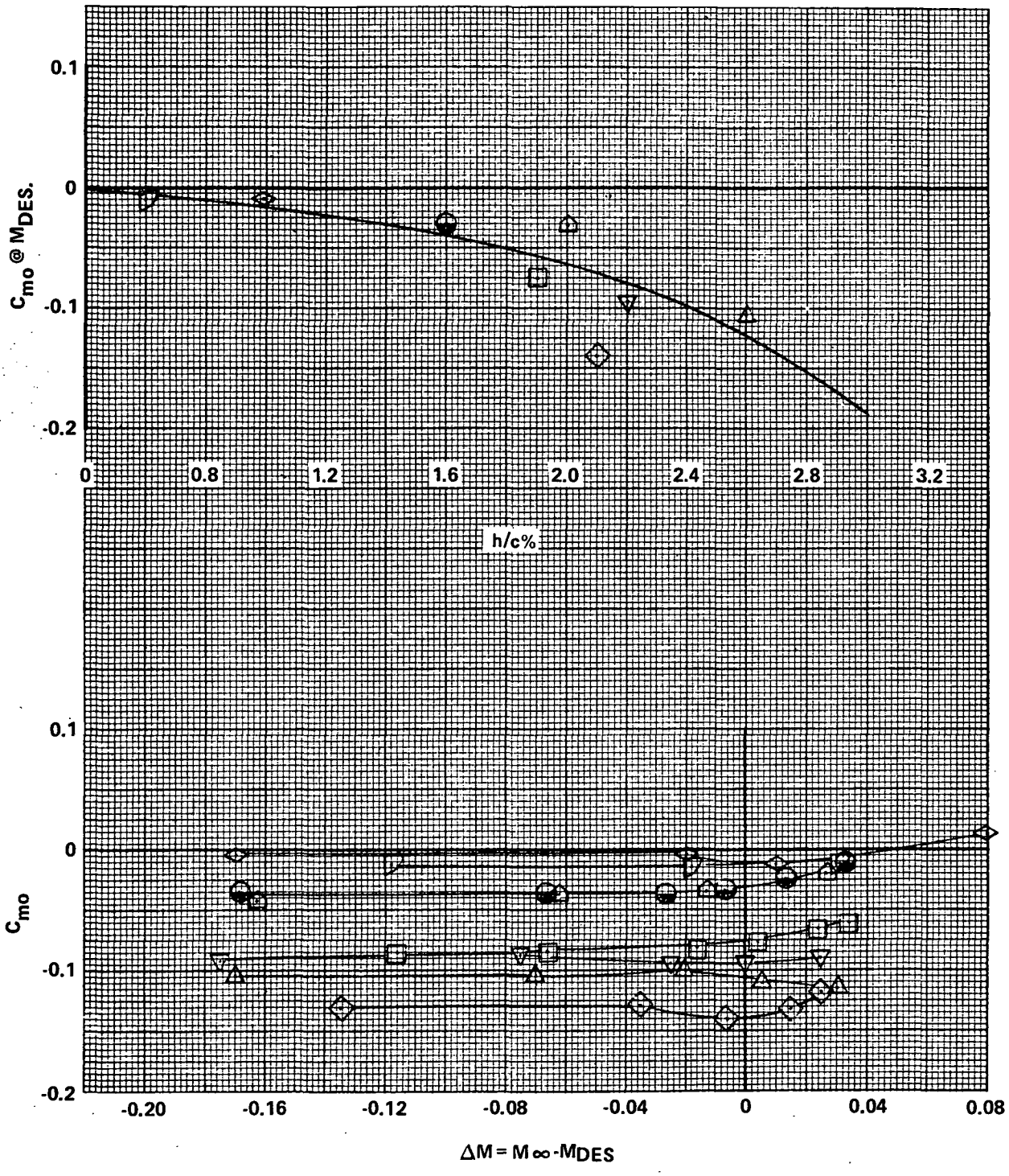

Figure 30. Zero Lift Pitching Moment Variation with Camber and Incremental Mach Number from Mach Design

4.6 Buffet Onset

For purposes of this discussion, buffet onset is defined as the break in axial force versus lift coefficient or for those tunnel models employing root strain gages as the lift coefficient corresponding to a rapid rise in the RMS root bending moments.

A systematic buffet investigation was conducted by NASA and results were reported in NASA TN 5805. The wings of this test series employed 63, 64, 65, 45°, and aspect ratios 4 to 6. Previous buffet correlation attempts by Lockheed employing the data of this report had shown a reasonably good correlation of buffet onset with $C_{L_{Design}}$. Some buffet data were obtained on the advanced airfoil designs employed in this study, and a comparison was made (Figure 31) to compare buffet characteristics of conventional and advanced airfoil sections.

The variation of the advanced W_7 and W_{10} wing/body C_L Buffet versus ΔM exhibits a vastly different character. W_{10} exhibits the same variation with ΔM as a conventional airfoil, while W_7, which is more representative of actual flight experience, has a very different variation. The reason for these differences in buffet onset variation are not understood and certainly additional effort is required in buffet prediction techniques.

4.7 Airfoil Section - Pressure Drag - Form Factor

The friction drag buildup process for preliminary design configurations will generally involve knowledge of both the wing and body form factors as a function of wing section and body geometry.

$$C_{D_o} = C_f \times F.F \frac{S_{Wet}}{S_{Ref}}$$

On Figure 32 this form factor has been developed for advanced airfoil sections and also presents data for a NACA 65 series section for reference. The parameter $F.F = C_{D_o}/2\ C_f$ is simply the 2-dimensional minimum section drag coefficient divided by twice the flap plate skin friction coefficient at the test Reynolds number. The factor of 2 accounts for both upper and lower surfaces. The data, from top to bottom on Figure 32, is from 2-D tests on a

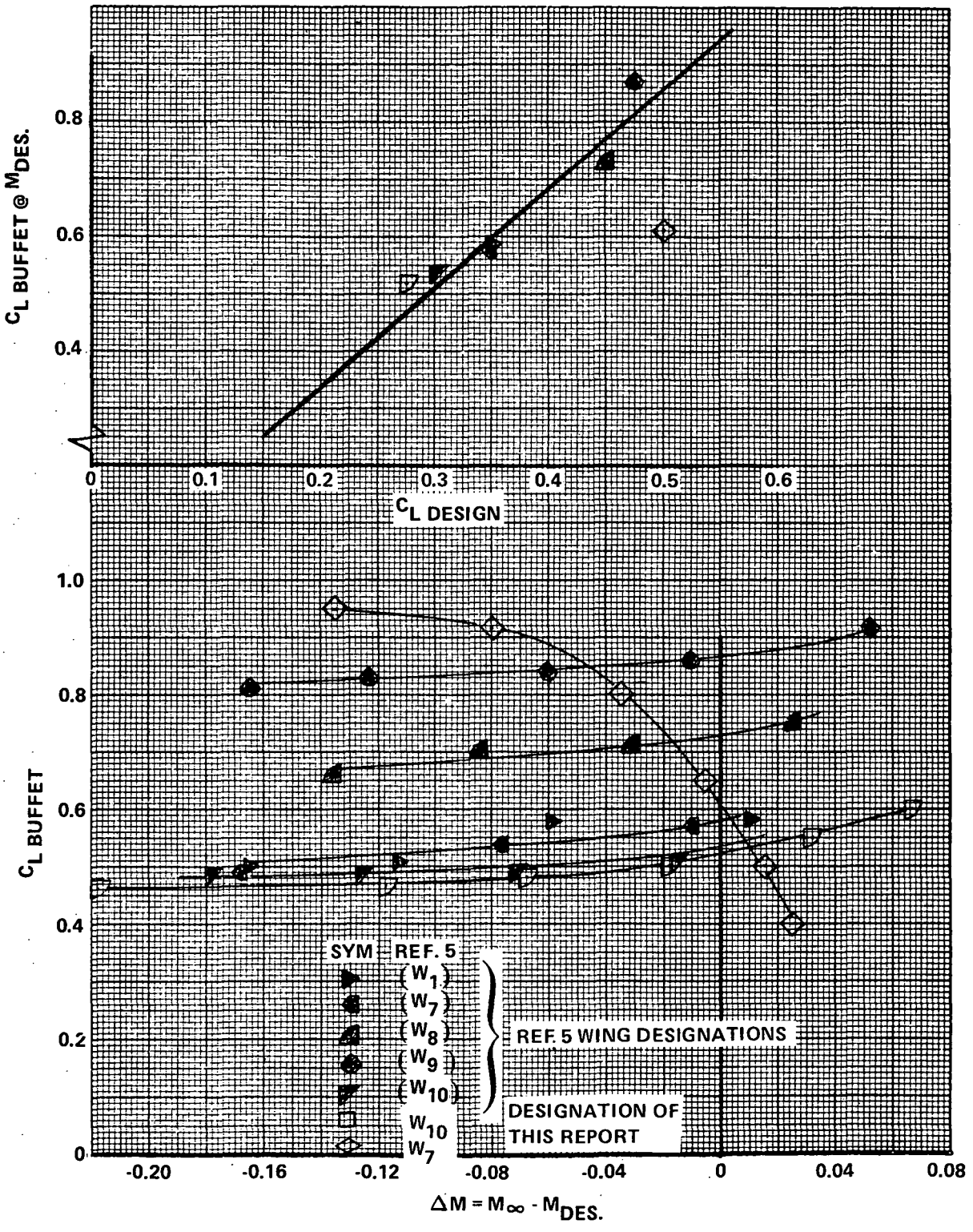

Figure 31. Lift Coefficient for Buffet Onset

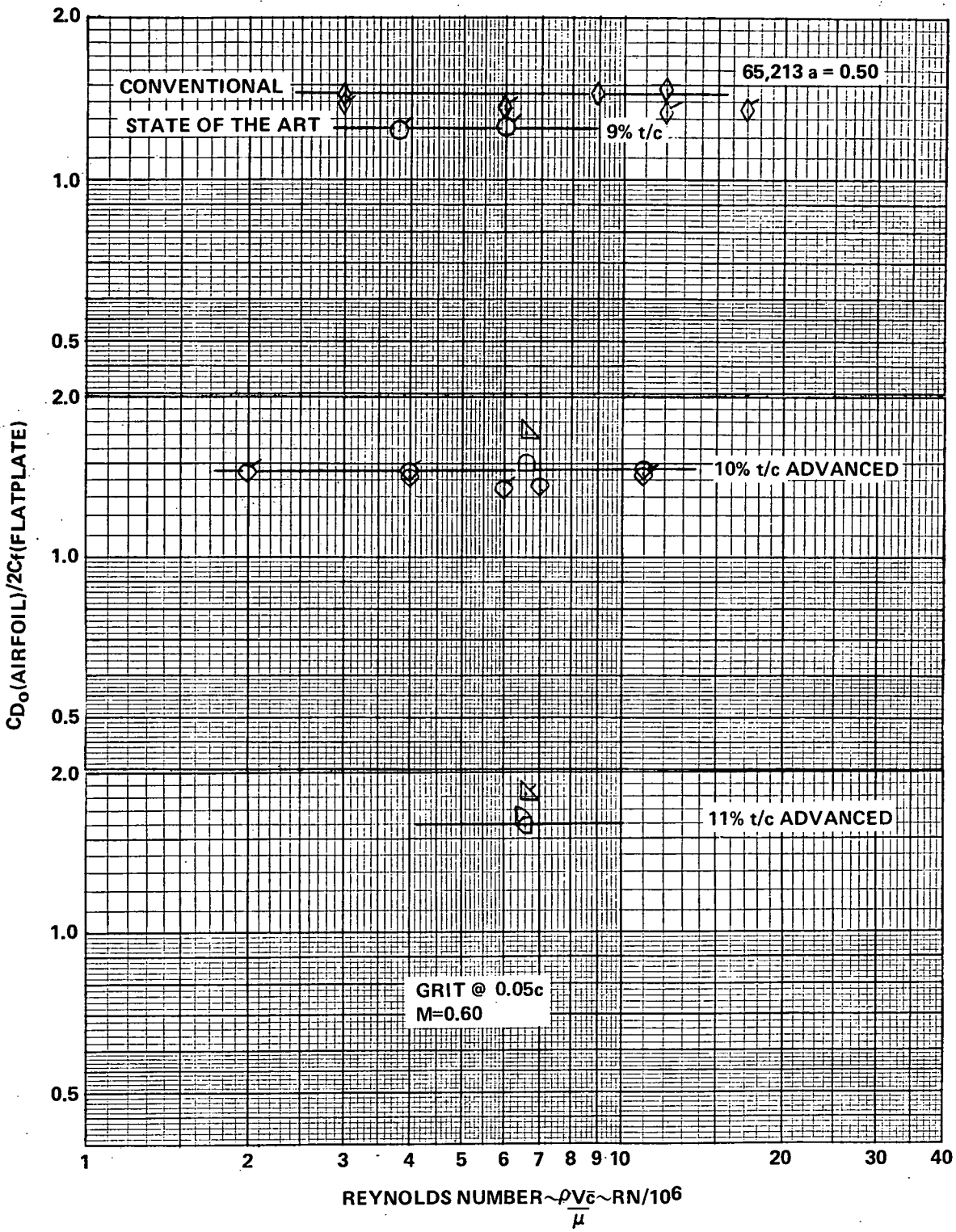

Figure 32. Conventional State of the Art, and Advanced Airfoil Section - Ratio of Minimum Drag to Theoretical Skin Friction Drag

conventional NACA 65, 213 a = 0.5 airfoil, 9 percent thickness ratio state-of-the-art airfoil, and 10 percent and 11 percent thickness ratio advanced airfoils, respectively. The flagged versus unflagged symbols represent same model tested in two different facilities. On Figure 33, the average fairing of $C_{D_o}/2\ C_f$, is shown as the form factor versus the section thickness ratio. The NACA 65 series airfoil results confirm the variation given in the RAS data sheets and USAF DATCOM. At a thickness ratio of 10 percent the advanced airfoil appears to carry an approximate 10 percent increased subsonic pressure drag over the conventional airfoil sections. Subsequent advanced airfoil test results (data unpublished) of 2nd generation designs are included on Figure 33. Additional information on 2nd generation airfoils is included in Appendix A.

Figures 34, 35, and 36, which were not derived as part of this study, are presented as part of the total drag buildup procedure to be discussed in a later section.

5. DRAG BUILDUP PROCEDURES

The correlation techniques developed in the previous sections can now be combined to define a systematic procedure for the total drag buildup of arbitrary transonic aircraft incorporating advanced airfoil wing sections.

The geometric characteristics of an example twin-engine transonic transport are itemized on Figure 37 and will be used to demonstrate the drag buildup process. It should be emphasized here that, any interference or compressibility drag of nacelles or tails, and incremental drag due to inlets, antennas, or other proturbences, is an additive drag element that must be derived from other sources.

The initial step in the drag buildup procedure, graphically described on Figure 38, involves the determination of the aircraft design lift coefficient and design Mach number. The derivation of $C_{L_{Design}}$ involves the determination of the minimum pressure drag at M = 0.60 at the nominal mission altitude. For this example 30,000 ft has been selected. Aircraft component drag buildup is on Figure 38 along with those text figures required for the computation. Using this computed $C_{D_{pmin}}$, percent wing camber, and wing aspect ratio; $C_{L_{Design}}$ is

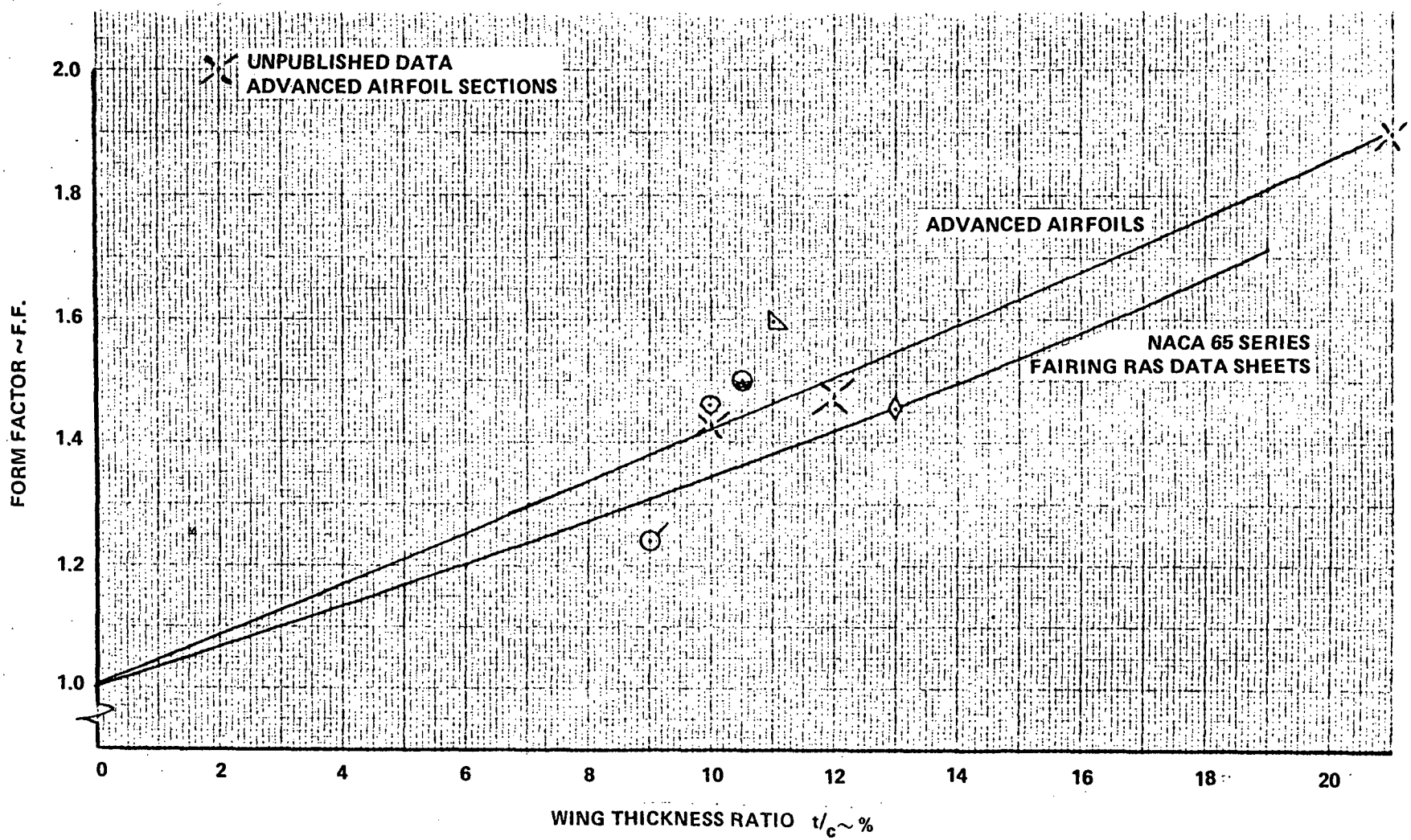

Figure 33. Wing Section Form Factors

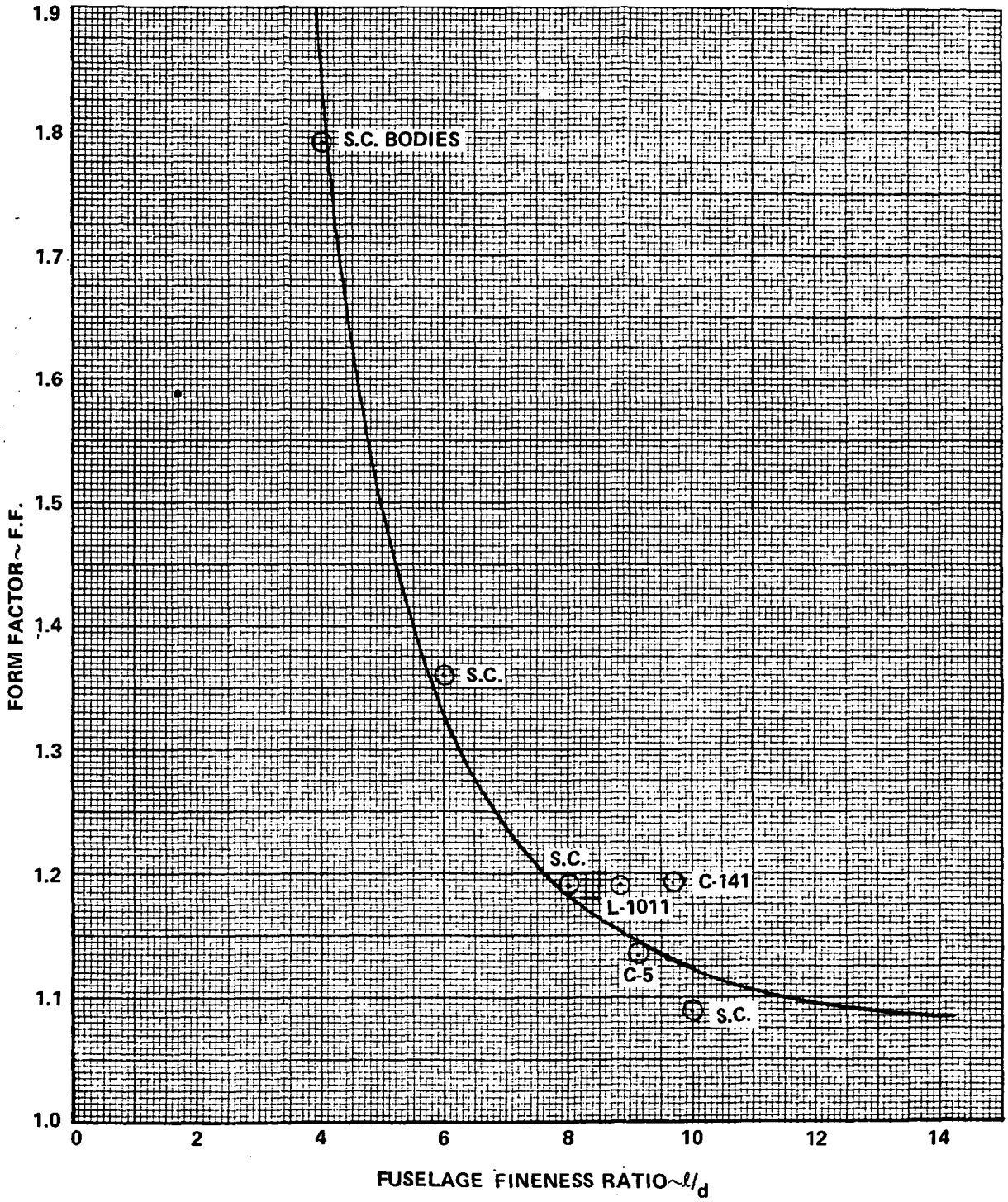

Figure 34. Body Form Factors

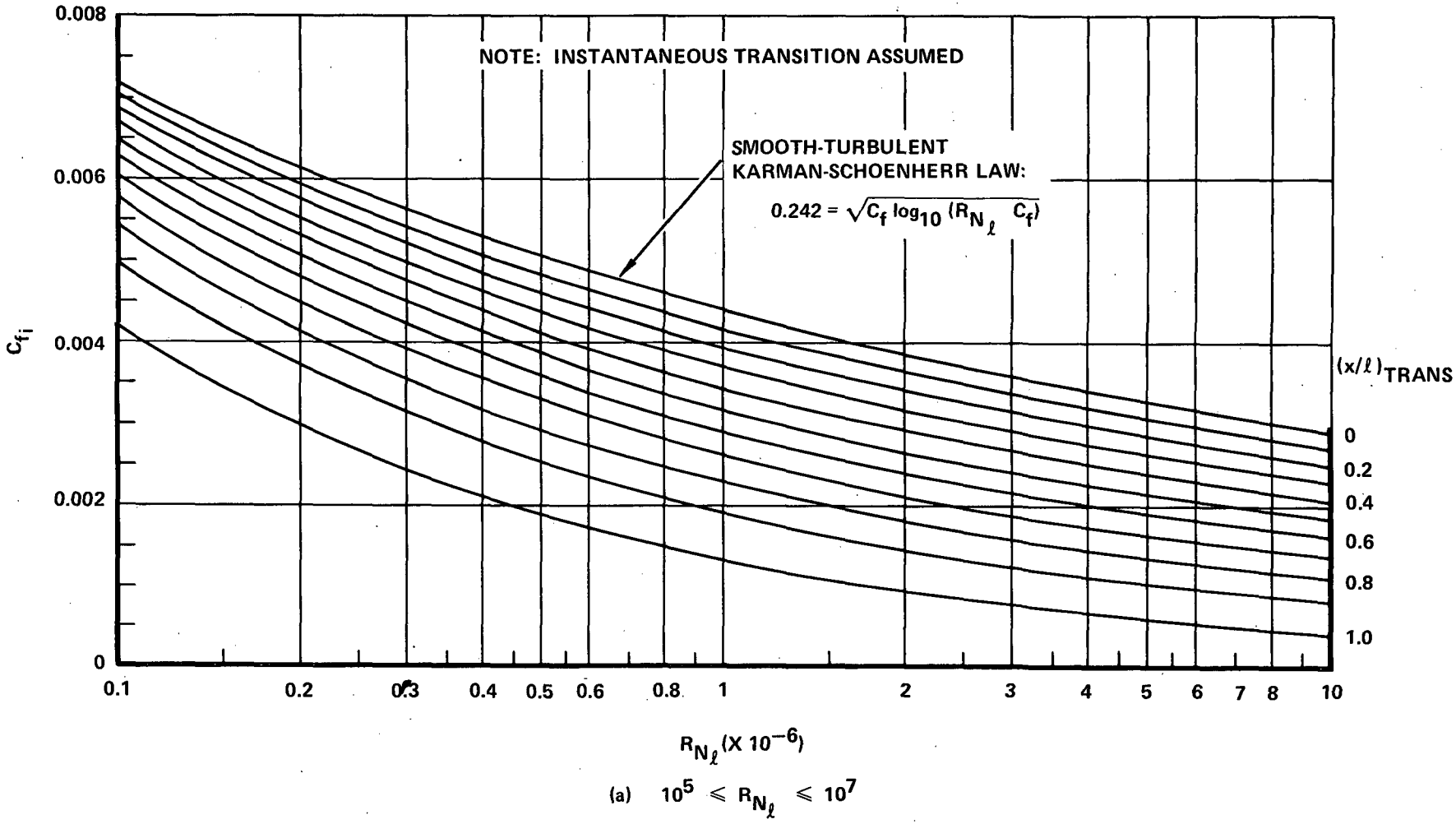

(a) $10^5 \leq R_{N_\ell} \leq 10^7$

Figure 35. Variation of Flat Plate Incompressible Skin Friction Coefficient with Reynolds Number (Sheet 1 of 2)

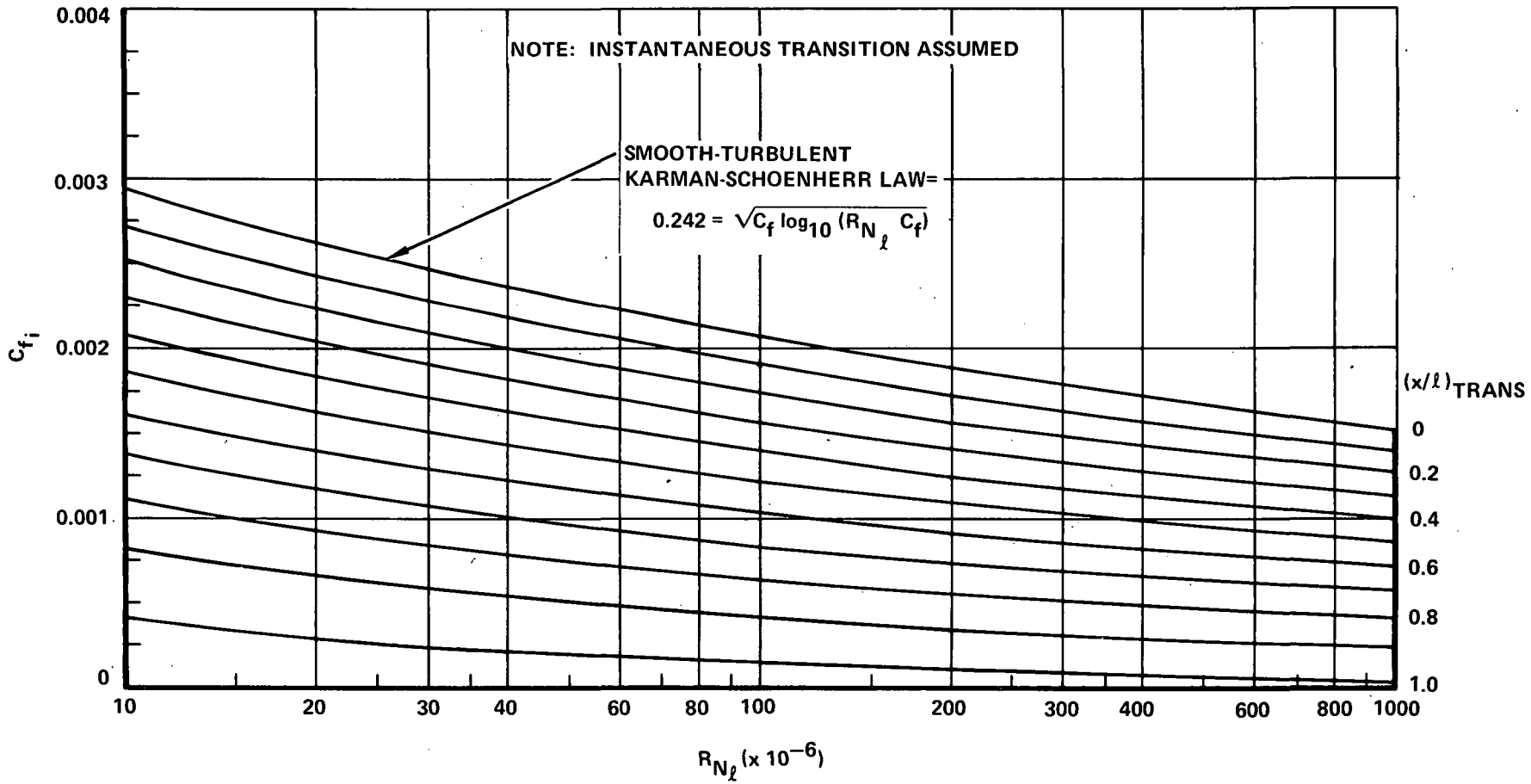

(b) $10^7 \leqslant R_{N_\ell} \leqslant 10^9$

Figure 35. Variation of Flat Plate Incompressible Skin Friction Coefficient with Reynolds Number (Sheet 2 of 2)

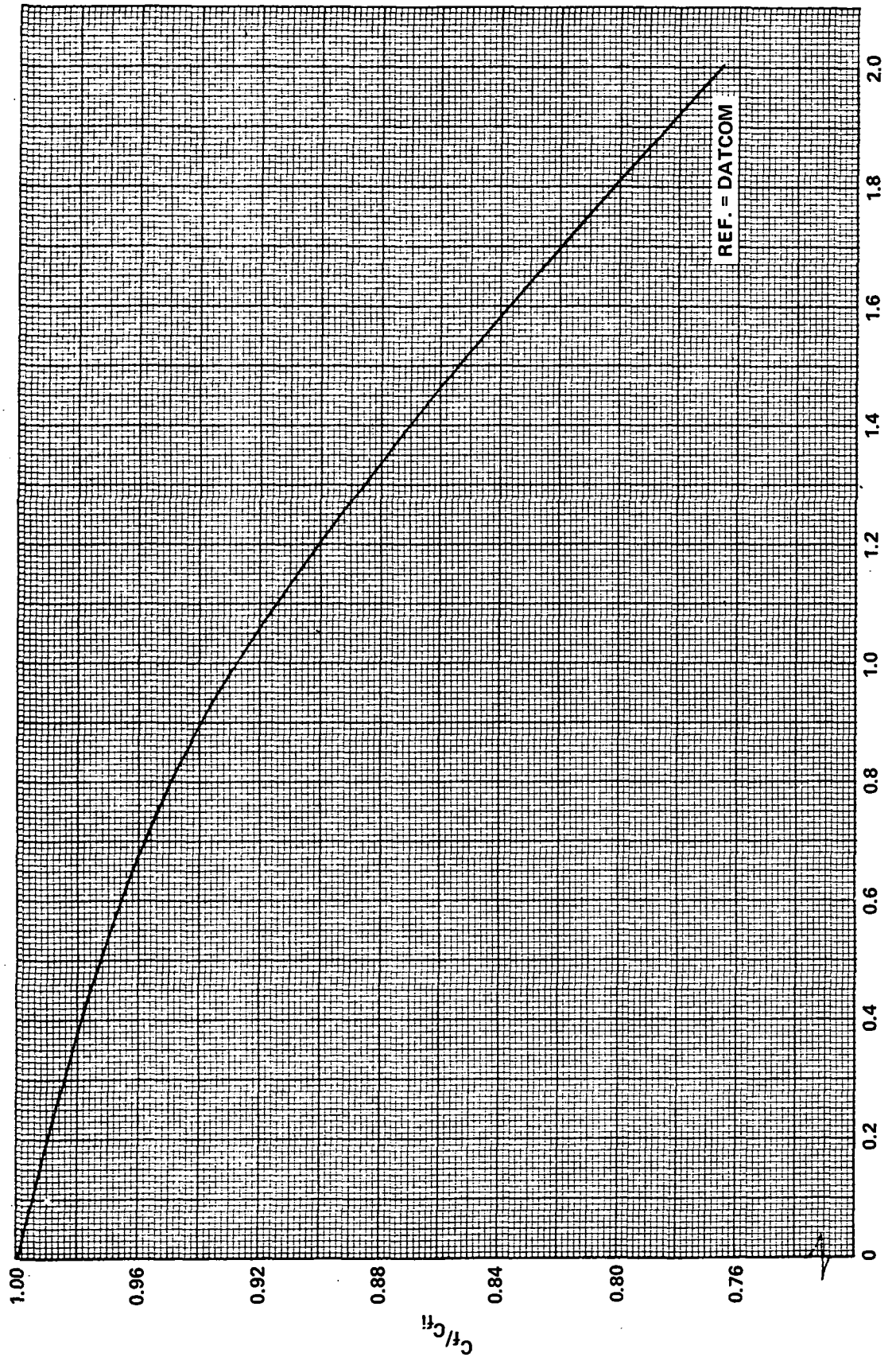

Figure 36. Compressibility Correction to Skin Function Coefficient

AIRCRAFT GEOMETRY	
AR	= 7.0
$\Lambda_{c/4}$	= 35°
λ	= 0.30
$(t/c)_{eff}$	= 13.0%
h/c	= 1.6%
$\ell_{t/c}$	= 2.7
S_{REF}	= 3456 ft^2

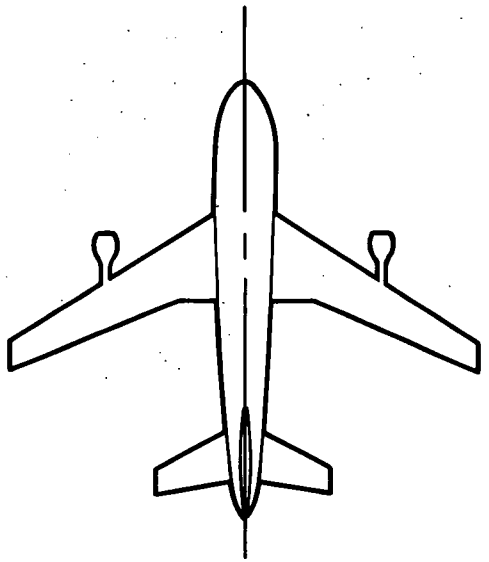

COMPONENT	REF LENGTH ft	S_{WET} ft^2	S_{WET}/S_{REF}	ℓ/d	t/c %
FUSELAGE	177	8483	2.455	9	–
WING	24.3	6100	1.765	–	13.0
HORIZONTAL	17.6	1970	0.570	–	9.0
VERTICAL	17.0	752	0.218	–	9.0
NACELLE	14.5	658	0.191	12	–
PYLON	21.9	261	0.076	–	8.0

Figure 37. Example Twin Engine - Advanced Transonic Transport Geometry

determined. Computation of Mach design involves determination of the 2-dimensional equivalent divergence Mach number for the wing section at the design lift coefficient. This $M_{D\ 2\text{-}D}$ is then corrected for wing aspect ratio and sweep to obtain the 3-dimensional drag divergence Mach number, which, at $C_{L_{Design}}$, is equivalent to M_{Design}.

At this point, the lift coefficient and Mach number have been determined for best cruise. The total drag polars can now be defined for any Mach-Altitude condition; however, for purposes of this example buildup, the best cruise Mach number is chosen. Note that if other than best cruise altitude is selected for off design polar determination, minimum pressure drag must be computed based on the Reynolds number and C_f associated with that altitude Mach number condition. In the final aircraft preliminary design sizing process, off design Mach number polars would also be investigated to assure an airframe-propulsion system match for all mission segments.

The next step in the drag buildup procedure involves the computation of the minimum pressure drag, the induced drag, compressibility drag, pressure drag, and trim drag at the design Mach number of 0.85 and altitude of 30,000 ft. These computations are shown on Figure 38 in tabular form. Most of the steps are self evident. Column (3) is equivalent to the trimmed $C_L = W/q\ S_{REF}$. The ΔC_L due to trim is an additional lift which must be carried on the wing to balance the tail down load required to trim the wing pitching moment. For this example a zero static margin was selected; hence, the required trim is only that amount necessary to overcome the negative c_{m_o} of the wing = -0.04. Perhaps, with advancement in active control technology, this trim requirement on resulting drag can be reduced to zero at the design conditions. Column (6) is the incremental lift that the wing is experiencing from the design lift coefficient. The remaining computations are relatively straightforward, with the possible exception of (17) and (20). In determining the ΔC_{D_p}, the parameter presented on Figure 29 must be crossplotted versus ΔC_L at $\Delta M = 0$ to allow interpolation of the pressure drag contribution at the ΔC_L represented by column (6). The final drag represented by the summation performed for column (20) must be plotted versus the $C_L = W/qs$ of column (3) to represent the trimmed aircraft polar. For determination of drag polars at other Mach-Altitude conditions, the same process is followed, i.e., computation of columns (1) through (20), respectively.

SELECT

AIRCRAFT GEOMETRY

SEE FIGURE 37

COMPUTE $C_{D_{P\ MIN}}$

M = 0.60 @ 30K

FIGS. 33&34

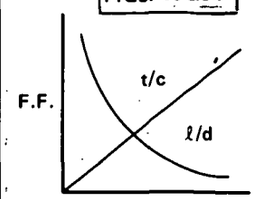

FIG. 35

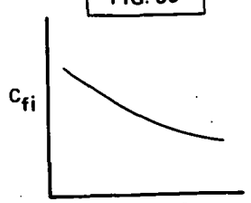

FIG. 36

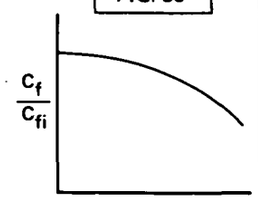

COMPONENT	RN/10^6	C_{fi}	F.F.	S_{WET}/S_{REF}	C_f/C_{fi}	$\Delta C_{D_{P\ MIN}}$
FUSELAGE	302	0.00175	1.15	2.455	0.966	0.0049
WING	41	0.00225	1.60	1.765		0.0061
HORIZONTAL	30	0.00240	1.31	0.570		0.0017
VERTICAL	29	0.00240	1.31	0.218		0.0007
NACELLE	25	0.00245	1.09	0.191		0.0005
PYLON	37	0.00230	1.28	0.076		0.0002
ROUGHNESS & LEAKAGE (NOMINAL 6%)			See Note Section 4.7			0.0009

$(RN/FT = 1.71 \times 10^6) \Delta C_{D_{P\ MIN}} = C_{fi} \times F.F. \times \frac{S_{WET}}{S_{REF}} \times \frac{C_f}{C_{fi}}$ TOTAL $C_{D_{P\ MIN}} = 0.0150$

COMPUTE $C_{L\ DESIGN}$

FIG. 15

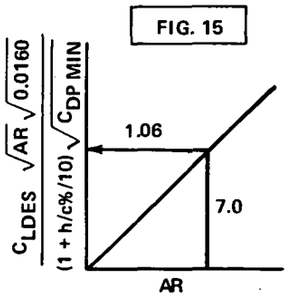

$$C_{LDES} = \frac{1.06 \times \sqrt{0.0150} \times 1.16}{\sqrt{7.0}\ \sqrt{0.0160}}$$

$C_{LDES} = 0.453$

COMPUTE M_{DESIGN}

FIGS. 7 - 14

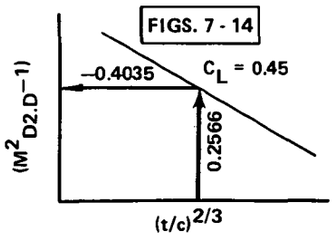

&

TABLES II & III

TABLE I

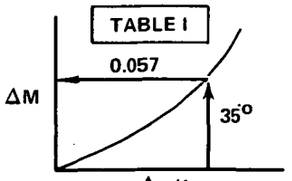

TABLE I

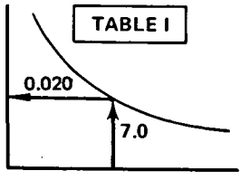

$M_{DES} = M_{D3\text{-}D} = M_{D2\text{-}D} + \Delta M_\Lambda + \Delta M_{AR}$

$M_{DES} = 0.85 = 0.772 + 0.057 + 0.020$

① $C_{L_{DES}}$	② M_{DES}	③ $C_{L_{TRIM}}$	④ $\Delta C_{L_{TRIM}}$	⑤ $C_{L_{WING}}$	⑥ $\Delta C_{L_{WING}}$	⑦ M_∞ / h
0.45	0.85	0.10 0.20 0.30 0.40 0.435 0.500 0.550 0.600 (SELECT)	0.015 FIG. 30 FIG. 37 $\Delta C_L = \frac{-C_{m_o}}{\ell_{v/\bar{c}}}$ Section 4.5 $\frac{(-)-0.04}{2.7}$ ③ + ④	0.115 0.215 0.315 0.415 0.450 0.515 0.565 0.615	−0.335 −0.235 −0.135 0.035 0 0.065 0.115 0.165 ⑤ − ①	0.85/30K (SELECT)

⑧ ΔM	⑨ $C_{D_{P\ MIN}}$	⑩ $CL^2/\pi AR$	⑪ $(1 + \frac{h}{c}/10)$	⑫ $(t/c)^{5/3}$	⑬ $(t/c)^{1/3}$	⑭ ⑪ X ⑫	⑮ ⑪ X ⑬
0	0.0148 @M=0.85	0.0006 0.0021 0.0045 0.0078 0.0092 0.0121 0.0145 0.0172	1.16	0.0334	0.5066	0.0388	0.588
$M_\infty - M_{DES}$		$\frac{⑤^2}{\pi AR}$	FIG. 37	TABLE III	TABLE III		

⑯ $\frac{\Delta C_{DC}}{(t/c)^{5/3}(1+\frac{h}{c}\%/10)}$	⑰ $\frac{\Delta C_{D_P}}{(t/c)^{1/3}(1+\frac{h}{c}\%/10)}$	⑱ ΔC_{D_C}	⑲ ΔC_{D_P}	⑳ ⑨ + ⑩ + ⑱ + ⑲ $C_{D\ TOTAL}$
0.067	0.00038 0.00033 0.0011 0.0025 0.0032 0.0083 0.0133 0.0197	0.0026	0.0002 0.0002 0.0006 0.0015 0.0019 0.0049 0.0078 0.0116	0.0182 0.0197 0.0225 0.267 0.0285 0.0344 0.0397 0.0426
FIG. 18 VS COL ⑧	FIG. 29 VS COL ⑥	⑯ X ⑭	⑰ X ⑮	PLOT VS COL ③

Figure 38. Drag Buildup Flow Diagram

FOLDOUT FRAME 1

FOLDOUT FRAME 2

6. 2-D AND 3-D COMPARISON OF COMPRESSIBILITY AND PRESSURE DRAG

The objective of this section is to establish an equivalence comparison between 2- and 3-dimensional compressibility and pressure drag which might permit (1) an assessment of an ultimate potential of advanced airfoil design practices, (2) indicate some of the penalties associated with applying 2-D characteristics to the 3-D wing, and (3) indicate a degree of data sensitivity to some of the major test variables.

On Figure 39 the fairing of the 3-dimensional wing-body compressibility and pressure drag increments; adjusted for the effects of aspect ratio, sweep, camber, thickness ratio, $C_{L_{Design}}$ and M_{Design}, using the methods developed in this report; are compared with 2-dimensional test data for a 10 percent thickness ratio, 1.64 percent camber, advanced airfoil section. The flexibility of the definition of advanced airfoils; sensitivity of the component drag data to the test variables; varying design techniques employed by the principal investigators in arriving at the 3-dimensional wing section, camber, and twist; and the varying degree of model refinement during testing all contribute to the data scatter previously evidenced in the 3-dimensional data. However, the conservatism in the faired 3-D data relative to the 2-D data appears mainly attributable to differences in test Reynolds Number, i.e., 3-D wing-body tests are generally conducted at RN = 2 to 3 million. Additional comparisons are noted on Figure 40 for other $\Delta C_{L's}$. The agreement between 2- and 3-D becomes increasingly better at the lower lift coefficient with increasing disagreement above Design C_L.

At the present stage of development of advanced airfoil design practices, it is believed that for preliminary design of aircraft for transonic cruise applications the potential of advanced airfoils is best represented by the 3-dimensional data fairings of the previous sections. Additional tests and data analysis, the subject of the next section, certainly are in order to sort out the 2-dimensional and 3-dimensional equivalence differences and in particular the sensitivity to Reynolds Number.

7. RECOMMENDATIONS

The advanced airfoil data correlation and drag buildup technique arrived at in this reporting may assist in determining the potential of advanced airfoil applications; however, there remain major and significant areas of further study. These study areas are itemized below:

1. Systematic definition of 2-D design-to criteria and testing to isolate the sensitivity and limitations of the geometric variation on
   - design lift coefficient and Mach number
   - lift coefficient for buffet onset
   - maximum lift coefficient
   - zero lift pitching moment
   - minimum pressure drag
2. Determination of the 2- and 3-dimensional equivalence in the above parameters and 3-D design procedures using 2-D data.
3. Systematic 3-D testing of higher aspect ratio wings including buffet onset studies.
4. Continued development of empirical relationships such as those developed in this study extending into maximum lift and pitching moment correlation.
5. Empirical correlation of lift, drag and moment characteristics of high-lift devices on wing/body's employing advanced airfoil sections.
6. Systematic wind tunnel investigations to determine the potential of advanced airfoil design practices for supersonic cruise applications.

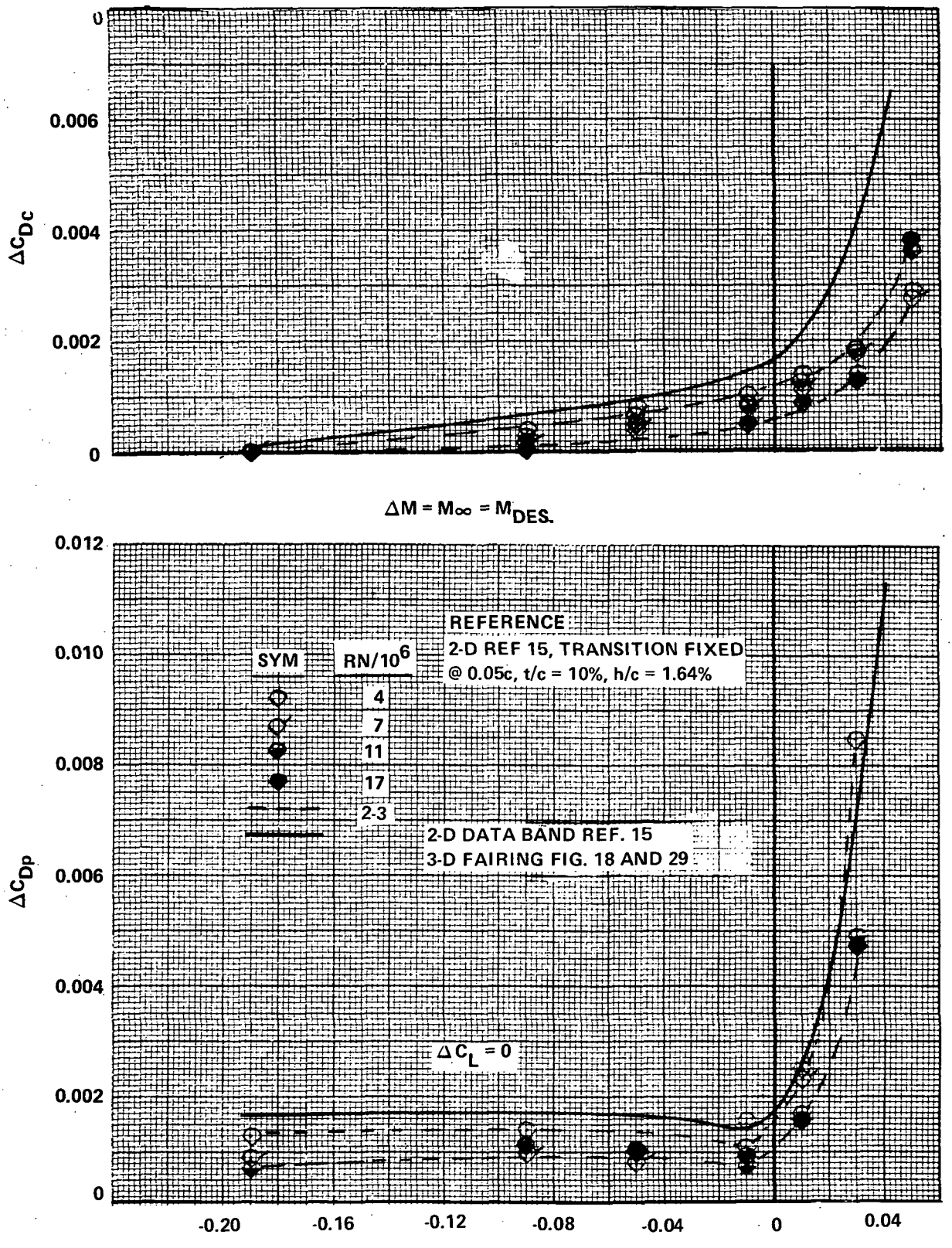

Figure 39. ΔC_{D_c} and ΔC_{D_p} Comparison - 3-D Fairing vs 2-D Test Results

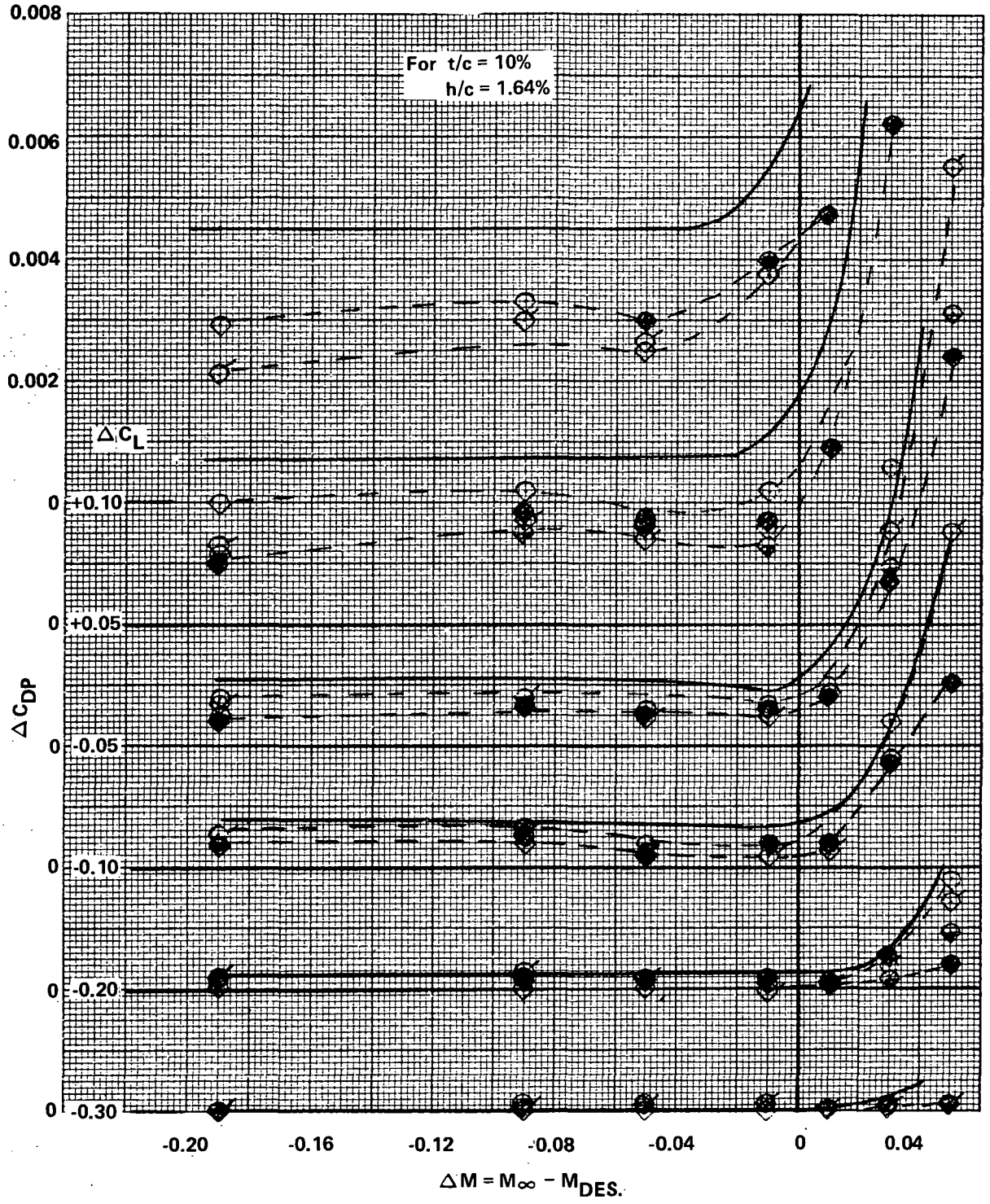

Figure 40. ΔC_{D_p} Comparison - 3-D Fairing vs 2-D Test Results

REFERENCES

1. Miranda, L. R.: Three-Dimensional Supercritical Wing Design. LR 27048, May 1975.

2. McDevitt, John B.: A Correlation by Means of Transonic Similarity Rules of Experimentally Determined Characteristics of a Series of Symmetrical and Cambered Wings of Rectangular Planform. NACA Report 1253.

3. Burdges, Kenneth P.; Blackwell, James A.; and Pounds, Gerald A.: High Reynolds Number Test of a NASA 65, -213, a = 0.5 Airfoil at Transonic Speeds. NASA CR-2499, 1975.

4. Abbott, Ira H.; and Von Doenhoff, Albert E.: Theory of Wing Sections.

5. Ray, Edward J.; and Taylor, Robert T.: Buffet and Static Aerodynamic Characteristics of Systematic Series of Wings Determined from Subsonic Wind-Tunnel Study. NASA TN D-5805, 1970.

6. Anon.: L-1011-1 Flight Performance, RB.211-22B Engines. LR 26189, December 1973.

7. Anon.: Transonic Wind Tunnel Tests of the 1/30 Scale L-1011 Airplane, Lockheed Tests No. N-227, N-236, N-241. Cornell Aeronautical Laboratory, Inc., Report No. AA-4006-W-1, March, June, July 1969.

8. Chudyk, D. W.: Wind Tunnel Test of a 1/30 Scale Model L-1011 Airplane Utilizing a Supercritical Wing. Calspan Report No. AA-4006-W-29, W.A. T06-53, June 1975.

9. NASA/Lockheed-California Company. Contract #N00019-73-C-0040, 1974. (Report to be published).

10. Blackwell, J. A.; Dansby, T.; Little, B. H., Jr.; Ryle, D. M., Jr.; Allison, H. B.: Aerodynamic Design, Test, and Analysis of the Lockheed-Georgia ATT-95 Aircraft. Lockheed-Georgia Company Report LG 72ER 0041, 1972.

11. Ferris, James C.: Static Aerodynamic Characteristics of a Model with a 17-Percent-Thick Supercritical Wing. NASA TMX-2551, 1972.

12. Graham, Lawrence A.; Jones, Robert T.; and Boltz, Frederick W.: An Experimental Investigation of the Oblique-Wing and Body Combination at Mach Numbers Between 0.60 and 1.40. NASA TMX-62,256, 1973.

13. Bartlett, Dennis W.; and Re, Richard J.: Wind Tunnel Investigation of Basic Aerodynamic Characteristics of a Supercritical-Wing Research Airplane Configuration. NASA TMX-2470, 1972.

14. Capone, Francis J.: Effect of Various Wing High Lift Devices on the Longitudinal Aerddynamic Characteristics of a Swept-Wing Fighter Model at Transonic Speeds. NASA TMX-3204, 1975.

15. Burdges, K. P.; Blackwell, J. A., Jr.; and Pounds, G. A.: High Reynolds Number Test of a NASA 10% Thick Supercritical Airfoil at Transonic Speeds. NASA CR-132468, 1975.

16. Harris, Charles D.: Aerodynamic Characteristics of an Improved 10-Percent-Thick NASA Supercritical Airfoil. NASA TMX-2978, 1974.

17. Harris, Charles D.; Blackwell, James A., Jr.: Wind-Tunnel Investigation of Effects of Rear Upper Surface Modification on a NASA Supercritical Airfoil. TMX-2454, 1972.

18. Harris, Charles D.: Aerodynamic Characteristics of Two NASA Supercritical Airfoils with Different Maximum Thicknesses. NASA TMX-2532, 1972.

19. Fournier, Paul G.; and Goodson, Kenneth W.: Low Speed Aerodynamic Characteristics of a 42° Swept High-Wing Model Having a Double-Slotted Flap System and a Supercritical Airfoil. NASA TMX-3036, 1974.

20. Bartlett, Dennis W.; and Harris, Charles D.: Effects of Wing Trailing-Edge Truncation on Aerodynamic Characteristics of a NASA Supercritical-Wing Research Airplane Model. NASA TMX-3024, 1974.

21. Goodson, Kenneth W.: Low Speed Aerodynamic Characteristics of a Rectangular, Aspect Ratio-6, Slotted Supercritical Airfoil Wing Having Several High-Lift Flap Systems. NASA TMX-2317, 1971.

22. Harris, Charles D.: Wind Tunnel Investigation of Effects of Trailing-Edge Geometry on a NASA Supercritical Airfoil Section. NASA TMX-2336, 1971.

23. McKinney, Linwood W.; Herman, Joseph F.; and Boden, Lawrence A.: Effect of Wing Mounted Nacelles on a 42° Swept Supercritical Wing Configuration at Near-Sonic Speeds. NASA TMX-2954, 1974.

24. Supercritical Wing Technology, - a Progress Report on Flight Evaluation. NASA SP-301, 1972.

25. Bartlett, Dennis W.; and Harris, Charles D.: Effects of Wing Trailing Edge Truncation on Aerodynamic Characteristics of NASA Supercritical-Wing Research Airplane Model. NASA TMX-3024, 1974.

26. Caldwell, A. L.; et al.: Technology Integration for Close Support Aircraft. AFFDL-TR-73-59, 1973.

27. Harris, Charles D.; and Bartlett, Dennis W.: Wind-Tunnel Investigation of Effects of Underwing Leading Edge Vortex Generators on a Supercritical-Wing Research Airplane Configuration. NASA TMX-2471, 1972.

28. Pyle, Jon S.; and Steers, Louis L.: Flight Determined Lift and Drag Characteristics of an F-8 Airplane Modified with a Supercritical Wing With Comparisons to Wind-Tunnel Results. NASA TMX-3250, 1975.

29. Revell, James D.: Analysis of Transonic Independent Research Data Based on Transonic Tests on Airfoils 1 to 4 Conducted at ARA 8" x 18" 2-D Transonic Wind Tunnel. LR 23162, 1970.

30. Bartlett, Dennis W.: Application of a Supercritical Wing to An Executive-Type Jet Transport Model. NASA TMX-3251, October 1975.

APPENDIX A

Subsequent to the development of the drag buildup procedures presented in the body of this report, additional advanced airfoil wing-body wind tunnel data was made available through NASA Langley. (See Figure A-1.)

Analysis of these data by the previously discussed procedures resulted in appreciable reduction in the parameters ΔC_{Dc} and ΔC_{Dp} with some slight penalty in drag divergence Mach number.

These new fairings of M_{D2-D}, ΔC_{Dp}, ΔC_{Dc} are noted on Figures A-2 through A-7 and are recommended for use as "Advanced Airfoil Design-Potential" drag buildup.

The more salient features of these advanced airfoils are

- A reduction in the compressibility drag parameter, i.e., drag creep for all Mach numbers. The fairing of the data on Figure A-3 reflects levels attained on 2-dimensional sections, i.e., W_{11}.
- The pressure drag parameter reflects appreciable reduction in pressure drag and the Mach number is increased towards Mach design. (See Figures A-3 through A-7.)
- Drag divergence Mach numbers are reduced approximately $\Delta M = \div .015$ over the Advanced Airfoil reported on in the body of this report. (See Figure A-2.)
- The form drag appears to be unchanged. Figure 33 form factors are still recommended.
- For a wing-body having an effective wing thickness ratio of 10 percent, the "Advanced Airfoil Design-Potential" compressibility and pressure drag would be approximately 14 drag count lower at M_{design} and $C_{LDesign}$ than the Advanced Airfoil reported on in the body of this report.

SYM.	AR	$\Lambda c/4^o$	$t/c_{EFF.}\%$	h/c @ .70Y/$\frac{b}{2}$ % CAMBER	$C_{L_{DESIGN}}$	M_{DESIGN}
	11.954	27	12.58	1.15	0.65	0.792
	11.954	27	14.58	1.38	0.65	0.765
	10.242	27	12.58	1.30	0.60	0.795
	11.48	30	12.22	1.12	0.60	0.815

Figure A-1. Wing-Body Data Base - Summary

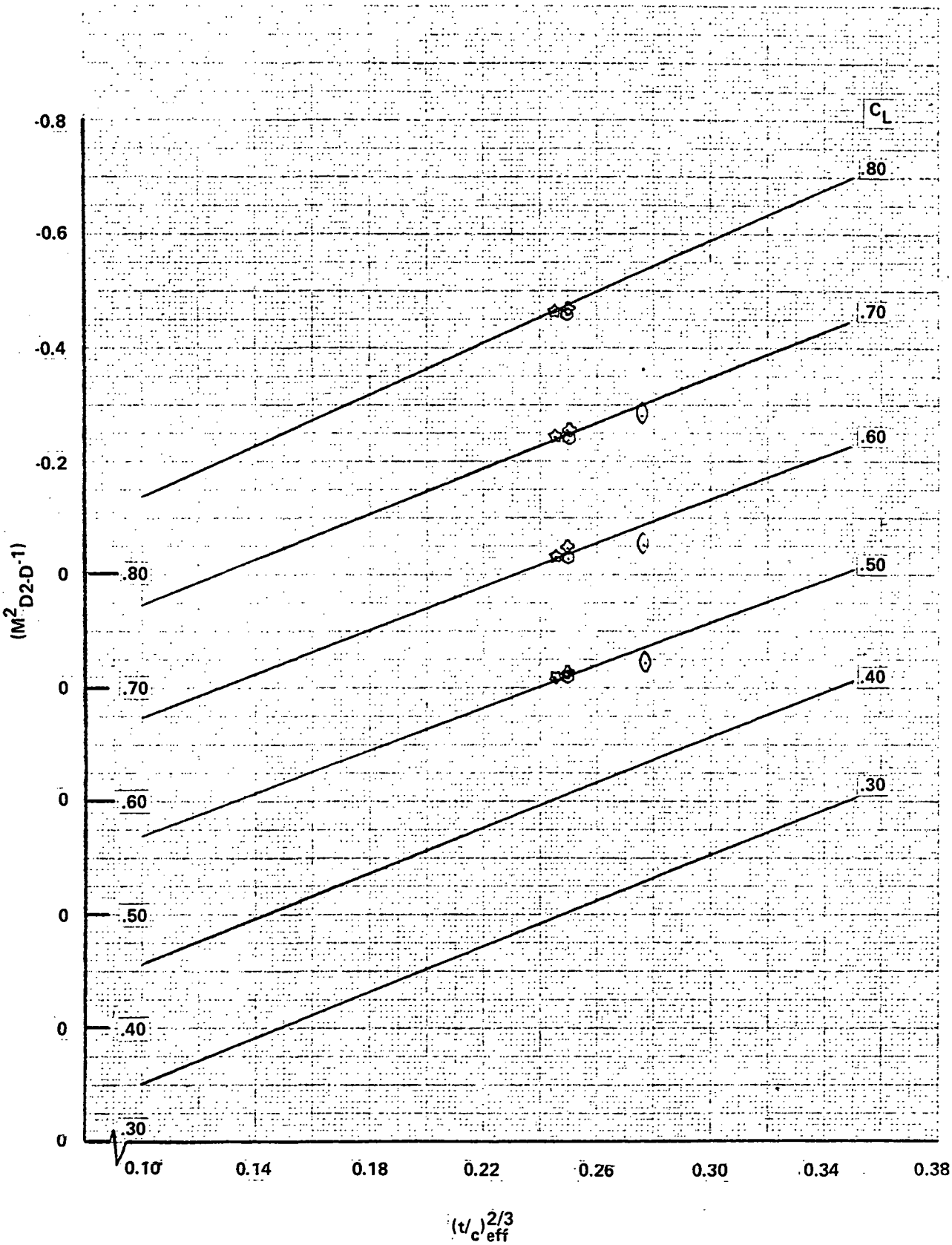

Figure A-2. Drag Divergence Mach Number - M_{D2-D}

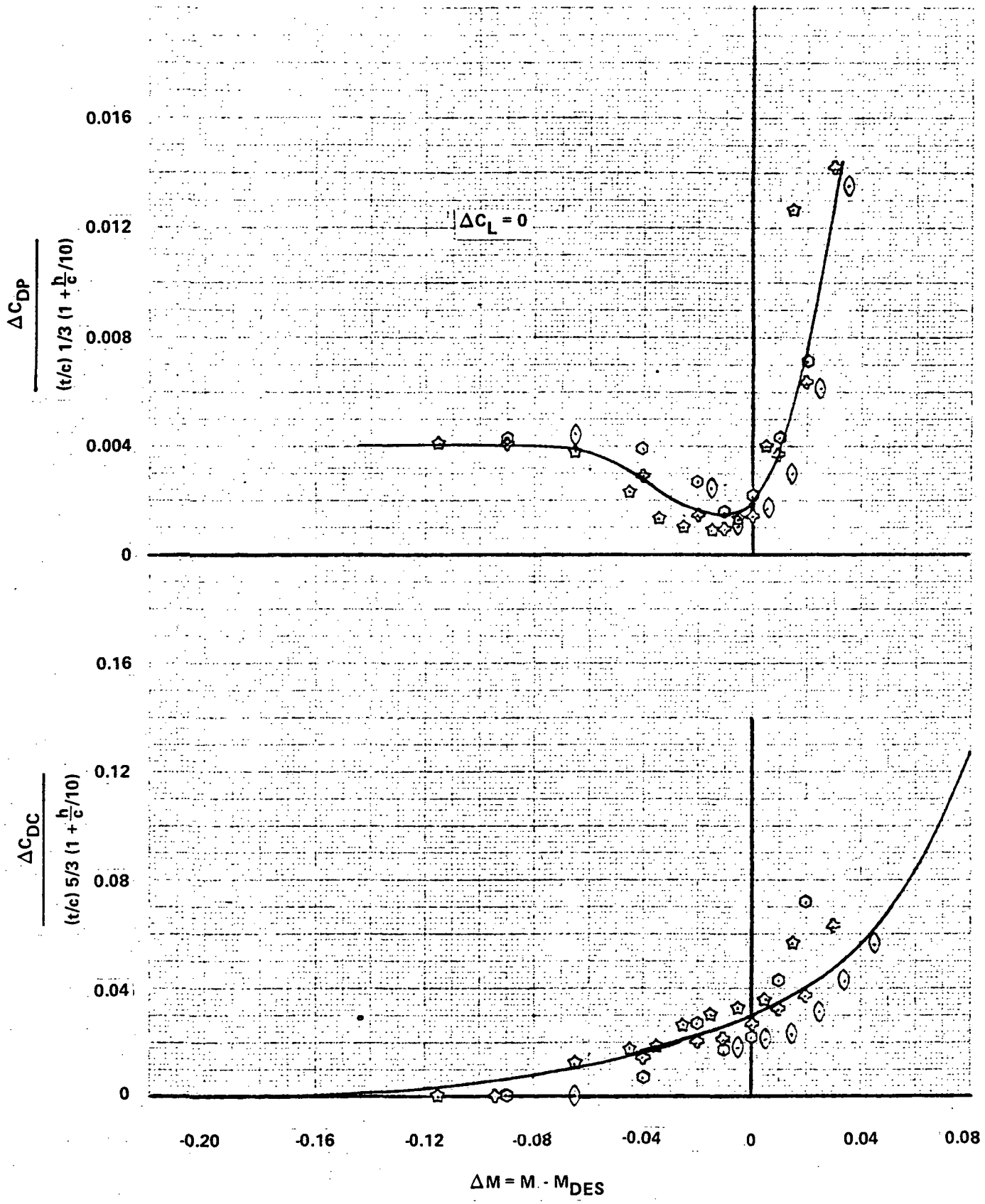

Figure A-3. Incremental Compressibility and Pressure Drag

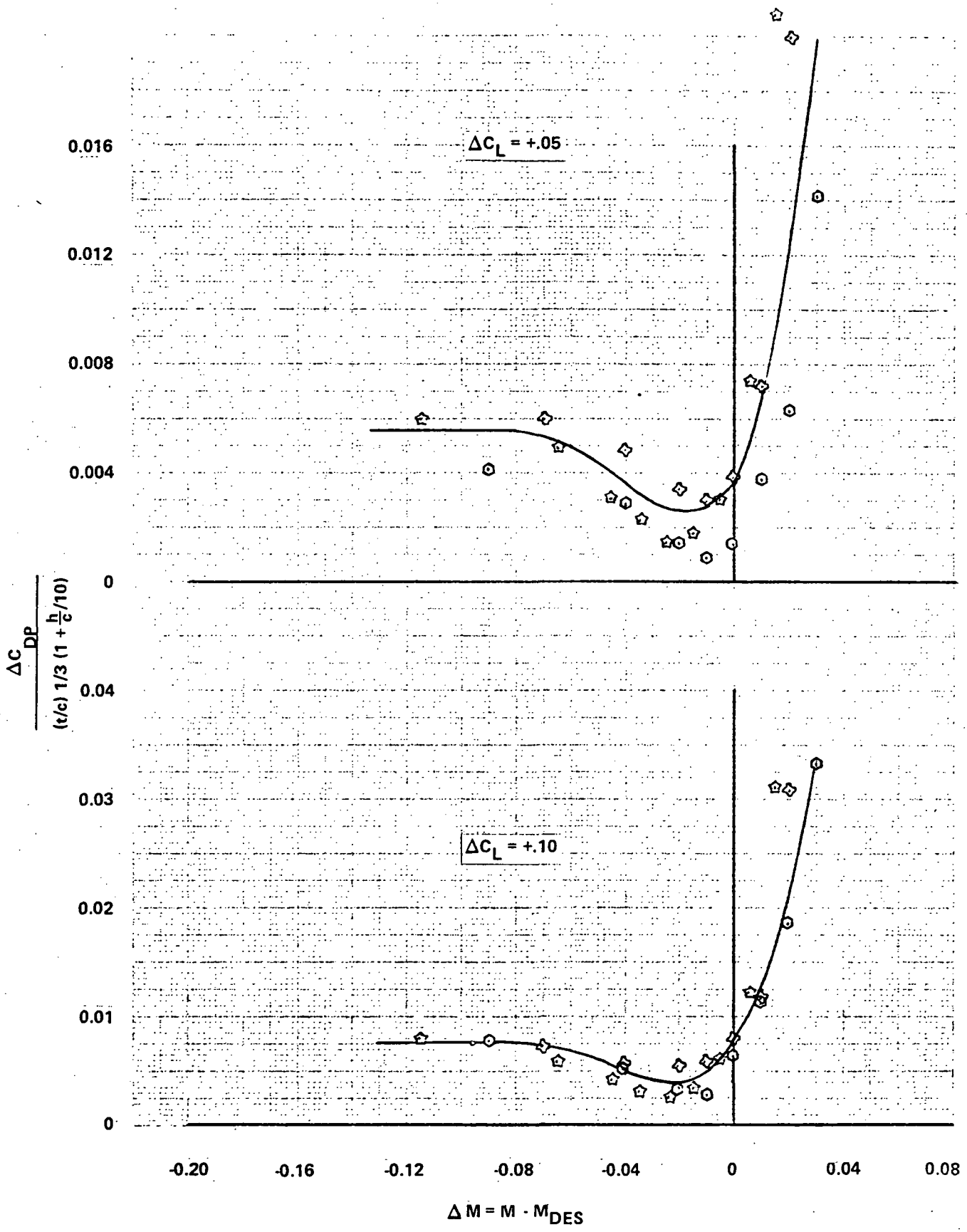

Figure A-4. Incremental Pressure Drag, ΔC_L = +0.05 and +0.10

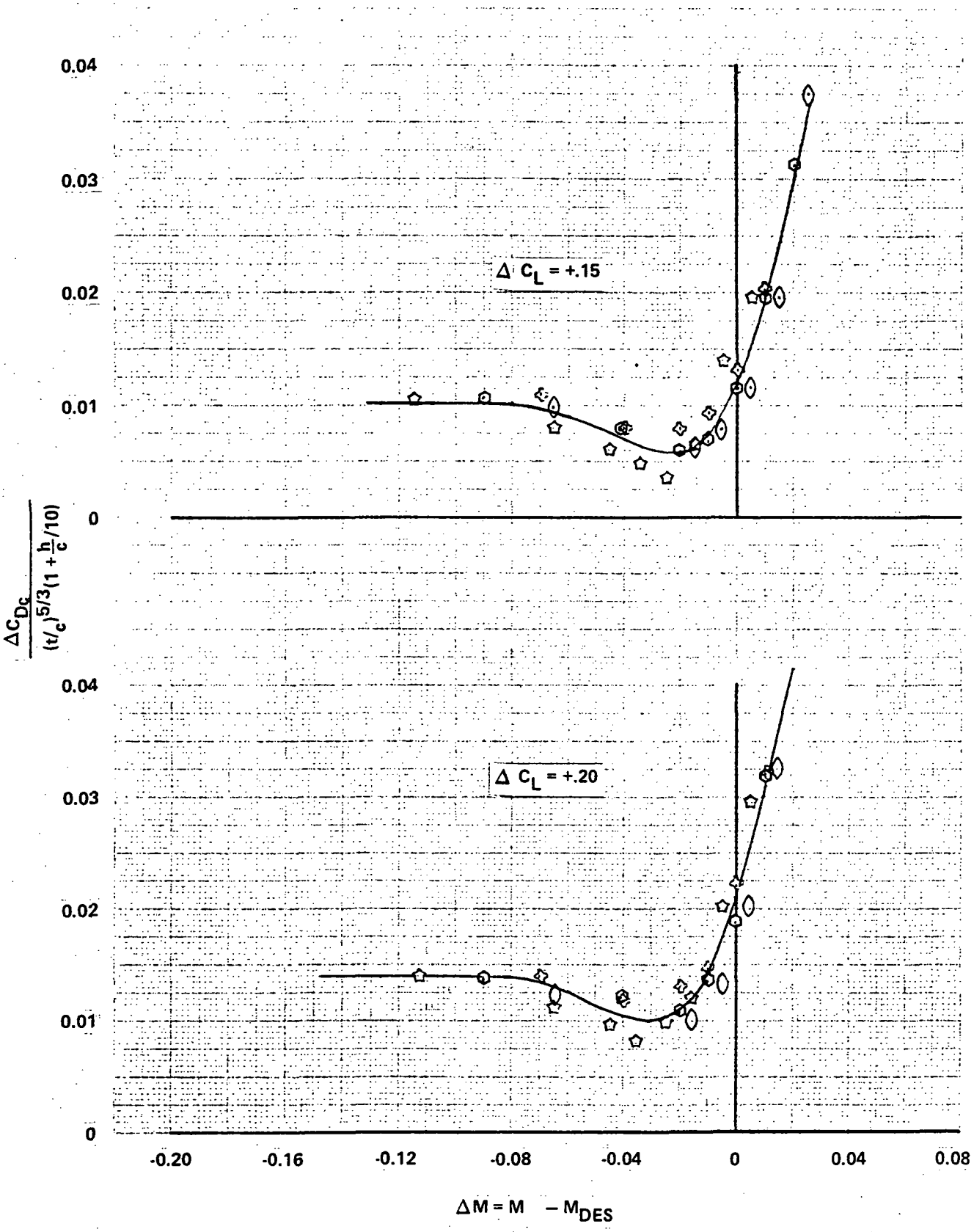

Figure A-5. Incremental Pressure Drag - ΔC_L = +0.15 and 0.20

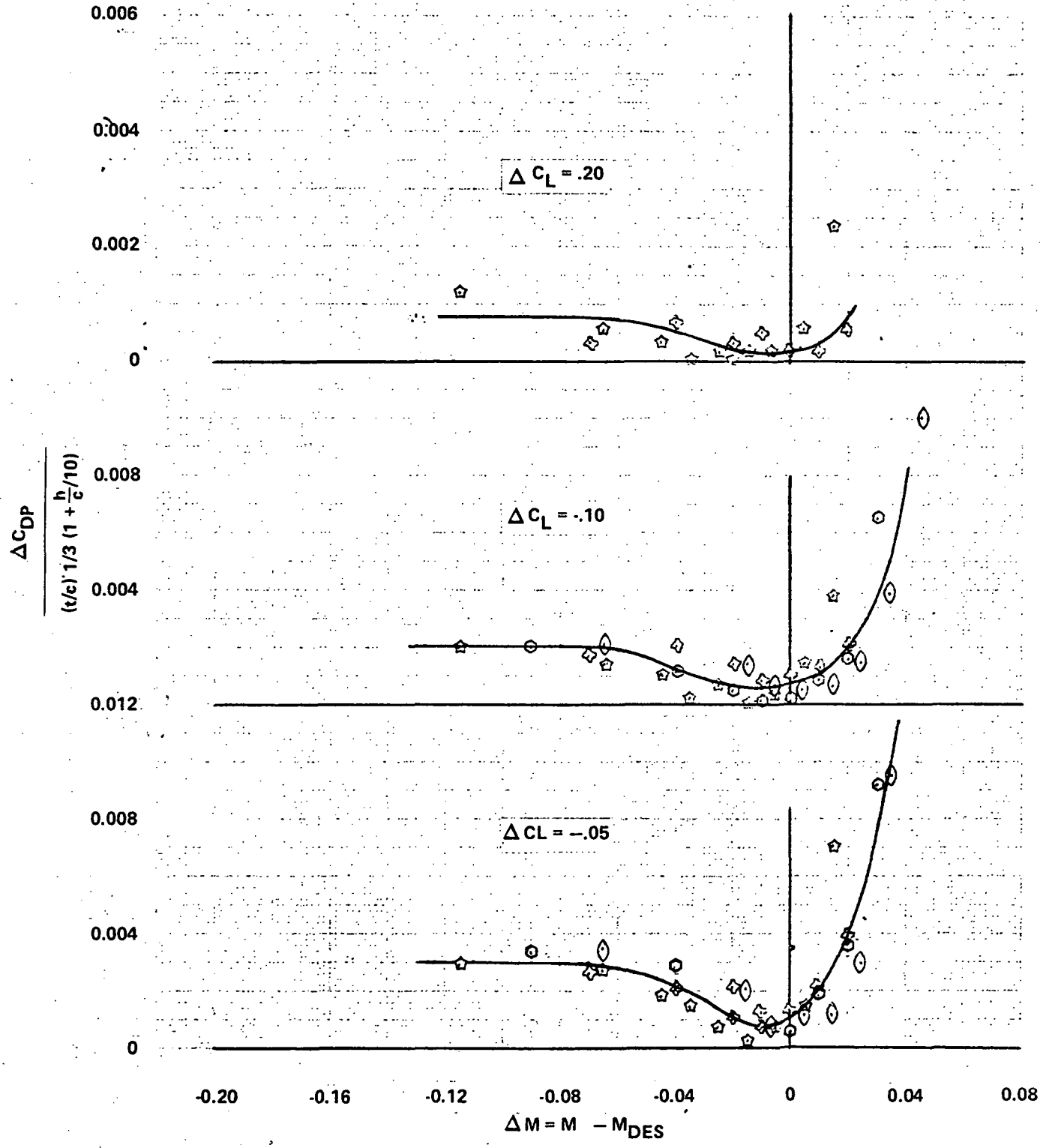

Figure A-6. Incremental Pressure Drag - ΔC_L = -0.05, -0.10 and -0.20

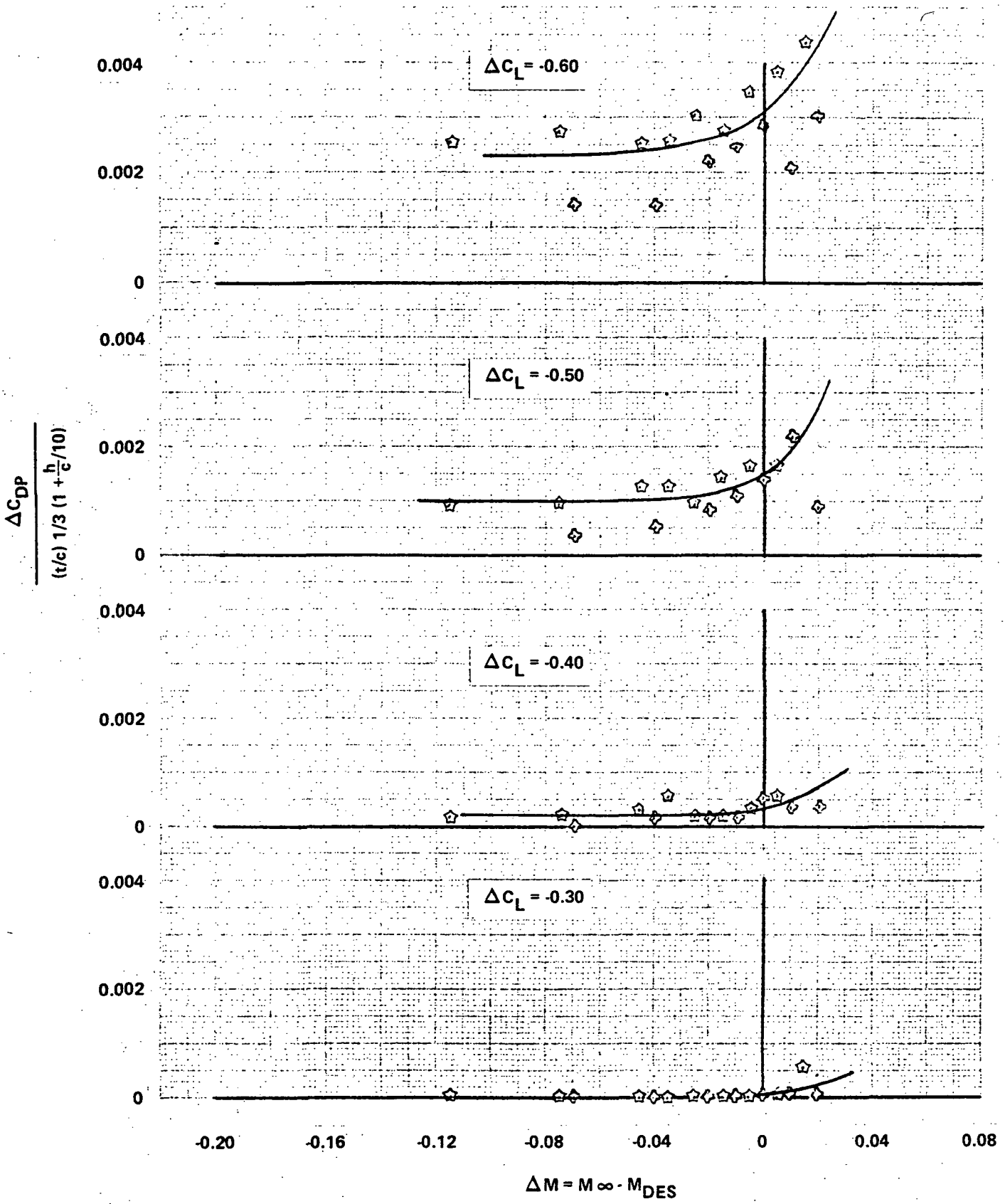

Figure A-7. Incremental Pressure Drag - ΔC_L = -0.30, -0.40, -0.50 and -0.60